Sex Differences in the Correlation between Empirical and Simulated Brain Connectomes

Master's Thesis Report

Author: Shraddha P. Jain [1, 2]
Primary Examiner: Prof. Dr. Joachim Krug [1]
Secondary Examiner: Dr. Oleksandr V. Popovych [2, 3]
Supporting Supervisor: Dr. Kaustubh R. Patil [2, 3]

[1]Department of Physics, University of Cologne
[2]Institute of Neuroscience and Medicine, Brain and Behaviour (INM-7), Forschungszentrum Jülich
[3]Institute of Systems Neuroscience, Medical Faculty, Heinrich-Heine University Düsseldorf

June 10, 2022

Acknowledgements

This research project has personally been a great experience. Through the project, I have not only gained a better understanding in the domain of neuroscientific research, but I have also learned useful skills in the field of statistics and data analysis. I would like to express my sincere gratitude to everyone who made it possible for me.

In particular, I would like to specially thank my research supervisors - Dr. Kaustubh R. Patil and Dr. Oleksandr V. Popovych at the Institute of Neuroscience and Medicine 7 (INM-7) - Forschungszentrum Jülich, for giving me the wonderful opportunity to pursue a research project with them in the form of an initial internship and subsequently a master thesis project. Both of them have helped me understand different aspects of the project in a very comprehensive way and I will always be very grateful to them for their relentless support, guidance and encouragement throughout the project. I would also like to express my sincere gratitude to Prof. Dr. Joachim Krug for gladly agreeing to be my supervisor at the University of Cologne and also for helping me with the administrative processes. I am also indebted to him for his key suggestions that helped me incorporate a different perspective into the analysis. I also thank Prof. Dr. Simon Eickhoff - the director of INM-7 and all the members of the Applied Machine Learning group as well as the Mathematical Neuroscience group for their selfless assistance and insightful discussions during our meetings and seminars. I am particularly grateful to Justin Domhof, Kyesam Jung, Shammi More, Sami Hamdan and Dr. Amir Omidvarnia for patiently helping me resolve the issues I faced during the project.

In addition, I would like to convey my sincere appreciation to Dr. Petra Neubauer-Guenther at the Physics Department of the University of Cologne for her unwavering support during the entire course of my master's study in Germany. Besides, my heartfelt thanks to Mrs. Herrmann at the examination office for kindly helping me with the bureaucracy.

I am also immensely thankful to my family, especially my parents who have been my greatest source of inspiration and moral support. Ma and Papa, thank you for always being there for me! Moreover, this acknowledgement would definitely be incomplete without thanking my dear friends, particularly Tushita, Vivek, Saurabh, Shivi, Priyanka, Nishant, Naren, Maheshwari, Keshvi, Ananya and Prajwal for having faithfully stood by me through thick and thin. It's because of their love and care that I made it this far. Last, but not the least, I would like to express my deepest gratitude to my Guru for His Grace in every step of my life.

Abstract

Investigation of sex differences in the brain connectomes, that is, comprehensive maps of the underlying structural and functional connections across different regions of the human brain defined by a specific parcellation scheme, has been an active field of research in neuroscience. There are largely two main approaches to study the complex dynamics of the brain - empirical neuroimaging techniques and whole brain dynamical models. The studies in the past, however, have utilized only the empirical brain data extracted from the neuroimaging techniques in their investigation of sex differences. The aim of this project, therefore, is to also include the simulated data generated from the whole brain dynamical models and examine the sex differences in its correlation with the empirical data, within a given brain parcellation scheme.
The analysis involves 272 subjects from the Human Connectome Project (144 females). For each individual under 11 brain parcellation schemes, we calculated an empirical structural connectivity (eSC), an empirical functional connectivity (eFC) using the empirical neuroimaging data and two simulated functional connectivity (sFC) matrices based on the ensembles of coupled phase- (PO) and limit-cycle (LC) oscillators. The sex difference was then investigated in the goodness-of-fit - the maximal Pearson's correlation coefficient between the sFC and the eFC matrices ($corr(sFC,\ eFC)_{max}$). We observed a significantly higher correlation for males within each of the 11 parcellation schemes. Since the models utilize the empirical information, we regressed out the brain size and empirical structure-function relationship, to check if the sex difference still persists. After the regression, this difference remains significant for 10 and 8 parcellation schemes for PO and LC model, respectively. We speculated that a potential reason for this could be the differences in the 'complexity' of the eFC matrix between the two sexes, which may in turn negatively influence the quality of their model fitting, i.e. a higher 'complexity' implying a lower fit. We then calculated three potential 'complexity' measures - the Shannon entropy $H(eFC)$, the standard deviation $\sigma(|eFC|)$ and the area under the eigen value curve $A(\lambda_{eFC})$ of the eFC matrix, to not only examine the sex differences in them, but to also investigate their ability to account for the sex differences in the goodness-of-fit. We found that the first two measures are significantly higher for males and are, therefore, positively correlated with the goodness-of-fit. However, the third measure is found to be significantly higher for females, resulting a negative correlation with the goodness-of-fit. The study was, therefore, successful in establishing the statistical differences in the goodness-of-fit and other properties of the eFC matrix between males and females. However, a precise interpretation of the term 'complexity' of a connectome and the validity of our hypothesis about its negative correlation with the goodness-of-fit demands further investigation.

Contents

Chapter 1

Introduction

To understand the complex dynamics of a human brain, it is a common practice in neuroscience to view the brain from the perspective of network theory. The empirical neuroimaging techniques as well as the dynamical whole brain models follow this approach, where the brain is represented as a network of distinct, but interacting brain regions, also referred to as the 'nodes' of the network and the 'edges' of the network are represented by the structural or functional connections between the nodes [29] [31]. The structural connections correspond to physical anatomical links between the brain regions, while the functional connections represent the synchronised co-activation of any pair of brain regions during a task performance or even the resting state of the brain. Brain connectomes are, therefore, comprehensive maps of neural connections in the brain [6] represented through mathematical matrices.

Investigating sex differences in these brain connectomes (both structural and functional) has been an active area of research in neuroscience. Previous studies have, however, explored only empirical brain data in this aspect. For instance, the study [40] investigated how the sex differences are encoded differently in the structure and the function of human brain. That is, for some brain regions, there might be only a structural or a functional difference between the male and female brain, while some brain regions may differ both in their structure and their function. As mentioned earlier, the functional connections across different brain regions exist even when the brain is in its resting state. Accordingly, some studies such as [32] have shown that there exist certain specific functionally connected regions (referred to as resting state networks or RSNs) in the human brain wherein, the resting state connectivity differs between males and females. Furthermore, a more recent study [39] implemented machine learning algorithms and successfully classified subjects according to their sex by utilizing the spatially specific resting state brain connectivity (empirical) data. In addition, the empirical structure-function correspondence in a male brain is also

found to be different from that in a female brain [16].

Therefore, the aforementioned studies investigating the sex differences in the organization of human brain have not included the simulated resting state connectivity of the human brain in their analysis. Hence, in addition to the empirical data recorded through the neuroimaging techniques, this project aims to also include the simulated data generated by whole brain dynamical models and subsequently examine how the quality of model fit, that is, the correlation between the simulated and the empirical functional connectomes, differs between males and females.
The following section provides a general background of a few concepts that constitute the major building blocks of the analysis in this project.

1.1 Background

1.1.1 Brain Parcellation

The human brain is spatially heterogeneous [9]. Different parts of the brain differ not only in their structure and function (local properties), but also in their connectivity to other parts of the brain (global properties). To understand the organization and function of the brain, we could consider the brain as a collection of hundred of thousands of voxels (volume elements) and record the data for each of these voxels. However, this would result in a very high dimensional data which is not optimal for our analysis. Brain parcellation is, therefore, a technique to delineate the whole brain into distinct, yet closely interacting regions, where each region consists of many voxels grouped together with respect to similarity in a specific neurobiological measure. The idea is to create a brain atlas where each region is homogeneous within itself, but differs from other regions. In this way, the dimension of brain data is reduced from hundreds of thousands of voxels to a few hundred brain regions or brain parcels [9].

There exist a plethora of possible methods and criteria to parcellate a brain and this is an open question in neuroscience as to which is the best way among many. Each parcellation method results in a different number of brain regions, and an example of this is illustrated in Figure 1.1, where the cortex of the human brain is delineated into distinct brain regions (represented by each color) and the numbers on the left represent the number of respective brain regions. The two common criteria based on which the brain is parcellated into distinct regions are its anatomical and functional properties. The anatomical properties include cytoarchitecture, myeloarchitecture, folding properties of the cerebral cortex etc [9] [31]. The Harvard - Oxford atlas, for instance, is based on parcellating brain cortex into 96 distinct parcels or brain

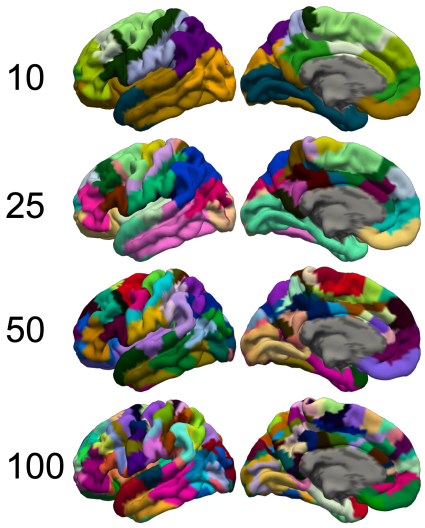

Figure 1.1: Illustration of delineation of the cortex of the human brain into distinct brain regions represented by each color. Each parcellation criteria gives rise to a different number of brain regions as indicated by the numbers on the left side of the figure. Figure taken from [3].

regions regions with respect to the cortical folding properties. On the other hand, for parcellation based on functional properties, the functional connectivity of each voxel is considered and voxels with similar connectivity (with the rest of the brain) are grouped together into a brain region through a machine learning (clustering) algorithm [31]. Here, functional connectivity refers to undirected statistical dependencies between a pair of voxels (either while the brain is at rest or during task performance) [29]. Examples of atlases defined based on resting state functional connectivity are Schaefer atlas (which can be further classified into parcellation schemes with 100, 200, 400 or 600 parcels) and Shen atlas (which can have 79, 156 and 232 parcels).

It is important to note that all the methods employed to define a particular brain atlas/parcellation scheme have inherent assumptions, advantages, and well as limitations. Therefore, neither the anatomical nor the functional properties are in anyway superior to the other, as each property represents different aspects of brain organisation [9].

1.1.2 Empirical Structural and Functional Brain Connectome

A connectome or a connectivity matrix is a comprehensive map of neural connections across different parts of the brain [6]. These connections can be at micro, meso as well as macro scales. Once the brain has been partitioned into distinct brain regions according to a certain criteria of parcellation, neuroimaging techniques are employed to record the signal from each of these regions either during the resting state of the brain, or during a cognitive task. Using this data extracted from the neuroimaging techniques, a structural or a functional connectivity matrix is generated that reflects anatomical links or statistical dependencies, respectively, between all the possible pairs of brain regions.

At a macro scale, for a particular choice of brain parcellation scheme, the structural connectivity (SC) is constructed from streamline tractography inferred from diffusion weighted magnetic resonance imaging (dw-MRI), which reveals physical anatomical links (axonal fibre bundles/streamlines) that interconnect the brain regions [31]. In principle, there are two kinds of SC matrices that can be constructed - empirical structural connectivity matrix (eSC) where each element corresponds to the number of streamlines that connect the two brain regions and the empirical path length (ePL) matrix where each element corresponds to the average length of those streamlines [8]. Besides, for the same parcellation scheme, the empirical functional connectivity matrix (eFC) is constructed by calculating the Pearson's correlation coefficient between the blood oxygen level dependent (BOLD) time series signal of all possible pairs of brain regions, recorded through the functional magnetic resonance imaging (fMRI). The activity of a brain region is directly proportional to the blood oxygen level (amplitude of the BOLD signal) in that region. Since a brain region is made up of numerous voxels, the BOLD signal recorded for a certain region in the brain is the average of the BOLD signals of all the constituent voxels and, therefore, reflects the collective activity of a large population of the underlying neurons. The eFC matrix constructed, therefore, represents the strength of synchronised co-activation between distinct regions of the brain [8].

It is should be noted that the structural connectivity matrix (SC) and the functional connectivity matrix (FC), however, do not specify any directionality of the underlying connections [29] and are, therefore, symmetric matrices.

1.1.3 Simulated Functional Connectome

One of the efforts to understand the complex dynamics and the activity of the brain, through the lens of Physics and Mathematics, is to simulate the mean activity of each of the brain regions using whole brain dynamical models. Similar to empirical neuroimaging methods, this approach also views brain cortex as a network of nodes obtained by partitioning the cortex into distinct brain regions (nodes or parcels) defined according to a parcellation criteria [8].

Some whole brain dynamical models are biologically inspired, like the neuronal mass model, while some oscillatory neuronal models like the phase oscillator model and the limit cycle model are rather abstract [4] and their neurobiological interpretation is difficult. In general, the mathematical models employed to simulate the neuronal activity of the brain involve a set of time dependent differential equations that can be numerically solved. As the brain is viewed as a network of nodes or brain regions defined by a selected parcellation scheme, the coupling strength between the nodes is calculated from the eSC matrix, whereas the delay in signal propagation between them is obtained from the ePL matrix. The models, therefore, utilize the empirical neuroimaging data in their simulations. The simulation results in a time series signal corresponding to each node of the network. For the selected parcellation scheme, the simulated functional connectivity (sFC) matrix (symmetric in nature) is subsequently constructed by calculating the Pearson's correlation coefficient between the simulated time series signal of all possible pairs of nodes or brain regions (similar to the calculation of the eFC matrix).

1.1.4 'Complexity' of a Connectome

Human brain is a hierarchical and modular (consisting of modules and sub modules [29]) organisation of different regions that constantly interact with each other, even when the brain is at rest. The empirical time series signals recorded through the fMRI technique for each brain region represent the collective dynamics of a large population of the underlying neurons. Since the dynamics can be periodic, random or chaotic, the time series signals also exhibit different levels of complexity, which in-turn introduces complexity in the eFC matrix [19].

The exact definition and quantification of 'complexity' of a connectome, however, remains an open question in neuroscience. In the recent literature, there have been a few attempts to quantify the 'complexity' of brain data. In the context of physiological time series signals, the temporal complexity of an empirical fMRI signal from

the human brain can be quantified in terms of 'entropy' which is a well established estimate in statistics to assess how complex a dynamical process is [19]. It essentially measures the lack of temporal order or predictability in the signal [26]. A large value of any of the entropy, therefore, implies a highly disordered signal and thus indicates that the underlying system is substantially complex [37] [26] [19]. The classical measures of entropy, however, are inaccurate in quantifying the complexity of the fMRI time series signal due to limited number of sampling points [19]. Hence, the more appropriate measures previously employed in the literature with regards to the entropy analysis of the fMRI data include the 'sample entropy' (SampEn) [26] [37] [19] which measures the rate at which new information is generated in a dynamical process [27], 'multi-scale entropy' (MLE) which is sample entropy over multiple time scales [27] [37] and 'approximate entropy' (ApEn) [37] [26](a variant of sample entropy [30]). Moreover, the study [19] uses SampEn to quantitatively characterize the complexity within the dynamic functional connectivity (a functional connectome that is time dependent). Besides, although the study [31] does not exclusively discuss 'complexity' of a connectome, it quantifies several properties of the empirical connectome by computing the data variables for every individual subject using their respective eFC matrices, in order to account for both intra-parcellation as well as inter-parcellation variance observed in the modelling results.

Aim of the Project

Specifically, this project considers the activity of a human brain in the absence of a cognitive task and therefore, both the empirical neuroimaging signals as well as the simulated time series signals that we considered, exhibit the resting state activity of the brain. The project aimed at investigating whether the quality of model fit, that is, the correspondence between the eFC matrix and the sFC matrix, referred to as the goodness-of-fit, is different for the group of males as compared to the group of females, within a selected parcellation scheme. Moreover, since the mathematical models utilize the empirical information, we also aimed to investigate if the sex differences persist after the other covariates with sex, like the brain size or the empirical structure-function correspondence are regressed out from the goodness-of-fit.
Furthermore, since the eFC matrix was used for model validation, the sex differences in the goodness-of-fit could also possibly be influenced by the presence of sex differences in the 'complexity' of the eFC matrix. Therefore, an additional aim of the project was to also quantify the 'complexity' of the eFC matrix, assess the statistical significance of the differences in the quantified measure between the group of males and females and also examine if the sex differences in the goodness-of-fit can be attributed to the variation in the 'complexity' of the eFC matrix between males and females within a selected parcellation scheme.

Chapter 2

Materials and Methods

In this chapter, we discuss the characteristics of the empirical data employed in the project, along with the brain parcellation schemes used, steps involved in the construction of the eSC, ePL, eFC matrices and whole brain dynamical models implemented for the construction of the sFC matrix for every individual subject. Furthermore, in addition to the methods employed for the calculation of 'complexity' measures, we also discuss a few statistical techniques relevant to the analysis.

2.1 Characteristics of the Empirical Data

In this study, we considered 272 healthy and unrelated subjects consisting of 144 females and 128 males. All the subjects belong to the age group of 22-37 years, where the mean age of the male group is 28.7 ± 3.6 (mean $\pm$ std) and that of the female group is 28.3 ± 3.5. Hence, the average age of both the groups is approximately the same as shown in Figure 2.1a, where the histograms of the males (in blue) and females (in red) are superimposed on each other and the respective box plots are not largely shifted with respect to each other. However, as shown in Figure 2.1b, in case of the brain sizes or the total intracranial volume (TIV measured in mm^3), the histograms and the box plots of the male group are largely shifted towards higher values as compared to those of the female group. The statistical significance of this difference was subsequently tested and quantified as described in detail in subsection 3.1.1.

The empirical data for these subjects was obtained from the Human Connectome Project (HCP) S1200 public release, which has the complete dwMRI data - for the construction of eSC and ePL matrices, the resting state fMRI (rs-fMRI) data - for the construction of the eFC matrix and the phenotypical data which includes the phenotypical features such as sex, age, brain size (TIV), etc of the subjects [31].

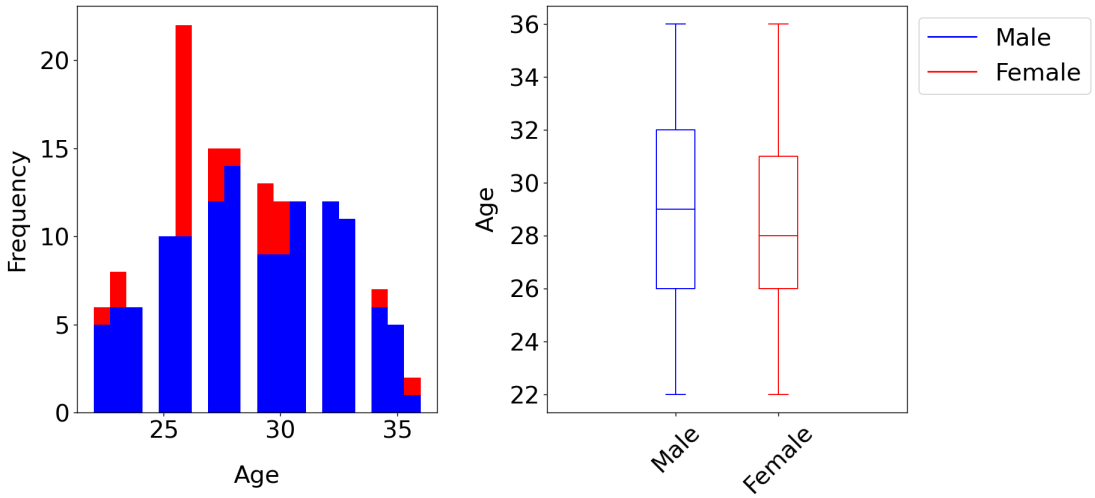

(a)

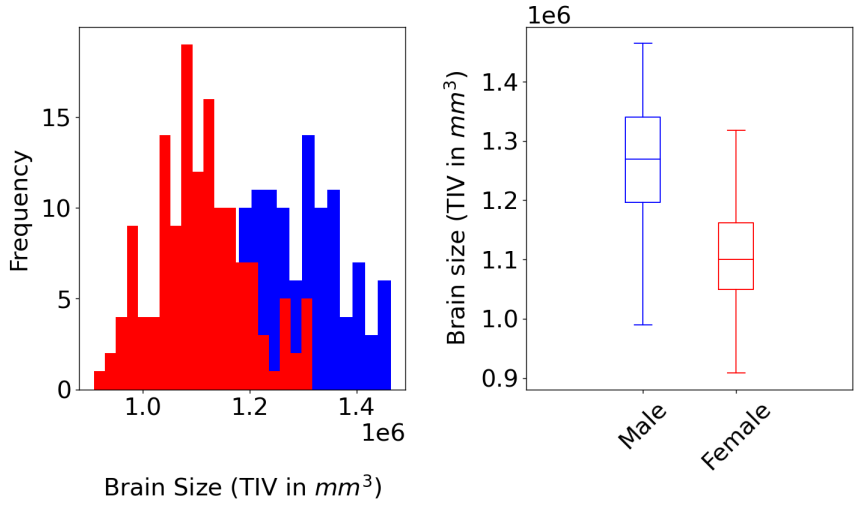

(b)

Figure 2.1: Illustration of the differences in the phenotypical characteristics between the group of males (in blue) and the group of females (in red) in the subjects considered. **(a):** Sex differences in the age. **(b):** Sex differences in the brain size or the Total Intracranial Volume (TIV measured in mm^3).

2.2 Brain Parcellation Schemes

We considered 11 cortical brain parcellation schemes in total which consisted of three atlas families: the anatomical Harvard-Oxford Atlas defined based on folding properties of the cortex, and the functional Shaefer Atlas and Shen Atlas which are based on grouping of voxels according to their similarity in the patterns of their respective resting state functional connectivity. Each of these families of atlases have several variations within themselves as follows:

1. Schaefer Atlas with 100, 200, 400 and 600 cortical parcels (referred to as S100, S200, S400 and S600) [31].

2. Shen Atlas with 79, 156 and 232 cortical parcels (denoted as Shen79, Shen156, and Shen232) [31].

3. The Harvard Oxford Atlas can be sub-classified based on the threshold of maximal probability of a voxel to be included in the parcel. Therefore, this Atlas family has parcellations with 0%, 25%, 35% and 45% (denoted as HO0%, HO25%, HO35% and HO45%) threshold of maximal probability. For example, the HO25% parcellation implies that every voxel with maximal probability below 25% will not be included in the parcel or brain region. Thus, the higher the threshold, the smaller is the size of the resulting brain region.
   The HO0%, HO25% and HO35% parcellate the brain into 96 cortical regions (parcels), however, HO45% results in 95 cortical regions as the left supracalcarine cortex region is excluded because no voxels within this region meet the threshold of 45% [31].

2.3 Construction of eSC and ePL Matrices from dwMRI Data

The connectomes considered in this study are defined at the macro scale. The SC matrices representing the undirected anatomical links in the brain were constructed using the dwMRI data which consisted of dwMRI images as well as T1-weighted images. Firstly, the complete dwMRI data underwent a preprocessing step implemented through an in house developed pipeline consisting of software packages such as Freesurfer, MRtrix3, ANT and FSL. The preprocessing procedure involves the following tasks: head motion correction and removal of noise and distortions caused by eddy currents for dwMRI images, image intensity normalization, tissue segmentation and reconstruction of the cortical surface for T1-weighted images and bias field correction for both dwMRI and T1-weighted images and registration of dwMRI images

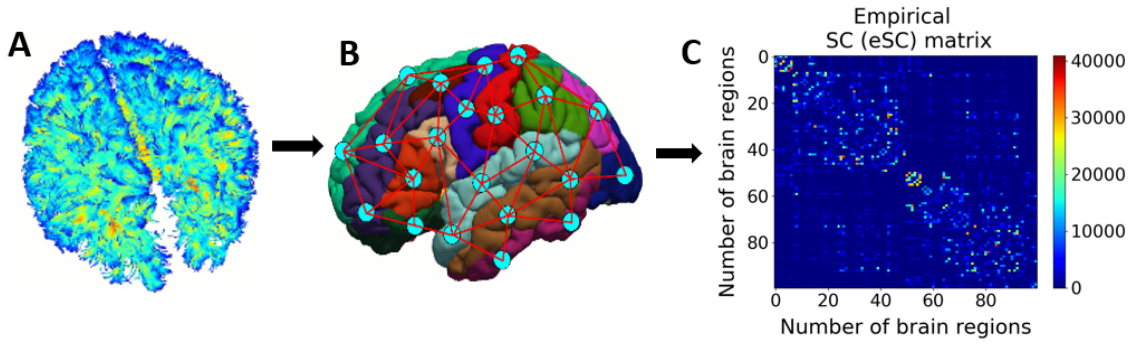

Figure 2.2: Schematic illustration of the construction of the eSC matrix of an individual subject for 100 cortical brain regions defined under the S100 parcellation scheme. **A**: Streamline tractography of the human brain inferred from diffusion weighted Magnetic Resonance Imaging (dw-MRI) scan. **B**: Schematic representation of the physical anatomical links between different brain regions. **C**: Example of the resultant eSC matrix for 100 cortical brain regions (self connections excluded). The color of each pixel in the eSC matrix signifies the count of the number of streamlines according to the color bar.

to the T1-weighted images through transformation function. Thereafter, MRtrix3 package was used to calculate the whole brain tractography through a probabilistic fiber tracking algorithm. Then, the FSL package was employed to transform the brain atlas images which were initially sampled in the standard space to the native space [31] [8]. In the end, using MRtrix3 on the whole brain tractography, the structural connectivity (SC) was calculated for each of the 11 brain parcellation schemes. This process yielded two symmetric NxN dimensional SC matrices - the eSC matrix and the ePL matrix signifying undirected anatomical links across N brain regions defined under a selected parcellation scheme. As already mentioned, the eSC matrix consists of the count of the axonal fibre bundles or streamlines connecting all possible pairs of the brain regions, whereas the ePL matrix consists of the average length of those streamlines.

Following the aforementioned procedure, we constructed the eSC and the ePL matrices for every individual subject, under each of the 11 parcellation schemes. A typical construction of the eSC matrix of a certain subject, for 100 cortical brain regions defined under the S100 parcellation scheme, is schematically illustrated in the Figure 2.2, where the process progresses from streamline tractography (extreme left) to establishing anatomical links between different brain regions (middle) and finally results in a 100x100 eSC matrix (extreme right).

2.4 Construction of eFC matrix from rs-fMRI Data

In order to compute the eFC empirical functional connectivity (eFC) matrix in this study, we considered the resting state fMRI signal (rs-fMRI) from the brain regions, that is, the fMRI signal was recorded in the absence of a cognitive task.
The rs-fMRI data was initially preprocessed (removal of noise) using the ICA FIX provided by the HCP repository [31]. For every subject, the preprocessed data consists of the resting state BOLD activity time series signal for all the N parcels (brain regions) defined under a selected brain parcellation scheme. The time series signal of each brain region represents its mean activity (at rest) since the signal is the average of the BOLD signals of all the underlying voxels that constitute that brain region. In this study, the rs-fMRI data of every subject included data from 4 different scanning sessions of 1200 time points each, for every brain region defined under a given parcellation scheme [31]. The time series data from all the 4 sessions were subsequently z-scored and concatenated to obtain a signal of 4800 time points in total per brain regions per subject.

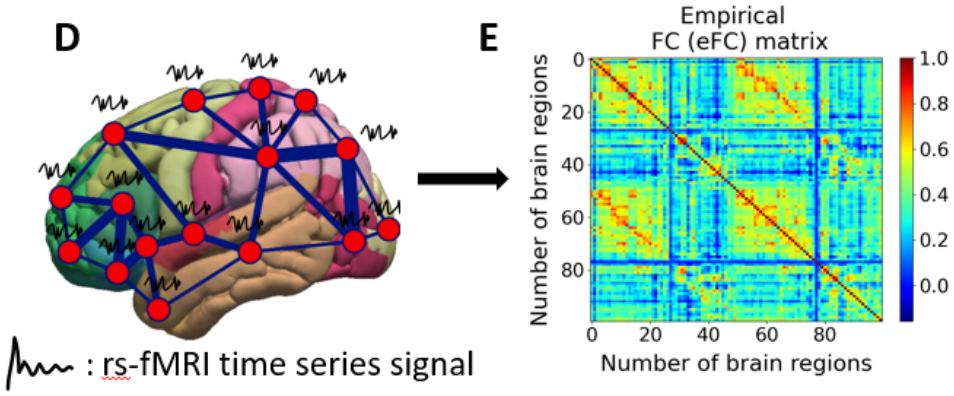

Figure 2.3: Schematic representation of the construction of the eFC matrix of an individual subject for 100 cortical brain regions defined under the S100 parcellation scheme. **D**: The BOLD time series signal recorded for every brain region through resting state functional Magnetic Resonance Imaging (rs-fMRI) (Figure by Justin Domhof, Institute of Neuroscience and Medicine - 7, Forschungszentrum Juelich.) **E**: Example of the resultant eFC matrix constructed by computing the Pearson's correlation coefficient between the time series signal of all possible pairs of 100 cortical brain regions. The color of each pixel in the eFC matrix signifies the value of the correlation coefficient according to the color bar.

The eFC matrix which represents the extent of undirected and synchronised co-activation [8] (in the resting state) between the brain regions was subsequently constructed for individual subject by calculating the Pearson's correlation coefficient between the concatenated time series signals of all possible pairs of N brain regions included in the chosen parcellation scheme, hence, resulting in one NxN dimensional symmetric eFC matrix per subject with diagonal entries equal to 1.
In this way, we calculated the eFC matrix for every subject, under each of the 11 parcellation schemes. Figure 2.3 illustrates the schematic construction of a typical eFC matrix of an individual subject for 100 cortical brain regions defined under the S100 parcellation scheme.

2.5 Whole Brain Dynamical Models

Similar to empirical neuroimaging techniques, the whole brain dynamical models also view the brain as a network of nodes. In this study, the resting state activity of the brain cortex was simulated with two slightly different approaches [8] using two models: The phase oscillator model (also known as the Kuramoto model) and the limit cycle model. In both of these models, the parcellated brain network is treated as an ensemble of coupled phase oscillators, that is, each brain region is analogous to a phase oscillator coupled with other brain regions. For every individual subject, the strength of this coupling was determined from the respective eSC matrix, while the ePL matrix was used to calculate the delay in signal propagation between the nodes of the model network [31]. The mean activity of each of these phase oscillators was subsequently simulated by numerically solving a system of time dependent differential equations corresponding to each oscillator. This resulted in a time series signal corresponding to each of the N nodes (brain regions) that constitute the model network. The difference between the two models, however, is that in the limit cycle model, the amplitude of the simulated time series signal is accounted for, whereas, in the phase oscillator model, it's not [31]. The time signals thus simulated are then used to calculate the sFC matrix for every subject, corresponding to each of the two models, under each of the 11 brain parcellation schemes.

2.5.1 Phase Oscillator Model

Mathematically, the phase oscillator model or the Kuramoto model is represented as:

$$\dot{\theta}_j(t) = 2\pi f_j + \frac{C}{N}\sum_{n=1}^{N}\omega_{jn}\sin(\theta_n(t-\tau_{jn}) - \theta_j(t)) + \eta_j \qquad (2.1)$$
$$j = 1, 2, ..., N$$

where, $\theta_j(t)$ is the time dependent phase corresponding to the jth phase oscillator (brain region) and the time series signal ($x_j(t)$) for the same oscillator is evaluated as $x_j(t) = sin(\theta_j(t))$. N represents the total number of phase oscillators (brain regions) under a given brain parcellation scheme, t is the time (considered in seconds) and η_j represents an independent noise in the system, sampled from the uniform distribution defined from -0.3 to 0.3. The parameters f_j, w_{jn} and τ_{jn} were evaluated for individual subjects from their respective empirical data. f_j is the natural frequency (in Hz) of the uncoupled jth oscillator and was calculated as the frequency of the maximal spectral peak (excluding frequencies below 0.01 Hz and above 0.1 Hz) of the empirical BOLD time series signal of the corresponding brain region. To do this,the empirical BOLD time series signals were transformed to the Fourier space and Welch's method was applied [8].
ω_{jn} is the coupling weight and τ_{jn} (in secs) is the delay in signal propagation between the jth and nth phase oscillator. ω_{jn} was calculated from the eSC matrix as $\omega_{jn} = k_{jn}/ < k_{jn} >$ where k_{jn} is the number of streamlines between jth and nth brain region i.e, the element of the eSC matrix corresponding to the jth row and nth column and $< k_{jn} >$ is the average of the whole NxN dimensional eSC matrix with diagonal equal to 0. Similarly, τ_{jn} was computed from the ePL matrix as $\tau_{jn} = L_{jn}/V$ where L_{jn} is the average length of streamlines between jth and nth brain region as given by the elements of the ePL matrix and V is the average speed with which the signal propagates between the brain regions.
In the calculation performed above, the diagonal entries of both eSC and ePL matrices were equated to 0 to exclude the self connecting streamlines, that is, $w_{jj} = k_{jj} = L_{jj} = 0$ [31] .

We defined two global parameters: global coupling strength C and global or average propagation delay τ (in secs) which essentially scale the extent of individual coupling and signal propagation speed, respectively. The speed V of signal propagation can be expressed in terms of τ as $V =< L_{ij} > /\tau$ where $< L_{ij} >$ denotes the average of the NxN dimensional ePL matrix with 0s on the diagonal. Hence, by varying τ, we can vary V, which in turn alters the individual propagation delay τ_{jn} [31]. Therefore, for every individual subject, C and τ can be varied such that for every combination of (C, τ), a new set of time series signals was generated.

2.5.2 Limit Cycle Model

The limit cycle model is a bit different from the phase oscillator model in the fact that the amplitude of the simulated time series signal is also taken into account in the limit cycle model; it is not restricted to [-1, 1] as is the case with the phase oscillator model.

$$\dot{z}_j(t) = (a_j + i2\pi f_j - |z_j(t)|^2)z_j(t) + \frac{C}{N}\sum_{n=1}^{N}\omega_{jn}(z_n(t-\tau_{jn}) - z_j(t)) + \xi_j \qquad (2.2)$$
$$j = 1, 2, ..., N$$

$z_j(t) = x_j(t) + iy_j(t)$ is a complex number where the real part $x_j(t)$ is the simulated time series signal corresponding to the jth phase oscillator (brain region). The amplitude a_j of the jth oscillator reflects the extent of time fluctuation of the empirical BOLD signal and was, therefore, calculated as the normalised standard deviation of the empirical BOLD time series signal ($std(BOLD_j)$) from the corresponding brain region j. The normalisation was performed in such a way that mean and standard deviation of a_j, thus calculated is equal to 0.5 and 0.4, respectively. In the absence of any coupling between the oscillators, each oscillator in the set up independently rotates with the natural frequency f_j (expressed in Hz) around its origin and spans a radius of $\sqrt{a_j}$. The term ξj represents an independent noise (complex number) sampled from the uniform distribution defined in the interval [-0.3, 0.3] [31]. The parameters f_j, ω_{jn}, τ_{jn}, C and τ carry the same meaning as in the Phase Oscillator model and were also calculated for every individual subject in the same way as explained in section 2.5.1.

In both the models, the differential equations were numerically solved using the Heun method of integration with a fixed time step $\Delta t = 0.06$ secs and each time series signal used to calculate the sFC matrix was 3500 secs long [31]. Subsequently, we constructed the simulated functional connectivity (sFC) matrix for every subject by computing the Pearson's correlation coefficient between the simulated time series signal of all possible pairs of N brain regions included in the selected brain parcellation scheme (similar to the construction of the eFC matrix as illustrated in Figure 2.3). The sFC matrix is, therefore, symmetric and has NxN dimensions with diagonal entries equal to 1. Since each combination of the global parameters (τ, C) resulted in a new batch of time series signals, correlating them, therefore, yielded as many sFC matrices per subject as the total number of combinations of (τ, C) for a given model and a given brain parcellation scheme.

2.6 Model Fitting

Under a selected brain parcellation scheme, the similarity between the sFC matrix and the eFC matrix for each subject was determined by computing the Pearson's correlation coefficient - $corr(sFC,\ eFC)$ between the vectors formed by extracting the upper triangular parts of the corresponding matrices excluding the diagonal [8].

For each of the two models simulated in this study, we used 64 different values of global coupling strength C and 48 different values of global delay τ equally spaced in the interval [0, 0.945] and [0, 94], respectively. Therefore, for a given model and a chosen brain parcellation scheme, each subject has one eFC matrix, and 3072 sFC matrices obtained by 64 x 48 different combinations of the global parameters C and τ, respectively [31]. This, therefore, resulted in 3072 values of $corr(sFC,\ eFC)$ per subject, plotted against the corresponding parameters on a 2D parameter plane. An example of such a parameter plane generated for an individual subject for the phase oscillator model, under the S200 parcellation scheme is shown in Figure 2.4a. The horizontal axis on the plane denotes the global delay τ, the vertical axis denotes the global coupling C and the corresponding $corr(sFC,\ eFC)$ is represented by a color according to the color bar.

Subsequently, a grid search was performed on the parameter plane to extract the best model fit, that is, the maximal coefficient of correlation between the sFC and the eFC matrix. This maximal value is referred to as the goodness-of-fit or $corr(sFC,\ eFC)_{max}$. An example of the goodness-of-fit extracted for an individual subject for the phase oscillator model, under the S200 parcellation scheme is shown as a white circle in Figure 2.4a, where the $corr(sFC,\ eFC)_{max} = 0.48$ and the corresponding optimal parameters are $\tau_{opt} = 0$ and $c_{opt} = 0.12$. The best fit sFC matrix corresponding to these optimal parameters is shown on the left in the Figure 2.4b, along with the respective eFC matrix on the right.
Thus, for each model and for each of the 11 parcellation schemes, the value of $corr(sFC,\ eSC)_{max}$ was extracted in the above mentioned manner independently for all the 272 subjects.

2.7 Statistical Methods

This section briefly introduces the statistical techniques employed for the investigation and quantification of the sex differences in various quantities considered in this project.

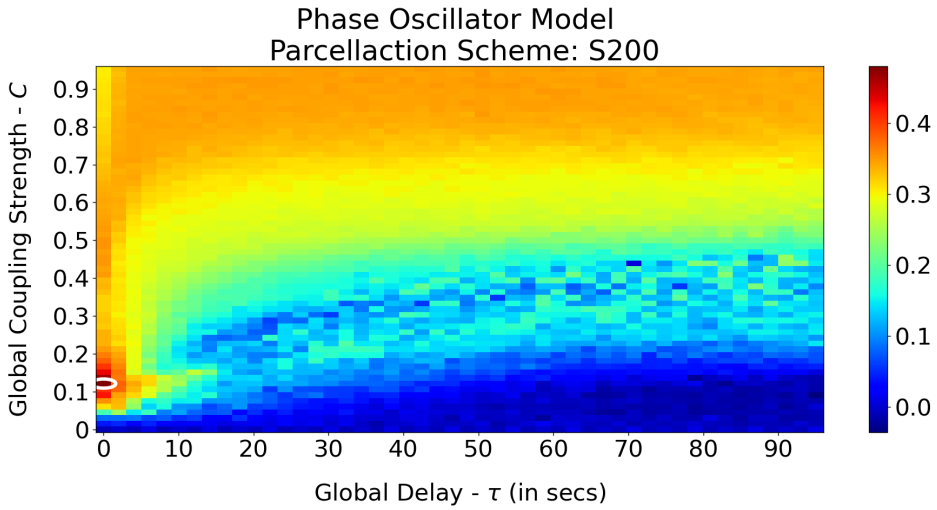

(a)

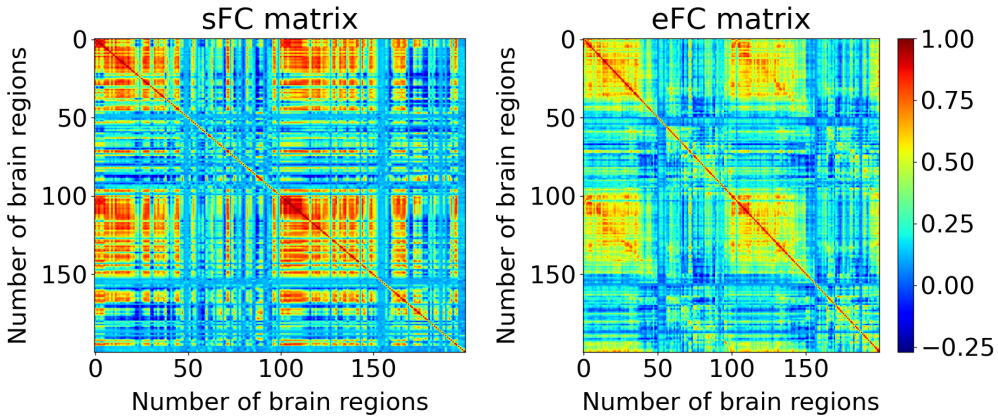

(b)

Figure 2.4: **(a):** Example of the parameter plane of an individual subject for the phase oscillator model under the S200 parcellation scheme; The horizontal and vertical axes represents the global delay τ and global coupling strength C, respectively, whereas, the color of each pixel represents the corresponding value of the $corr(sFC,\ eFC)$ according to the color bar; The white circle indicates the goodness-of-fit or $corr(sFC,\ eFC)_{max} = 0.48$, corresponding to an optimal global delay $\tau_{opt} = 0$ and optimal global coupling strength $C_{opt} = 0.12$. The simulated functional connectivity (sFC) matrix of the same subject corresponding to the aforementioned optimal model parameters is shown on the left in **(b)**, and on the right is the respective empirical functional connectivity (eFC) matrix, both of which are defined for the S200 parcellation scheme.

2.7.1 Fisher's Z Transform

The Pearson's correlation coefficient r varies from a minimum of -1 to a maximum of 1 and its distribution is often highly skewed if the value of r is close to the two extremes. This causes a problem in applying the statistical methods such as hypothesis tests and other general arithmetic operations [14]. Fisher's Z transformation solves this issue by transforming the correlation coefficients from the range (-1, 1) to a range ($-\infty$, $+\infty$) and it also makes the distribution fairly symmetric [14]. The Fisher's Z transformation of r is defined as its inverse hyperbolic tangent i.e. $\tanh^{-1}(r)$ or $arctanh(r)$ whose domain and range vary are the open interval (-1, 1) and ($-\infty$, $+\infty$), respectively. An example of the Fisher's Z transformation is illustrated in Figure 2.5

In this study, all the correlation coefficients were transformed using the Fisher's Z transformation prior to employing them for any arithmetic operations, statistical tests or regression analysis, except for the calculation of $corr(sFC,\ eFC)$ where no Fisher's Z transformation was performed.

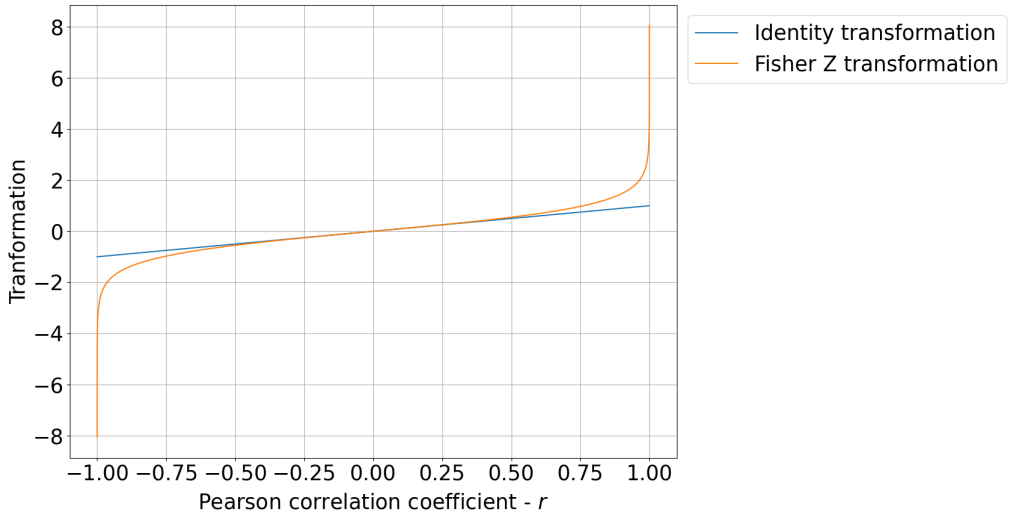

Figure 2.5: Illustration of the Fisher's Z transformation of a Pearson's correlation coefficient r; The plot in blue represents an identity transformation (for comparison), while the one in orange represents the Fisher's Z transformation; This plot is inspired from [14].

2.7.2 Wilcoxon Rank Sum Test

Wilcoxon rank sum test (also called Mann Whitney U test) is a non parametric statistical hypothesis testing method used to test the null hypothesis (H_0) that the two independent groups of samples being compared are drawn from the same population distribution [38]. This test is referred to as a non parametric test or a distribution free test because it does not assume that the underlying distribution of the two groups of samples is of a specific kind, as opposed to the parametric Student's t test, where the groups being compared must be sampled from a normal distribution [18]. For our analysis, even though a Fisher's Z transformation is performed on the correlation coefficients, the resulting distributions are not exactly normal and, therefore, a non parametric test is more appropriate.

The Wilcoxon rank sum test requires that the two groups are independent of each other [24] and the test is based on comparison between the medians of the two groups [38]. There exist two variations of this test: One-sided test and two-sided test. One-sided test is used when the speculation a priori (alternative hypothesis) is that the median of one group is higher than the other. However, if there is no such prior speculation with regards to positive or negative differences, a two sided test is employed, as is the case for our analysis. Therefore, the null (H_0) and alternative (H_A) hypothesis of the two sided Wilcoxon rank sum test are as follows:

- H_0: The two groups of samples being tested, are drawn from the same underlying population distributions [24].
- H_A: The two groups of samples are drawn from two different population distributions [24].

p-Value

A decision on which of the above mentioned hypothesis should be accepted/rejected is made based on the $p-value$ deduced from the test. The $p-value$ or the significance level is a statistical measure defined as the probability of obtaining test results at least as extreme as the results actually observed, under the assumption that the null hypothesis is true . If the $p-value$ is too small, then it implies that observing such results would be very unlikely if the null hypothesis were true [28]. The threshold for $p-value$ (denoted as α) commonly used in statistics is 0.05, therefore, allowing a maximum of 5% error in our judgement. If the $p-value$ deduced from the test is lower than 0.05, it is stated that there is a strong evidence to reject the null hypothesis (H_0) in favour of the alternative hypothesis (H_A). Otherwise, it is concluded that there is not enough evidence to reject the null hypothesis (H_0) [25].

In this study, the Wilcoxon's sum ranks test was implemented through an in-built function `scipy.stats.ranksums(X, Y)` from Python's `Scipy` library [5]. This function accepts the data from two samples (X = males and Y = females) as input and returns two values: a test-statistic which quantifies the difference in the medians of the two samples, and a $p - value$ which is used to decide whether the difference observed is of any statistical significance or not.
The sign of the test-statistic depends on the order of the input for the function. In our case, we used the group of males (X) as the first input and the female group (Y) as the second input. Thus, a positive and statistically significant test-statistic indicates that the group of males has a higher value (of the quantity being tested) than that of the females, whereas a statistically significant negative test-statistic indicates that female group has a higher value than that of the male group. The conclusions of the test, however, are only valid at the group level and not on the individual subject level.

2.7.3 Effect Size Measure (ESM)

In the context of performing a two samples null hypothesis test, the effect size is a statistical measure used to quantify the difference between the two groups of samples being compared. Traditionally, hypothesis tests only focused on the $p - value$ to either accept or reject the null hypothesis. However, the $p - value$ does not reveal any information about the magnitude of difference between the two groups. In the modern approach, the need to report the corresponding effect size measure, along with the $p - value$ is gaining importance [35] [23].

The applicability of an effect size measure depends on certain restrictions on the underlying distributions of the samples being tested. Therefore, the effect size measures for parametric and non parametric tests are different. The commonly used effect size measures for parametric tests are Cohen's D, Hedge's g or Glass's Delta because all of these measures depend on the normality of the distribution and are calculated using the means and standard deviations of the two samples [23]. The effect size measures for non parametric tests are not so well established as those for parametric tests [35]. However, there have been a few suggestions online and in the literature [35], which include the Cliff's Delta which is more robust for skewed distributions [23], Rank Biserial Correlation, "Rosenthal correlation", etc [1].
The "Rosenthal correlation" used in this study is easy to calculate and interpret, as it is evaluated by simple dividing the test-statistic (obtained from the Wilcoxon rank sum test) by the square root of the sum of sample sizes of both the groups (272 in our case) as shown in Equation 2.3 [1]. The effect size measure thus obtained, is denoted as ESM and Table 2.1 shows the interpretation of the magnitude of the ESM (|ESM|) as prescribed by [7].

$$\text{ESM} = \frac{\text{test-statistic}}{\sqrt{Total\ number\ of\ subjects}} \tag{2.3}$$

|ESM|	**Interpretation**
(0.0, 0.2)	Very low
[0.2, 0.4)	Low
[0.4, 0.6)	Moderate
[0.6, 0.8)	Strong
[0.8, 1.0)	Very strong

Table 2.1: Interpretation of the magnitude (absolute value) of the effect size measure (|ESM|) according to [7].

The calculation of ESM was implemented in this study through the in-built function `compute_effsize_from_t()` from Python's `Pingouin` library [36]. This function takes the test-statistic and the total sample size (272 in our case) as input and returns the ESM, whose sign is same as that of the test-statistic. Hence, it not only quantifies the difference, but also indicates which of the two groups has a higher value of the quantity being tested.

It is now clear that the two major takeaways from a two sample statistical hypothesis test are the ESM and the $p - value$ which report the magnitude of the difference between the two groups, and the corresponding statistical significance of the difference, respectively.

2.7.4 False Discovery Rate (FDR) correction

The results of the statistical hypothesis tests are prone to errors where a null hypothesis is rejected even when it is in fact true. These errors are termed as 'false positives' or 'false discoveries' or 'type 1 errors' in the context of statistical hypothesis testing. In situations where multiple hypothesis tests are performed and compared with each other, there is an increased probability of the false positives [13]. False Discovery Rate (FDR) correction is, therefore, a statistical technique to control the rate of the false discoveries (FDR) in statistical hypothesis tests when multiple comparisons are performed. Mathematically, the FDR is defined as the ratio of number of false positives to the total number of times the null hypothesis is rejected. If FP is the number

of false positives and TP is the number of true positives (situations when the null hypothesis should be rejected), the FDR is given as [12],

$$FDR = \frac{FP}{FP + TP} \tag{2.4}$$

In this study, since we conducted the hypothesis testing for 11 different parcellation schemes and compared them with each other (through $p-value$ plots), in order to mitigate the rate of type 1 errors, all the 11 $p-values$ were corrected for the FDR through the inbuilt python function - `statsmodels.stats.multitest.fdrcorrection()` [20].

2.7.5 Multiple Linear Regression

Linear Regression is a statistical technique that uses the least squares method to model the best fit linear relationship of a dependent variable with respect to an independent variable. When there are multiple dependent variables, this technique is referred to as Multiple Linear Regression [21] [17]. For the multivariate regression model to be applicable, the independent variables should not be very highly correlated with each other.

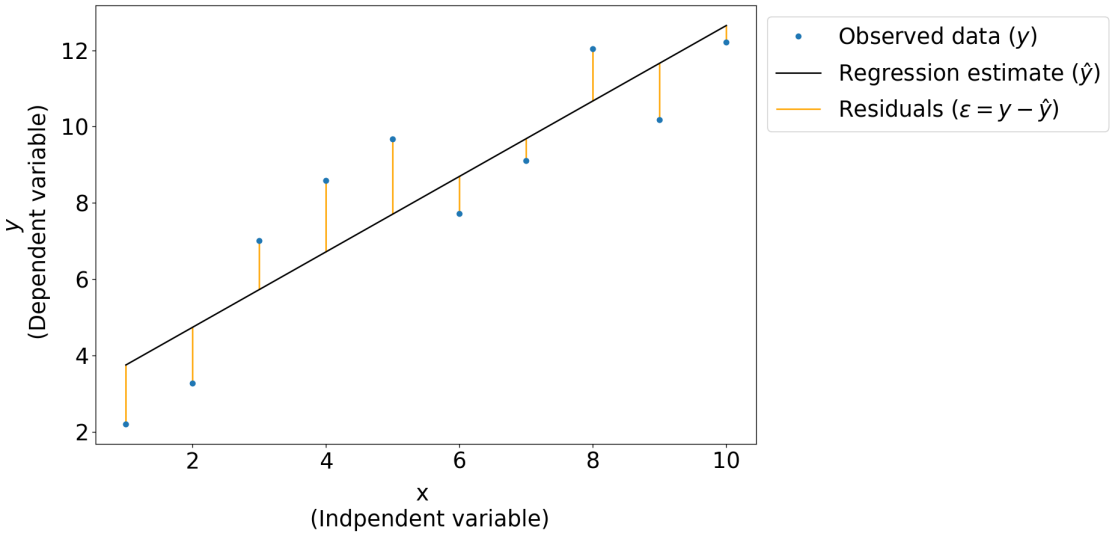

Figure 2.6: Illustration of a univariate linear regression, modelling the relationship between the dependent variable y and the independent variable y. Each dot corresponds to the observed value of the dependent variable and the solid black line represents it regression estimate ($\hat{y}$). The residuals ($\epsilon = y - \hat{y}$) are represented through the orange bars.

Let $x_1,\ x_2\ , x_3, ..., x_n$ be n independent variables and y be the dependent variable which contains the information about the observed data. Then, $\hat{y}$ is a function of the independent variables and represents the estimated value of the dependent variable according to the regression equation [17]:

$$\hat{y} = \alpha_0 + \alpha_1 x_1 + \alpha_2 x_2 + \alpha_3 x_3 + ... + \alpha_n x_n \tag{2.5}$$

where $\alpha_0,\ \alpha_1,\ \alpha_2,\ ....,\ \alpha_n$ are the coefficients estimated through the method of least squares in the regression analysis. Since $\hat{y}$ is the estimated outcome and y is the actual observed outcome, the error in the model is $\epsilon = y\ -\ \hat{y}$, which are also known as the residuals of the regression model. Figure 2.6 illustrates an example of a typical univariate regression model, where eat dot represents the observed data (y), the black solid line corresponds to the line of best fit obtained through linear regression ($\hat{y}$) and the orange bars represent the residuals (ϵ).

Regression of Confounds

In this study, the multiple linear regression is used to regress out the effect of known confounds from the quantities being tested for sex differences. From literature, we have identified two confounds as listed below:

1. Brain size: It has been established in the literature that, from a statistical perspective, the total intracranial volume (TIV measured in mm^3) of the brain, also known as the brain size, is significantly higher in males than it is in females. In this study, the list of brain sizes for all subjects was obtained from the phenotypical data in the HCP repository [15] [22] [33].

2. $corr(eFC,\ eSC)$: Additionally, the empirical structure-function correspondence (or the $corr(eFC,\ eSC)$) is statistically higher in females than in males [16]. To calculate the $corr(eFC,\ eSC)$ for each individual subject, we first transformed the respective eFC matrix using the Fisher's Z transformation (since the elements of the eFC matrix are already correlation coefficients), then vectorised the transformed eFC matrix and the eSC matrix by extracting the corresponding upper triangular parts excluding the diagonal, and finally calculated the Pearson's correlation coefficient between the two resultant vectors.

The validity of stated differences in both the confounding variables was also checked for the data set used in this study (discussed in detail in the subsection 3.1.1). Since the whole brain dynamical models discussed in section 2.5 utilize the empirical information, any possible sex differences in the modelling results could potentially be influenced by the sex differences inherent in the confounds. We, therefore, regressed out the confounds to check if the sex differences still persist in $corr(sFC,\ eFC)_{max}$.

The sex differences in the brain size (TIV) have been established in the literature for a long time now, and there are numerous studies strongly supporting this claim [15] [22] [33]. Hence, as a first step, only the brain size (TIV) was regressed out of $corr(sFC,\ eFC)_{max}$ to investigate if the sex differences are preserved after regression. Mathematically, this process is a uni-variate linear regression model and is represented as:

$$\hat{y} = \alpha_0 + \alpha_1 x_1 \tag{2.6}$$

where x_1 (independent variable) in our case was the brain size (TIV measured in mm^3), $\hat{y}$ is the regression estimated value for the goodness-of-fit and it, therefore, incorporates the effects of brain size. The residuals were calculated by subtracting $\hat{y}$ from the actual goodness-of-fit or $corr(sFC, eFC)_{max}$. Thus, the residuals calculated are free from the effects of brain size and were subsequently retested for sex differences through the Wilcoxon rank sum test.

The second confound - $corr(eFC, eSC)$ has been investigated only recently, and hence, there is not enough evidence in the literature to support the existence of sex differences in $corr(eFC, eSC)$. As a next step in the regression analysis, we regressed out both the known confounds - the brain size (TIV) as well as the $corr(eFC, eSC)$ from $corr(sFC,\ eFC)_{max}$. Since $corr(eFC, eSC)$ and $corr(sFC,\ eFC)_{max}$ are both correlation coefficients, they were transformed through the Fisher's Z transformation prior the regression and the residuals calculated were subsequently back transformed using inverse Fisher's Z transformation. We then re-investigated if the sex differences in the residuals are preserved after regression of both the confounds. Since there are two variables involved, this case of regression represents a multivariate linear regression model and is similar to Equation 2.6, except with an extra term x_2 on the RHS, representing the second confound - $corr(eFC, eSC)$ (Fisher's Z transformed).

$$\hat{y} = \alpha_0 + \alpha_1 x_1 + \alpha_2 x_2 \tag{2.7}$$

Here, $\hat{y}$ is also the regression estimated value for the goodness-of-fit, but it incorporates the effects of both the brain size as well as the empirical structure function correspondence - $corr(eFC, eSC)$. The residuals evaluated in this case are, therefore, free from the effects of both the confounding quantities. Subsequently, the residuals were retested for sex differences through the Wilcoxon rank sum test and the ESM was reported along with its statistical significance ($p - value$).

2.8 'Complexity' Measures

Inspired from all the relevant studies mentioned in the context of 'complexity' of brain data, we also proposed a few quantities calculated from the eFC matrices of individual subjects, as potential 'complexity' measures. They are:

1. Shannon entropy of the eFC matrix - $H(eFC)$.
2. Standard deviation of the eFC matrix - $\sigma(|eFC|)$.
3. Area under the eigen value curve of the eFC matrix - $A(\lambda_{eFC})$.

2.8.1 Shannon Entropy of the eFC Matrix - $H(eFC)$

Although the entropy measures in the literature are mostly studied in the context of time varying signals, the study in reference [19] evaluates the sample entropy of the dynamic functional connectivity (dynamic eFC) matrix rather than that of the fMRI time series signal. The dynamic eFC is calculated by considering the time varying correlations between the signals from individual brain regions across small time windows [19]. Since the eFC matrix for every subject in this study is evaluated just once considering all the time points (concatenated time series signal from 4 different fMRI scans), the eFC matrix is static or time independent. sample entropy (which is relevant to time varying entities) in this case is, therefore, not applicable. Hence, we consider the classical 'Shannon entropy' of the eFC matrix - $H(eFC)$ as a potential complexity measure.

The information theory defines the Shannon entropy of a random variable X, as the average level of uncertainty or the lack of predictability associated with the its possible outcomes $x_1,\ x_2, ...,\ x_N$. If $P(x_i)$ is the probability of occurrence of the outcome x_i, the formula for the Shannon Entropy $H(X)$ is given by [11],

$$H(X) = -\sum_{i}^{N} P(x_i)\ ln(P(x_i)) \tag{2.8}$$

In this project, we considered the functional connectivity between the brain regions as the random variable, and the elements of the eFC matrix as the various possible outcomes of the functional connectivity. The $H(eFC)$ was calculated separately for every individual subject under each parcellation scheme by employing the following steps:

1. Firstly, to simplify the calculation, we vectorised each eFC matrix by extracting its upper triangular part excluding the diagonal.

2. The vector obtained in the previous step was converted into a frequency distribution (array of counts) defined in the interval [-1, 1].

3. Lastly, the Shannon Entropy of the resultant frequency distribution was calculated using the in-built Python function - `scipy.stats.entropy()` and this measure is denoted as $H(eFC)$.

The uncertainty associated with the possible values of functional connectivity adds an element of complexity to the connectome. Accordingly, We speculated that a high value of the $H(eFC)$ corresponds to a more complex eFC matrix.

2.8.2 Standard Deviation of the eFC Matrix - $\sigma(|eFC|)$

Among many, one of the data variables considered in [31] is std[aver(eFC)] which is evaluated by first considering the column-wise averages of the eFC matrix, and then calculating the standard deviation of those column-wise averages. The relationship between the std[aver(eFC)] and the Fit(sFC, eFC) is shown in Figure 2.7, where it is observed that the two quantities are positively correlated and the former can, therefore, explain the latter's variance across subjects within a given parcellation scheme (colored lines) as well as across different parcellation schemes (solid black line) [31].

Inspired from the data variables evaluated in the study [31], we also calculated a property of the eFC matrix, that is, the standard deviation of the set of elements of the matrix. In general, the standard deviation σ of a random variable X measures the spread of its distribution with respect to the mean μ. A narrow distribution has a low value of σ, whereas, a high σ value corresponds to a broad distribution [34]. The formula for $\sigma(X)$ is,

$$\sigma(X) = \sqrt{\frac{\sum_i^N (x_i - \mu)^2}{N}} \tag{2.9}$$

where x_i is the ith data point and N is the total number of data points.
Similar to the calculation of $H(eFC)$, we considered the functional connectivity between the pairs of brain regions as the random variable and the elements of the eFC matrix as its possible outcomes. For every individual subject under each of the 11 parcellation schemes, to calculate the standard deviation of the eFC matrix, we first extracted the upper triangular part of the matrix into a vector, transformed it through the Fisher's Z transformation, and then evaluated standard deviation of the absolute values of the resultant vector and back transformed it through the inverse Fisher's Z transformation. Henceforth, standard deviation of the eFC matrix is denoted as $\sigma(|eFC|)$.

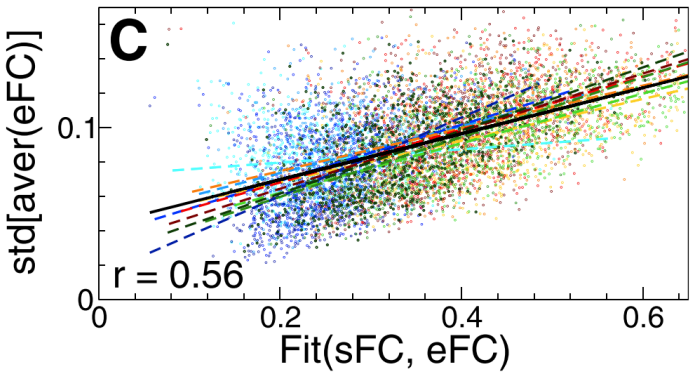

Figure 2.7: Relationship between the std[aver(eFC)] and goodness-of-fit (denoted as Fit(sFC, eFC) in the study) for the phase oscillator model. Each dot in the scatter plot corresponds to an individual subject, and the color represents the various parcellation schemes examined. The solid black line is obtained by considering the collective data from all the subjects under all the parcellation schemes. It, therefore, represents the joint linear regression resulting in a joint correlation coefficient of $r = 0.56$. Figure reproduced from [31].

Since the elements of the eFC matrix represent the extent of synchronised co-activation [8] (synchronicity) between different pairs of brain regions, the standard deviation of the eFC matrix - $\sigma(|eFC|)$, therefore, measures the spread in the synchronicity of the brain regions, with respect to the mean of the matrix. A higher value of $\sigma(|eFC|)$ implies that the elements of the eFC matrix are broadly distributed and are, hence, largely dissimilar to each other. This means that there is a large variation in the extent to which the activities of different pairs of brain regions are synchronised, whereas a low value of $\sigma(|eFC|)$ results from a narrow distribution and in that case, the activities of most of the pairs of brain regions are synchronised to a similar extent. We, therefore, speculated that a higher value of $\sigma(|eFC|)$ corresponds to a more 'complex' eFC matrix.

2.8.3 Area under the Eigen Value Curve of the eFC Matrix - $A(\lambda_{eFC})$

In linear algebra, a matrix M can be treated as linear transformation which when operated on an eigen vector V, results in the same vector, but scaled by a factor λ known as the eigen value of the matrix corresponding to the eigen vector V [10]. Mathematically, the transformation can be expressed as $MV = \lambda V$ and a set of lin-

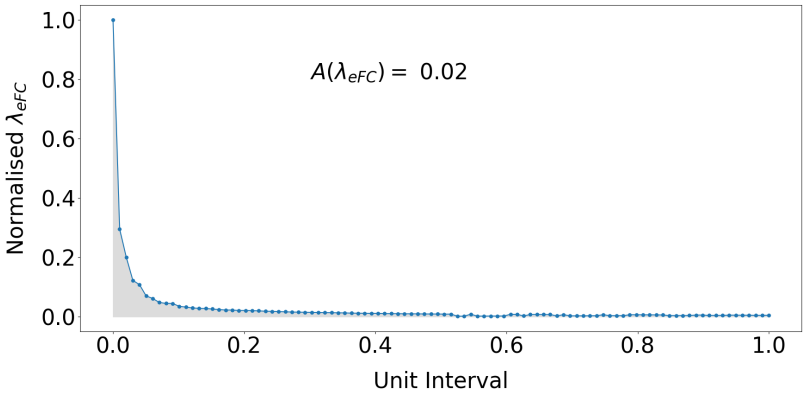

Figure 2.8: Illustration of curve obtained by plotting the normalised eigen values of the eFC matrix (λ_{eFC} shown as dots) against a unit interval [0, 1] for an individual subject under the S100 parcellation scheme. The shaded region represents the area under the curve denoted as $A(\lambda_{eFC})$.

early independent eigen vectors form the eigen basis of the matrix M.

In our project, we considered the eFC matrix of every individual subject under each parcellation scheme, as a linear transformation and evaluated all its eigen values (λ_{eFC}) (without a Fisher Z transformation). Since the dimension of the eFC matrix is NxN, (N is the number of brain parcels (N) under each parcellation scheme) the matrix has N eigen values, of which some may or may not be degenerate. As the eFC matrix is real valued and symmetric, all its eigen values are real, and all the corresponding eigen vectors are mutually orthogonal. The eFC matrix is, therefore, diagonalizable. Thereafter, for every individual subject, we calculated the area ($A(\lambda_{eFC})$) under the curve that was obtained by plotting the normalised eigen values against a unit interval [0, 1]. An example of one such plot for an individual subject under the S100 parcellation scheme is shown in Figure 2.8, where each dot represents a normalised eigen value of the eFC matrix for that subject. The trapezoidal rule used to calculate the $A(\lambda_{eFC})$ was implemented through Python's in-built function `scipy.integrate.trapezoid()`. Since both the vertical and the horizontal were are normalised, the magnitude of $A(\lambda_{eFC})$ directly reflects the shape of the eigen value curve. A steeper curve has a lower $A(\lambda_{eFC})$ compared to that of a more gradually falling curve. In order to understand how the shape of the eigen value curve potentially reveals the 'complexity' of the eFC matrix, let us consider an extreme case where out of N eigen values, only one of them is non zero, while rest are all zero. The value of $A(\lambda_{eFC})$ in this case is minimum. Since the eFC matrix is a diagonal matrix

(D_{eFC}) in its eigen basis, with eigen values on the diagonal, the eFC matrix in its original vector space can be reconstructed as:

$$eFC = PD_{eFC}P^{-1} \tag{2.10}$$

where P is a NxN matrix whose columns are the orthogonal eigen vectors of the eFC matrix. If D_{eFC} has only one non zero diagonal entry, this follows the simplest case of reconstruction as the contribution from the other diagonal entries is zero. Hence, the least value of $A(\lambda_{eFC})$ corresponds to the simplest case. Next, if we consider another extreme where all the eigen values of the eFC matrix are non zero and equal, the value of $A(\lambda_{eFC})$ in this case is maximum. Since the all the diagonal entries in D_{eFC} are non zero and equal, this case indicates the highest complexity as all the eigen values contribute equally in the reconstruction of the eFC matrix to its original vector space. Accordingly, we speculated that a high value of $A(\lambda_{eFC})$ corresponds to a high 'complexity' of the eFC matrix. It is, however, important to note that the physical or neurobiological interpretation $A(\lambda_{eFC})$ is not yet clear and the justification as to why it can be regarded as a potential 'complexity' measure is mathematical.

2.9 Workflow of the Analysis in the Study

A succinct version of the entire methodology followed in the project is illustrated through a flow chart in Figure 2.9, where for every individual subject under a particular choice of brain parcellation scheme, we independently calculated one eSC, ePL and eFC matrix, two sFC matrices and, consequently, two values of $corr(sFC,\ eSC)_{max}$ corresponding to the two models analysed. Hence, for each model, this process resulted in a list containing 272 values of $corr(sFC,\ eFC)_{max}$ for each of the 11 parcellation schemes. Similarly, each of the three 'complexity' measures described in section 2.8 were calculated separately for every subject from their respective eFC matrices, resulting in three such lists (corresponding to three measures) under each parcellation scheme.

For a chosen model and a chosen brain parcellation scheme, the list containing 272 values of $corr(sFC,\ eSC)_{max}$ (Fisher's Z transformed) was subsequently split into two groups - males (128 subjects) and females (144 subjects). Sex differences were then investigated between these two groups (within a parcellation scheme) through the Wilcoxon rank sum test and the magnitude of the difference was quantified in terms of the ESM. Since we calculated the model parameters for each subject using their respective empirical structural and functional data, the sex differences observed in the goodness-of-fit could possibly be influenced by the empirical covariates

with sex, namely the brain size (TIV) and the empirical structure-function correspondence ($corr(eFC,\ eSC)$). We, therefore, regressed out the two confounds from $corr(sFC,\ eSC)_{max}$ through multiple linear regression in order to check if the sex differences in it persist even after eliminating the confounding effects. Despite regression of the confounds, the sex differences in the goodness-of-fit could also be influenced by the sex differences in the 'complexity' of the eFC matrix that was used for model validation. Hence, we quantified three potential 'complexity' measures in terms of the properties of the eFC matrix and the sex differences in each of the three measures were also investigated similar to the procedure followed in case of $corr(sFC,\ eSC)_{max}$. In addition, for a selected model, we also examined the relationship between each of the 'complexity' measures and the confound regressed goodness-of-fit by evaluating the Pearson's correlation coefficient between the two quantities across individual subjects within a selected brain parcellation scheme. We, therefore, assessed if the the variation in the value of $corr(sFC,\ eSC)_{max}$ between males and females despite regression of the confounds, within a selected parcellation scheme, could be accounted for, by the variation in the 'complexity' of the eFC matrix. The process was repeated for all the remaining brain parcellation schemes and for the second model as well.

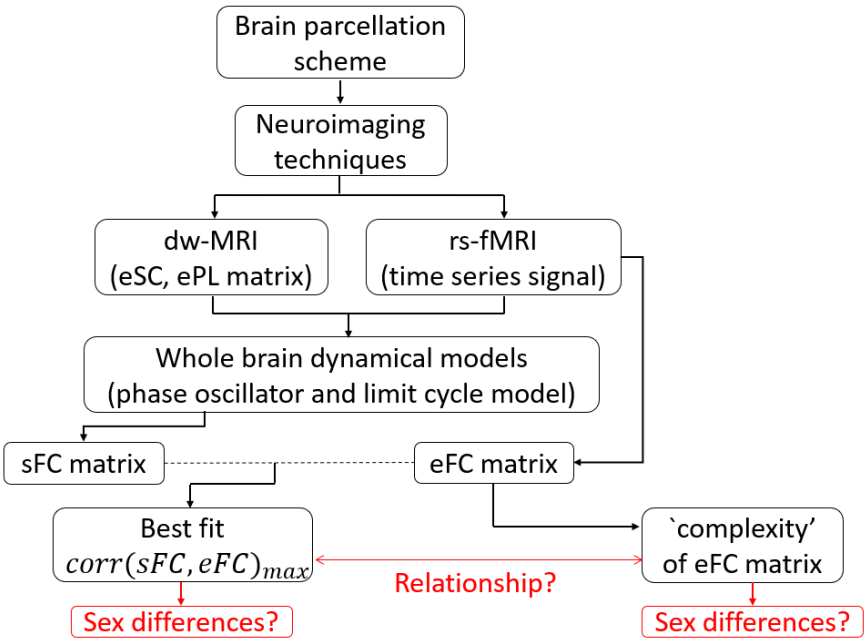

Figure 2.9: Flow chart summarising the general workflow of the analysis performed in the study. The main invesitigations of the project are shown in red. This figure is inspired from [8].

Chapter 3

Preliminary Analysis, Results and Interpretation

In this chapter, we discuss the initial analysis performed with regards to the investigation of sex differences in the goodness-of-fit within each parcellation scheme and for both the models. We also discuss the results obtained and their interpretation, which leads us to the main question of the project. The chapter is concluded with the proposal of an initial hypothesis as a potential reason for the preliminary results observed.

3.1 Sex Differences in $corr(sFC,\ eFC)_{max}$

For a selected brain parcellation scheme and model, the list of 272 values of the goodness-of-fit or the $corr(sFC,\ eFC)_{max}$ as extracted from the parameter plane was separated into two groups consisting of 128 males and 144 females, respectively. Since the two groups are independent and their population distribution is not normal, the Wilcoxon Sum Ranks test was implemented on the Fisher's Z transformed values of $corr(sFC,\ eFC)_{max}$ so as to investigate the differences in its value between the two groups (males and females). Subsequently, the effect size (ESM) was reported along with its statistical significance ($p - value$). This procedure was then repeated for all the remaining 10 parcellation schemes and also for the second model.
The qualitative differences in the value of $corr(sFC,\ eFC)_{max}$ between the group of males (in blue) and the group of females (in red) within each of the 11 parcellation schemes are illustrated in Figure 3.1a and Figure 3.1b for the phase oscillator model and limit cycle model, respectively. It is observed that the box plots of the male group are shifted towards higher values of $corr(sFC,\ eFC)_{max}$, relative to that of the female group, and this observation is consistent across all the parcellation schemes.

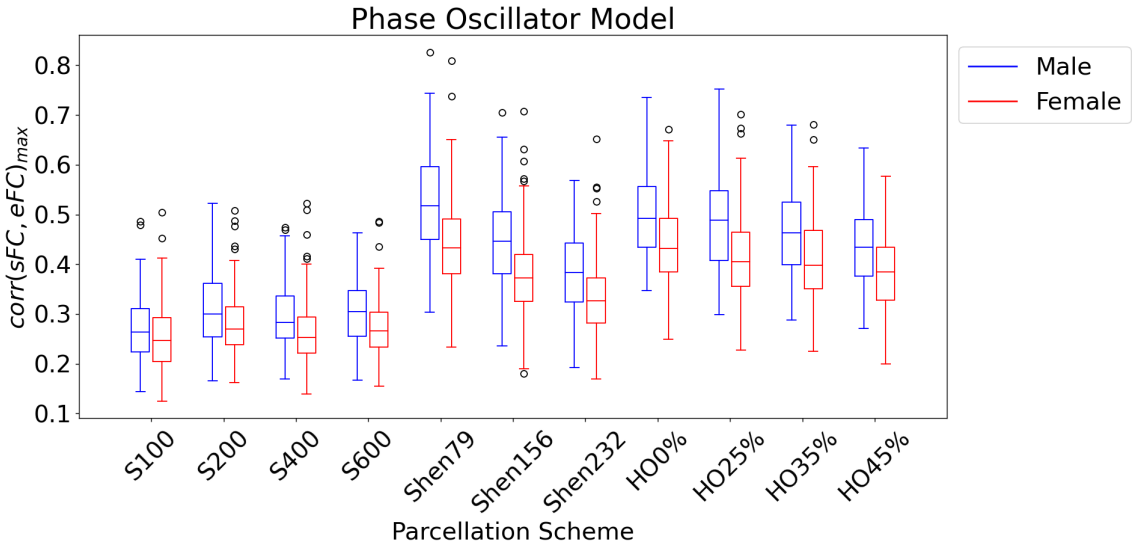

(a)

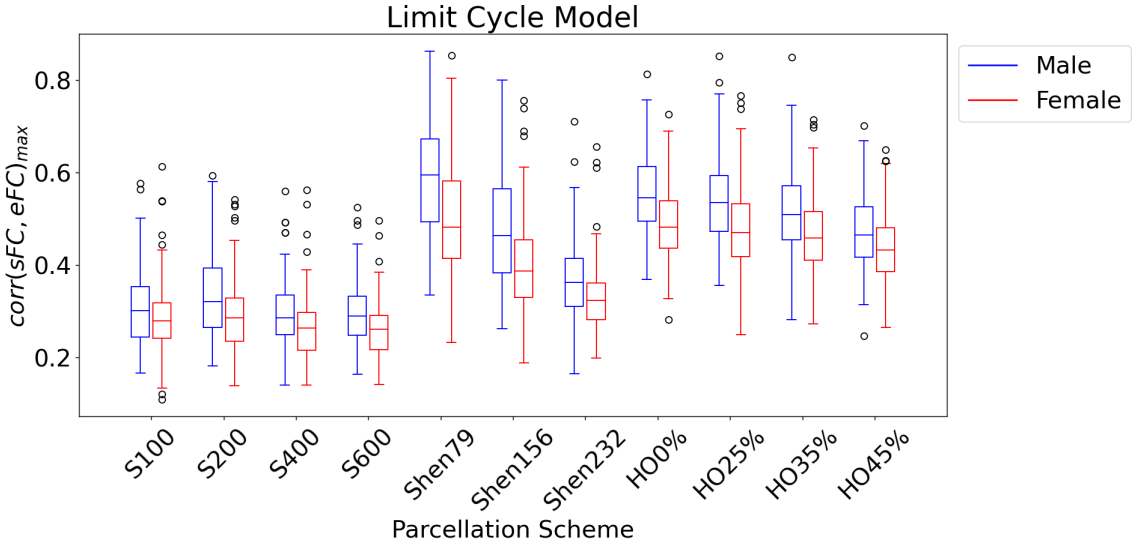

(b)

Figure 3.1: Box plots illustrating the qualitative difference in the value of $corr(sFC,\ eFC)_{max}$ between the male group (blue) and that of the female group (red) within each of the 11 parcellation schemes for **(a)** the phase oscillator model and **(b)** the limit cycle model.

The Wilcoxon rank sum test performed to statistically test and quantify the differences in the value of $corr(sFC,\ eFC)_{max}$ between the groups of males and females within a given parcellation and a given model, resulted in a test-statistic, which was used to quantify the magnitude of the observed difference in terms of the ESM. The test also yielded a $p-value$ which represents the statistical significance of the observed difference. The $p-values$ were all corrected for FDR since the analysis involved multiple comparison of the $p-values$ across different parcellation scheme. The plots for the ESM and the $p-value$ (FDR corrected) are shown in Figure 3.2a for the phase oscillator model and in Figure 3.2b for the limit cycle model, where, for both of the models, the ESM is positive and varies from values close to 0.1 to 0.4, which, therefore, implies that the magnitude of the effect size measure varies from 'very low' to 'low' (according to Table 2.1). The highest and lowest ESM was obtained for the Shen79 and S100 parcellation scheme, respectively, in the case of the phase oscillator model, whereas, the limit cycle model results in the highest and lowest ESM for the HO0% and S100 parcellation, respectively. Besides, we also found that all the $p-values$ (FDR corrected) are below the threshold of $\alpha = 0.05$, indicating that the ESMs calculated for all the parcellation schemes and for both the models are statistically significant. The fact that the ESM is not only positive, but also statistically significant suggests that for both the models, within a selected parcellation scheme, the group of males has a statistically significant higher value of $corr(sFC,\ eFC)_{max}$ than that of the corresponding group of females.

3.1.1 Regression of Confounds

Although we observed sex differences in the value of $corr(sFC,\ eFC)_{max}$ within a parcellation scheme, as mentioned earlier, these differences could potentially be influenced by other covariates with sex like the brain size (TIV) and the empirical structure-function correspondence ($corr(eFC,\ eSC)$) as the models utilize the empirical information in their simulations. We first performed a statistical investigation of the sex differences in both of the aforementioned confounding variables through the Wilcoxon rank sum test.

Brain size (TIV in mm^3)
As already mentioned and shown in Figure 2.1b, there exists a statistically significant difference in the TIV between the male and the female group. On performing the Wilcoxon rank sum test on the TIV data of the two groups, we found that the ESM = 0.65, which is considered 'strong' in magnitude and the $p-value = 10^{-27}$, which is well below the significance threshold of $\alpha = 0.05$. The positive and statistically significant ESM, therefore, indicates that the brain size or the TIV of the considered subjects is

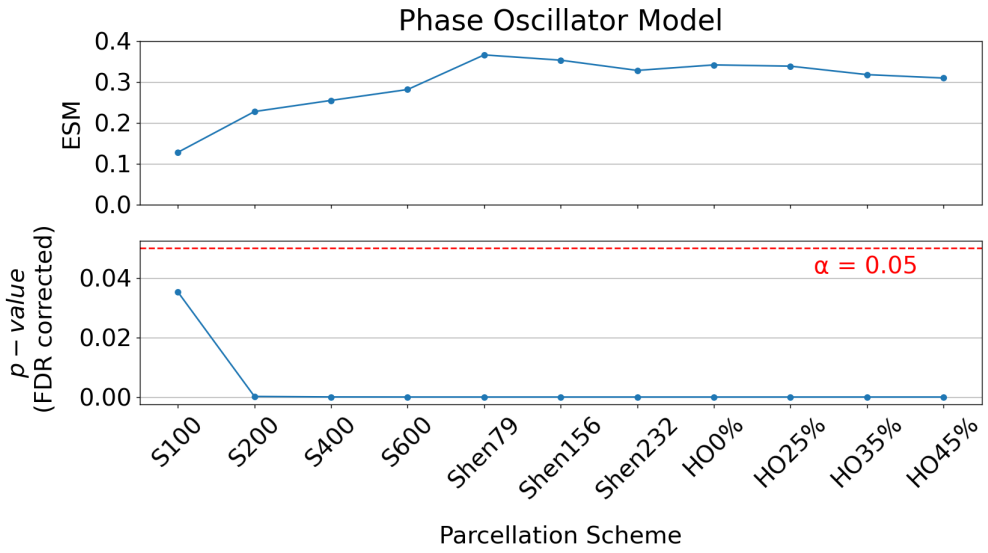

(a)

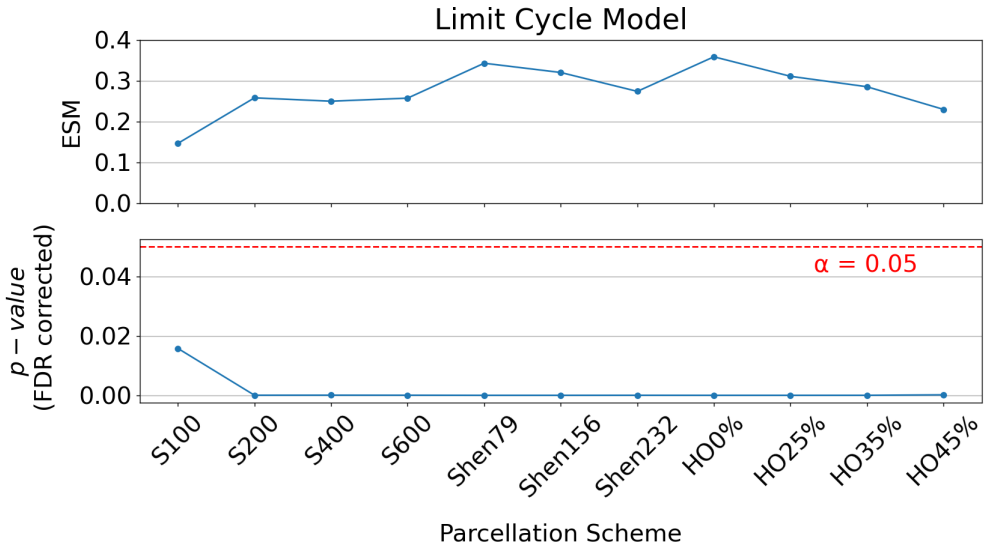

(b)

Figure 3.2: Quantification (ESM) and statistical significance (FDR corrected $p - value$) of the sex differences in $corr(sFC,\ eFC)_{max}$ within each of the 11 parcellation schemes (horizontal axis) for **(a)** the phase oscillator model **(b)** the limit cycle model; The red line indicates a statistical significance threshold of $\alpha = 0.05$.

statistically higher for the group of males and the difference is statistically significant.

Empirical structure-function correspondence - *corr*(*eFC*, *eSC*)
The box plots shown in Figure 3.3a illustrate the qualitative differences in the value of $corr(eFC,\ eSC)$ between the male group and the corresponding female group within each of the 11 parcellation schemes. We observed that the plots for the group of females (in red) are shifted towards higher values relative to the group of males (in blue). On performing the Wilcoxon Sum Ranks test between the group of males and females within each parcellation scheme, we obtained the ESM as well as the $p-value$ as shown in Figure 3.3b. The ESM is negative and varies from values close to -0.1 to -0.3 ('very low' to 'low'). However, the $p-value$ exceeds the threshold of 0.05 for S100 and HO0% parcellation schemes. For the rest of the 9 parcellation schemes, the negative ESM and also statistically significant as the corresponding $p-values$ are below the significance threshold. Therefore, the results indicate that within a selected parcellation scheme (except S100 and HO0%), the empirical structure-function correspondence or the $corr(eFC,\ eSC)$ is statistically higher for the group of females as compared to the group of males and the magnitude of the difference is statistically significant. Our results for both the brain size as well as the $corr(eFC,\ eSC)$ were, therefore, in line with the results in the literature [15] [22] [33] [16].

The model parameters in both the models studied were calculated from the individual empirical data of the subjects. The observed sex difference in the value of $corr(sFC,\ eFC)_{max}$ could, therefore, be potentially influenced by the inherent sex differences in the brain size and the empirical structure function correspondence. Hence, to eliminate the effects of the two confounds, they must be regressed out from the $corr(sFC,\ eFC)_{max}$. It must be noted that the regression analysis was performed for each of the 11 parcellation schemes under each of the two models, independently. As mentioned earlier, since the brain size is a confound with stronger evidence for sex differences in the literature, we initially regressed out only the TIV from the $corr(sFC,\ eFC)_{max}$. As a second step in the regression analysis, both the TIV as well as the $corr(eFC,\ eSC)$ were regressed out from the $corr(sFC,\ eFC)_{max}$. Considering the fact that the $corr(sFC,\ eFC)_{max}$ and $corr(eFC,\ eSC)$ are correlation coefficients, they were transformed through the Fisher's Z transformation, before the regression analysis was performed. The residuals hence calculated were back transformed using inverse Fisher's Z transformation. Subsequently, for a given model, and a selected brain parcellation scheme, the list of 272 residuals was again split into two groups of males and females and re-investigated for sex differences through the Wilcoxon Sum Ranks test. The process was then repeated for the remaining parcellation schemes as well as the second model.

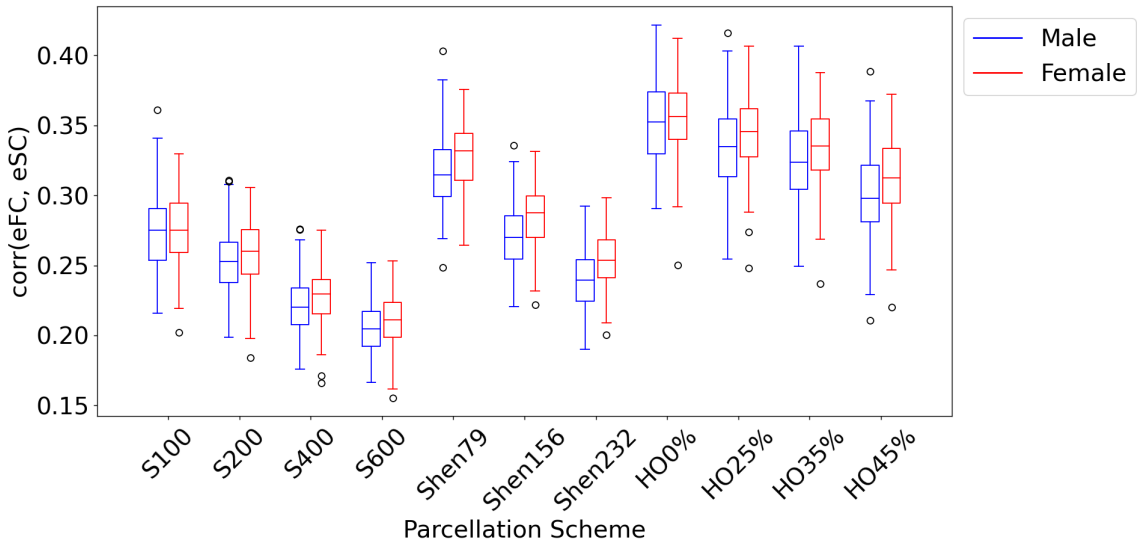

(a)

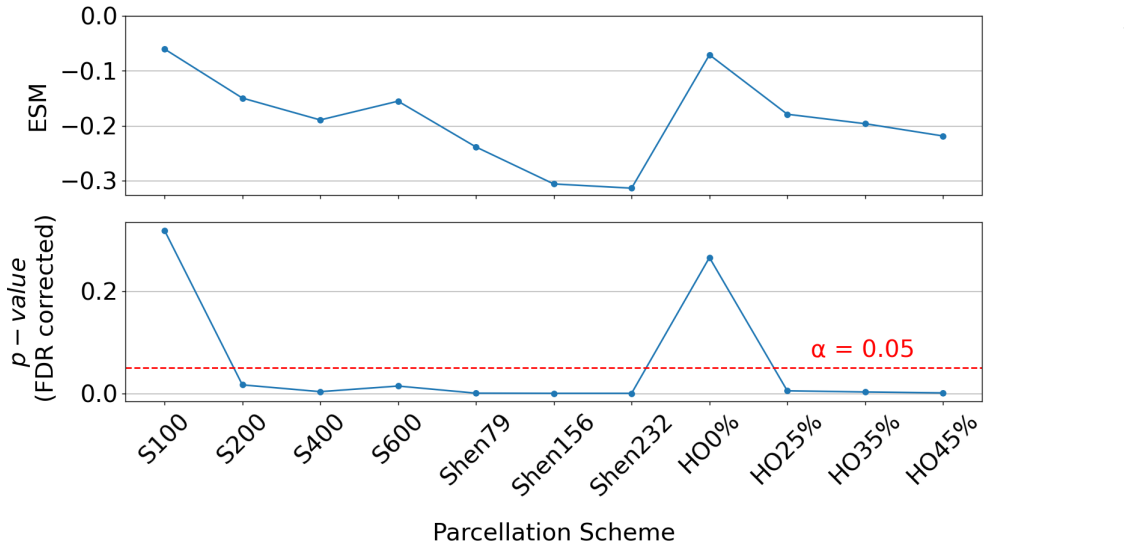

(b)

Figure 3.3: **(a):** Box plots illustrating the qualitative difference in the value of $corr(eFC,\ eSC)$ (empirical structure-function correspondence) between the male group (blue) and that of the female group (red) within each of the 11 parcellation schemes.
(b): Quantification (ESM) and statistical significance (FDR corrected $p - value$) of the sex differences in $corr(eFC,\ eSC)$ within each of the 11 parcellation schemes (horizontal axis). The red line indicates a statistical significance threshold of $\alpha = 0.05$.

Phase Oscillator Model

For the phase oscillator model, Figure 3.4a shows the results after regression of just the TIV and Figure 3.4b shows the results after both the TIV as well as the $corr(eFC,\ eSC)$ have been regressed out from the $corr(sFC,\ eFC)_{max}$. The colored box plots (blue for males and red for females) represent the value of $corr(sFC, eFC)_{max}$ after regression of the confounds and the dashed box plots (grey) represent its value prior to the regression. We observed that after regression of just the TIV (Figure 3.4a), the box plots of $corr(sFC,\ eFC)_{max}$ shift towards lower values relative to the those before regression (in grey) for all the parcellation schemes, whereas, when both the confounds (TIV and $corr(eFC,\ eSC)$) were regressed out, a mixed repositioning of the box plots (with respect to the grey plots) is observed as shown in Figure 3.4b. However, the relative shift between the box plot of the males and females within a parcellation scheme, remains intact in both the cases of regression analysis, with the box plot corresponding to the male group shifted towards higher values of $corr(sFC,\ eFC)_{max}$ than that of the corresponding female group.

We retested for the statistical significance and the magnitude of the sex differences in $corr(sFC,\ eFC)_{max}$ through the Wilcoxon rank sum test, for each case of regression and the results for the phase oscillator model are shown in Figure 3.6a. The plot in blue corresponds to the results before regression of the confounds (for comparison) and the plot in orange corresponds to the results after regression of only the TIV , where we observe that the ESM remains positive, but decreases in magnitude and the $p-value$ exceeds the threshold of $\alpha = 0.05$) for the S100 parcellation. The green plot corresponds to the results after both the TIV and the $corr(eFC,\ eSC)$ have been regressed out, and in this case as well, the ESM is positive, but further decreases in magnitude and the $p - value$ also surpasses the threshold of 0.05 for the S100 parcellation. The positive and statistically significant value of ESM, therefore, implies that within each of the parcellation schemes except S100, the group of males has a statistically significant higher value of the $corr(sFC,\ eFC)_{max}$ than the corresponding group of females, notwithstanding the regression of one or both the confounds.

Limit Cycle Model

Similar to the results for the phase oscillator model, even in case of the limit cycle model, the box plots for both males and females, for all the parcellation schemes reposition themselves towards lower values of $corr(sFC,\ eFC)_{max}$ after regression of the TIV alone as shown in Figure 3.5a. Moreover, when both the TIV as well as the $corr(eFC,\ eSC)$ were regressed out, we observed a mixed repositioning of the box plots relative to the ones before regression (shown in grey) as illustrated in Figure 3.5b. However, the box plot for group of males remains shifted towards higher values of $corr(sFC,\ eFC)_{max}$ relative to that of the group of females within a given

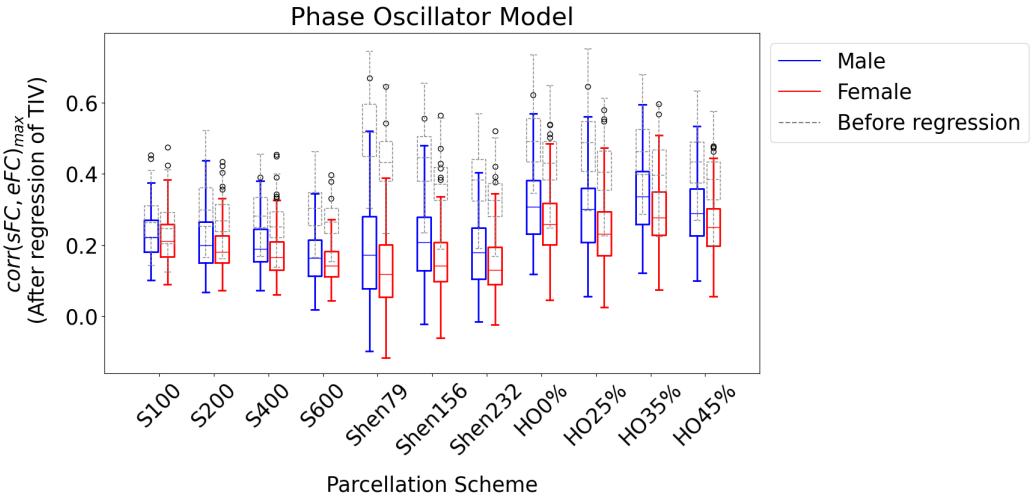

(a)

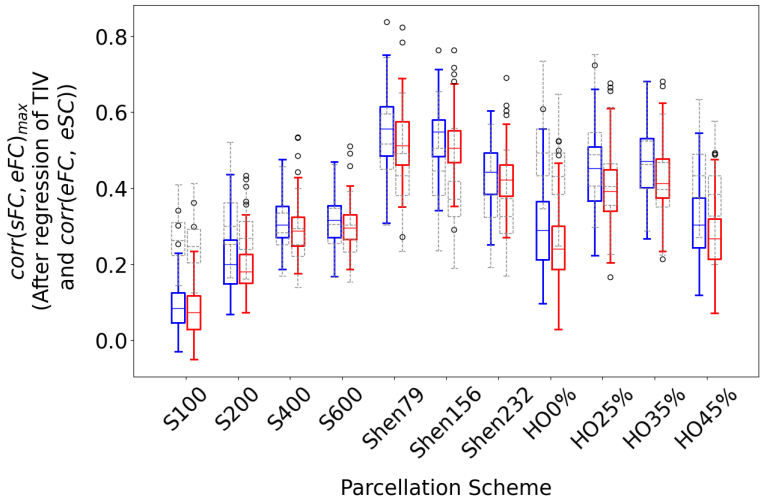

(b)

Figure 3.4: Box plots illustrating the qualitative difference in the value of $corr(sFC,\ eFC)_{max}$ between the male group (blue) and that of the female group (red) within each of the 11 parcellation schemes for the phase oscillator model **(a)** after regression of the TIV and **(b)** after regression of the TIV and $corr(eFC,\ eSC)$.

parcellation scheme, despite regression of one or both the confounds.
In order to statistically test and quantify the observed sex differences in the value of $corr(sFC,\ eFC)_{max}$ for the limit cycle model, after regression of the confounds, we performed the Wilcoxon rank sum test between the group of males and females within each of the 11 parcellation schemes. Figure 3.6b shows the plots for the ESM and $p - value$ for all the parcellation schemes, before regression (in blue), after regression of just the TIV (in orange) and after regression of the TIV as well as the $corr(eFC,\ eSC)$ (in green). For the case where only the TIV was regressed out, we found that the ESM is still positive, but its magnitude reduces relative to the case before regressing of the confounds. Moreover, the ESM for all the parcellation schemes except S100 is rendered statistically insignificant as the corresponding $p - value$ exceeds the threshold of $\alpha = 0.05$.
For the case where both the confounds have been regressed out, the ESM remains positive, but further decreases in magnitude and the $p - value$ increases beyond the threshold of 0.05 for three parcellation schemes that are S100, S600 and Shen232, rendering the respective ESMs statistically insignificant. The results for the limit cycle model, therefore imply that from a statistical perspective, the group of males has a significantly higher value $corr(sFC,\ eFC)_{max}$ relative to the corresponding group of females within all parcellation schemes except S100 for the case where only the TIV was regressed out, and for all parcellation schemes except S100, S600 and Shen232 for the case where both the confounds were regressed out.

Combining the observations from the analysis performed for both the models, the preliminary results can, therefore, be summarised as: The value of $corr(sFC,\ eFC)_{max}$ before the regression of the confounds, is observed to have a statistically significant higher value for the male group as compared to that of the female group, within all the 11 parcellation schemes considered, under both the phase oscillator model as well as the limit cycle model. Nevertheless, regression of the brain size (or TIV) alone, renders the sex difference statistically insignificant for the S100 parcellation, in case of both the models studied. After regression of both the confounds i.e. the brain size (TIV) and the empirical structure-function correspondence ($corr(eFC,\ eSC)$), we observed that the sex differences between the two groups within a parcellation scheme, are statistically significant, with the group of males having a statistically higher value relative to the corresponding group of females for all the parcellation schemes except S100 for the phase oscillator model and S100, S600 and Shen 232 for the limit cycle model. Therefore, for the phase oscillator model, 10 parcellation schemes (i.e. excluding S100) and for the limit cycle model, 8 parcellation schemes (i.e. excluding S100, S600 and Shen232) were considered to be of interest with regards to the presence of sex differences in the confound regressed goodness-of-fit.

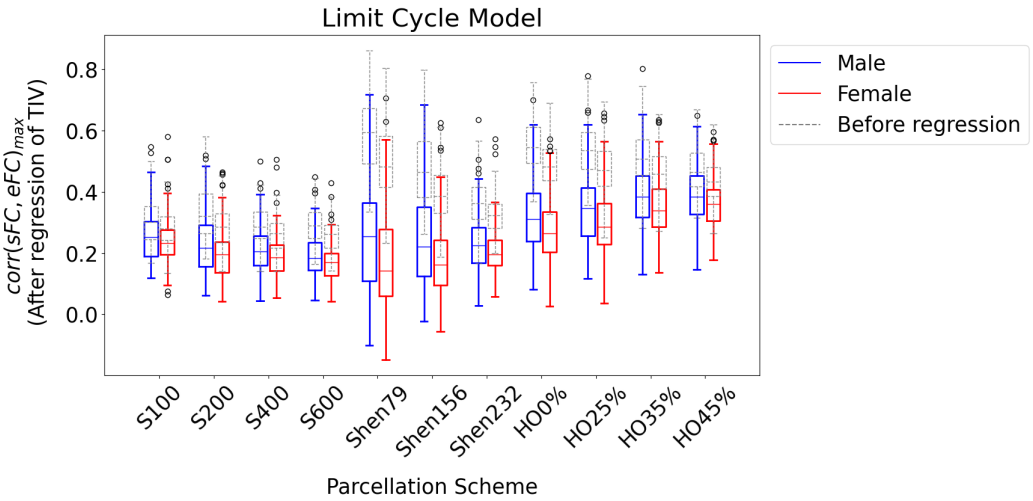

(a)

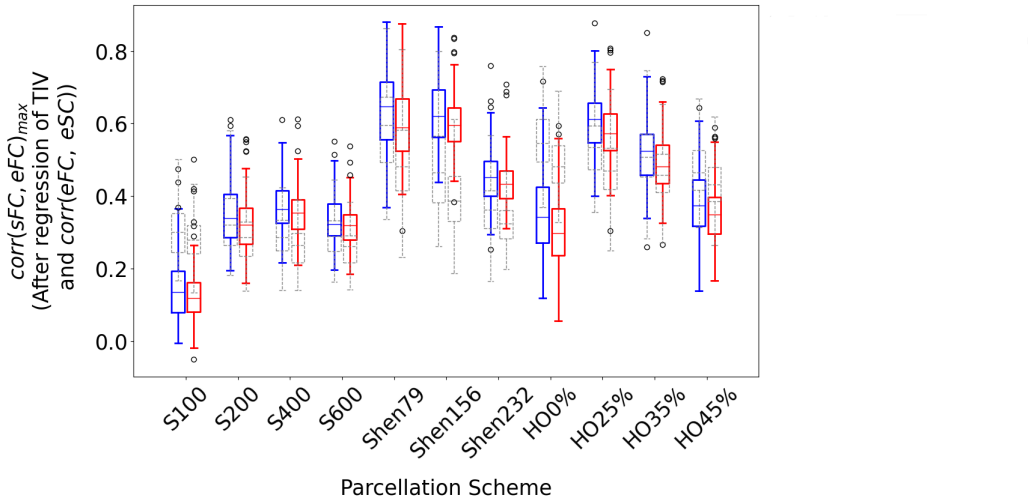

(b)

Figure 3.5: Box plots illustrating the qualitative difference in the value of $corr(sFC,\ eFC)_{max}$ between the male group (blue) and that of the female group (red) within each of the 11 parcellation schemes for the limit cycle model **(a)** after regression of the TIV and **(b)** after regression of the TIV and $corr(eFC,\ eSC)$.

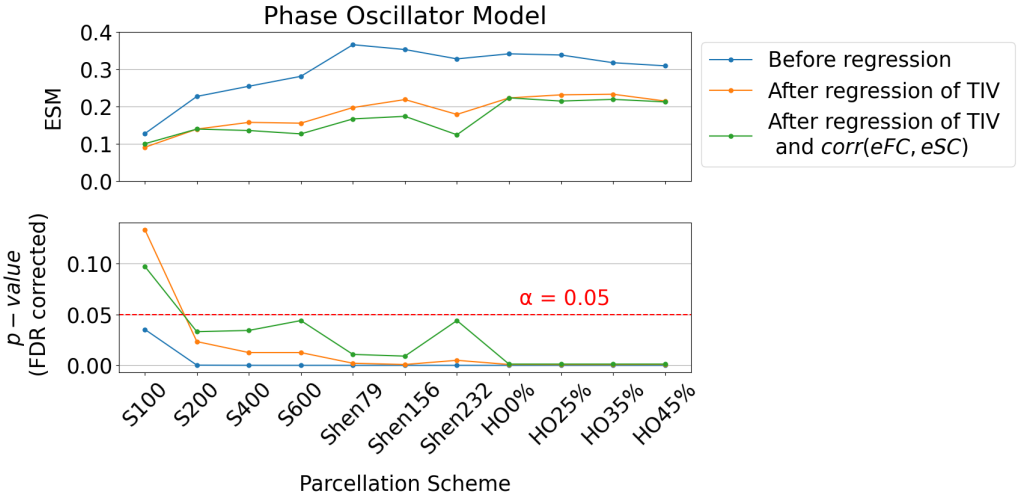

(a)

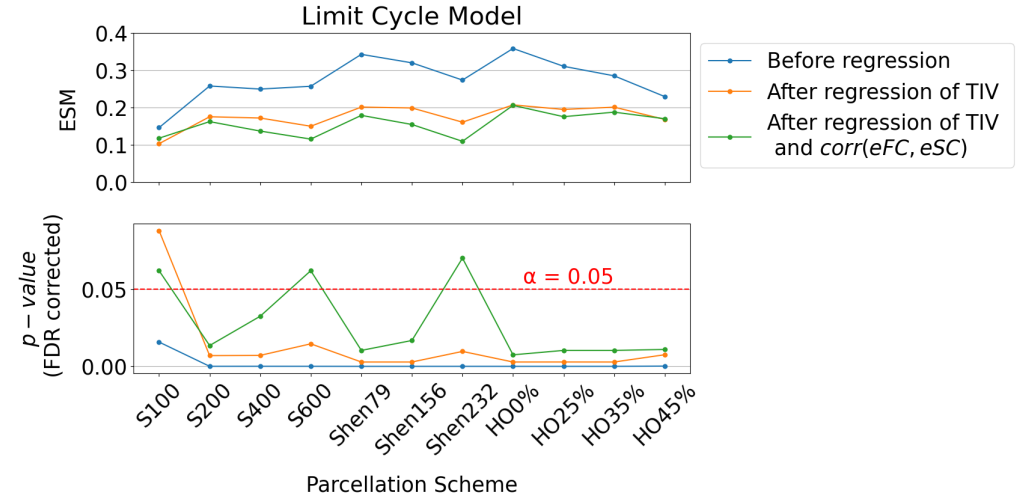

(b)

Figure 3.6: Quantification (ESM) and statistical significance (FDR corrected $p - value$) of the sex differences in $corr(sFC,\ eFC)_{max}$ within each of the 11 parcellation schemes (horizontal axis) for **(a)** the phase oscillator model and **(b)** the limit cycle model, before regression of the confounds (in blue), after regression of the TIV (in orange) and after regression of both the TIV and $corr(eFC,\ eSC)$ (in green); The red line indicates a statistical significance threshold of $\alpha = 0.05$.

3.2 Main Question of the Project

The initial question of this study was whether there exist any sex differences in $corr(sFC,\ eFC)_{max}$. Through the preliminary analysis, we observed that for a chosen parcellation scheme and a chosen whole brain dynamical model, there are indeed sex differences in $corr(sFC,\ eFC)_{max}$. The fact that these differences persist for most parcellation schemes under both the models analysed, despite regressing out the possible influences of the confounds, indicates that the goodness-of-fit inherently contains statistically significant sex differences independent of the influence from the sex differences in the brain size and empirical structure-function correspondence. Based on the preliminary results obtained in section section 3.1, the main question of the project is, therefore, as follows:

For a selected whole brain dynamical model, within a selected brain parcellation scheme of interest, why does the group of males have a statistically significant higher value of the goodness-of-fit ($\boldsymbol{corr(sFC,\ eFC)_{max}}$) as compared to that of the group of females, even after regression of the possible confounds?

3.3 Our Hypothesis

One possible explanation for the relatively higher value of the goodness-of-fit for the group of males with respect to the group of females, could be the influence of the sex differences in the 'complexity' of the eFC matrix since it is used to validate the model. For the case of females, the model may not be able to capture the 'complex' nature of the eFC matrix and hence results in a sFC matrix that fits poorly to the eFC matrix, as compared to that of the males. Our hypothesis was, therefore, as follows:

The higher the 'complexity' of the eFC matrix, the lower is the value of the goodness-of-fit ($\boldsymbol{corr(sFC,\ eFC)_{max}}$). Hence, statistically, the group of females has a more 'complex' eFC matrix as compared to that of the group of males, within a selected brain parcellation scheme.

As per this hypothesis, since the goodness-of-fit is lower for the group of females, we expect that the 'complexity' measures calculated in section 2.8 have a statistically significant higher value for group of females as compared to that of the group of males and that the measures negatively correlate with the confound regressed goodness-of-fit within a selected parcellation scheme of interest (for both the models).

Chapter 4

'Complexity' Analysis and Results

In this chapter, we show the results of the investigation of the sex differences in each of the three measures of 'complexity' and also their relationship with the confound regressed goodness-of-fit within a parcellation scheme and for both the models.

4.1 Shannon Entropy of the eFC Matrix - $H(eFC)$

4.1.1 Sex Differences in $H(eFC)$

Under each of the 11 parcellation schemes, the $H(eFC)$ was calculated for every individual subject (272 in total) and this list was then split into two groups of males (128) and females (144) for the investigation of sex differences in the value $H(eFC)$.

The box plots illustrating the qualitative differences in the value of $H(eFC)$ between the group of males and the corresponding group of females within each of the 11 parcellation schemes for the case before regression of confounds and for the case where only the TIV was regressed out are included in section 7.1 of the Appendix (Figure 7.1 and Figure 7.2, respectively) and the box plots corresponding to the case where both the TIV as well as $corr(eFC,\ eSC)$) were regressed out, are shown as colored plots in Figure 4.1, where the grey plots correspond to the case before regression (for comparison). The observations in all the above three cases are as follows:

1. Before the regression of any confounds, the box plots of the group of males are shifted towards higher values of $H(eFC)$ relative to those of the corresponding group of females within each of the 11 parcellation schemes except S100, where the shift is in the opposite direction (Figure 7.1 - Appendix).

2. After we regressed out only the TIV, we observe a downward repositioning of all the box plots across all the parcellations schemes except S100. However, the

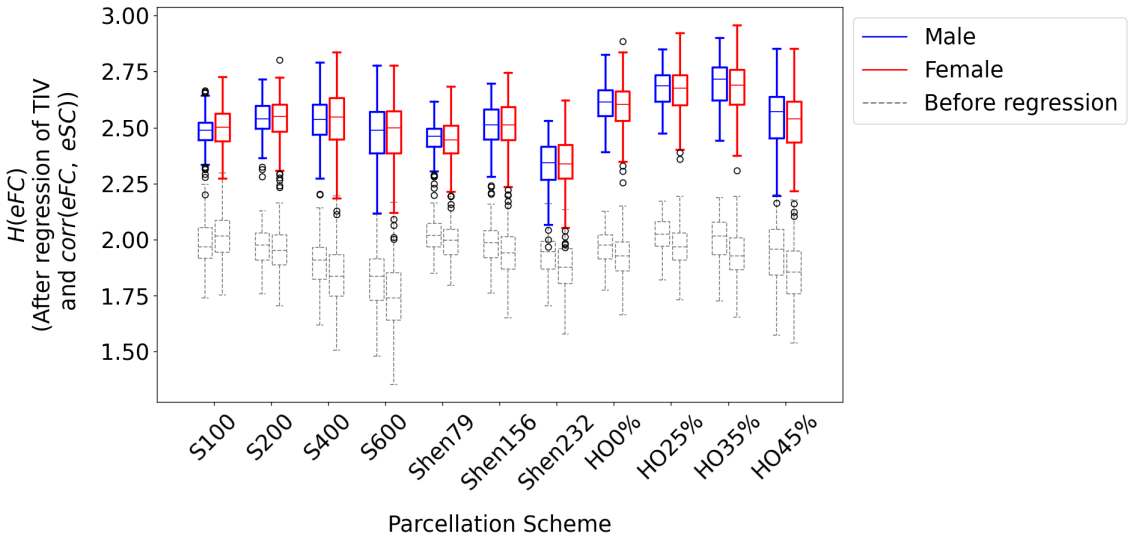

Figure 4.1: Box plots illustrating the qualitative difference in the value of $H(eFC)$ between the male group (blue) and that of the female group (red) within each of the 11 parcellation schemes. The plots in grey correspond to the value of $H(eFC)$ before regression of the confounds and the colored plots represent its value after regression of both the TIV and $corr(eFC,\ eSC)$

direction of the relative shift between the box plots of the male group and the female group within a given parcellation scheme remains same as the case before regression, but with a reduced gap between their respective medians (Figure 7.2 - Appendix).

3. When both the TIV and $corr(eFC,\ eSC)$ are regressed out from $H(eFC)$ (Figure 4.1), it is observed that the box plots across all the parcellation schemes reposition upwards (colored plots) relative to those before regression (in grey). However, within a selected parcellation scheme, the box plots of the group of males remain shifted above those of the corresponding group of females, but the gap between their respective medians further reduces.

The qualitative differences observed through the box plots were subsequently quantified through the Wilcoxon rank sum test between the group of males and females within each of the 11 parcellation schemes. The test yielded a $p - value$ (statistical significance) and a test-statistic which was used to calculate the ESM for the corresponding parcellation scheme.

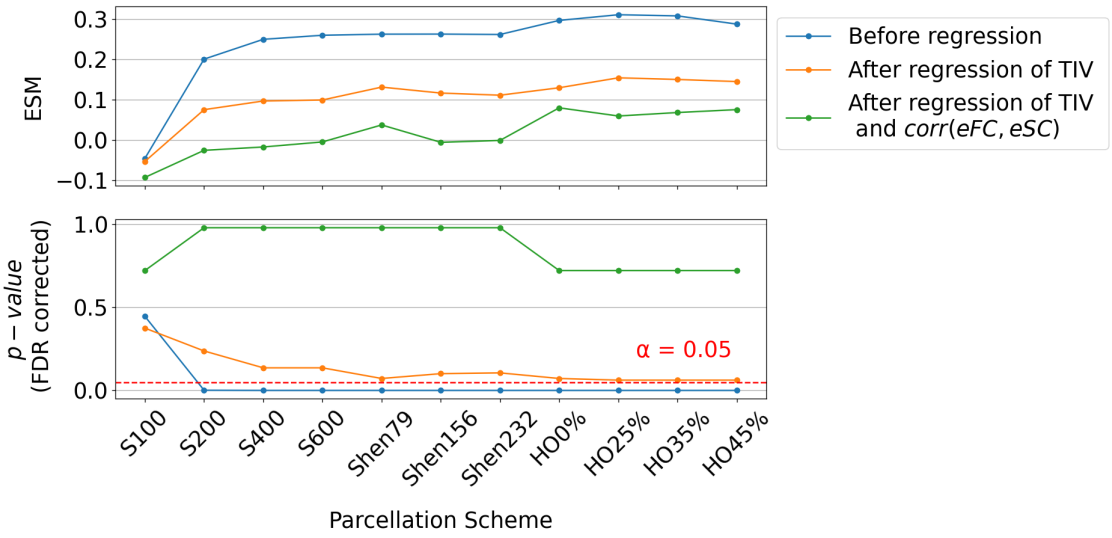

Figure 4.2: Quantification (ESM) and statistical significance (FDR corrected $p-value$ of the sex differences in $H(eFC)$ within each of the 11 parcellation schemes before regression of confounds (in blue), after regression of the TIV (in orange) and after regression of both the TIV and $corr(eFC,\ eSC)$ (in green); The red line indicates a statistical significance threshold of $\alpha = 0.05$.

The results of the test are illustrated in Figure 4.2 for the case before regression of the confounds (in blue), after the regression of just the TIV (in orange) and after regression of both the TIV and $corr(eFC,\ eSC)$) (in green). In all the three cases, we observed that the ESM for every parcellation scheme except S100 is positive. However, it reduces in magnitude after each confound is regressed out. On the other hand, the $p-value$ for each of the parcellation schemes excluding S100, is below the significance threshold of 0.05 only in the case where no confounds are regressed out. Regressing of confounds causes the increase of the $p-value$ beyond the threshold. This implies that the ESM quantifying the sex differences in the value of $H(eFC)$ with each parcellation scheme is statistically significant (except S100) only before regression of the confounds. Consequently, it can in turn be concluded that within each of the parcellation schemes except S100, the group of males has a statistically significant higher value of $H(eFC)$ than the corresponding group of females only when the confounds are not regressed out. Therefore, for all the further analysis on Shannon Entropy of the eFC matrix, we excluded the S100 parcellation scheme and also considered $H(eFC)$ without regressing out the confounds.

Parcellation Scheme	Phase Oscillator Model		Limit Cycle Model	
	r	$p-value$ (FDR corrected)	r	$p-value$ (FDR corrected)
S200	0.13	0.03	0.20	10^{-4}
S400	0.16	10^{-3}	0.26	10^{-5}
S600	0.24	10^{-5}	-	-
Shen79	0.36	10^{-9}	0.39	10^{-11}
Shen156	0.31	10^{-7}	0.38	10^{-11}
Shen232	0.30	10^{-7}	-	-
HO0%	0.29	10^{-6}	0.33	10^{-8}
HO25%	0.21	10^{-4}	0.25	10^{-5}
HO35%	0.28	10^{-6}	0.30	10^{-7}
HO45%	0.33	10^{-8}	0.35	10^{-9}

Table 4.1: Pearson's correlation coefficient r between $H(eFC)$ (without regression of any confounds) and $corr(sFC,\ eFC)_{max}$ (after regression of both the TIV and $corr(eFC,\ eSC)$) and its statistical significance (FDR corrected $p-value$) for the phase oscillator model and the limit cycle model under each of the 11 parcellation schemes.

4.1.2 Relationship of $H(eFC)$ with $corr(sFC,\ eFC)_{max}$

For each of the two models analysed, the relationship between the $H(eFC)$ (without regression of any confounds) and the $corr(sFC,\ eFC)_{max}$ (with both the confound regressed out) was examined within each of the 10 parcellation schemes of interest (excluding S100) for phase oscillator model and 8 parcellation schemes of interest for the limit cycle model (excluding S100, S600 and Shen232). The other parcellation schemes were excluded because within them, the sex differences in the goodness-of-fit do not survive after regression of both the confounds. Therefore, within a selected parcellation scheme of interest, the relationship was examined by evaluating the Pearson's correlation coefficient r between the two quantities. We found that for both the models, the values of r are positive and vary from values close to 0.1 to 0.3. Besides, they are also statistically significant as the corresponding $p-values$ (FDR corrected) are well below the significance threshold of 0.05 as shown in Table 4.1.

For both the models, the highest and lowest statistically significant values of r are obtained for the Shen79 and the S200 parcellation scheme, respectively. The relationship for the Shen79 parcellation is illustrated in Figure 4.3a for the phase oscillator model where the value of r is 0.36 and it is statistically significant as the corresponding $p - value << 0.05$. Likewise, Figure 4.3b illustrates the relationship for the limit cycle model under the Shen79 parcellation scheme with a statistically significant value of $r = 0.39$. The plots for all the remaining parcellation schemes of interest are included in subsection 7.1.1 of the Appendix.

Since we observed a positive correlation, we next examined whether altering the $H(eFC)$ affects the $corr(sFC\ eFC)_{max}$ for a given parcellation scheme and we selected the S200 parcellation scheme for this analysis. One of the ways to alter the $H(eFC)$ for every individual subject is the thresholding procedure (described in subsection 4.1.3). In addition, for the same parcellation scheme, the phase oscillator model was re-simulated for every subject in order to obtain the new goodness-of-fit that corresponds to best fit between the sFC matrix and the thresholded eFC matrix. Thereafter, the relationship between the altered $H(eFC)$ and the re-simulated goodness-of-fit was re-investigated across varying thresholds.

4.1.3 Thresholding of the eFC Matrix

In the thresholding process, the elements of the eFC matrix that have a magnitude (absolute value) below a chosen threshold value, were set to zero. The chosen threshold values were: {0 (no threshold), 0.1, 0.2, 0.3, 0.4, 0.5, 0.6, 0.7}. The values 0.8 and 0.9 were not considered since most of the elements of the eFC matrix become zero at those values of the threshold. The resulting eFC matrix that is thresholded at a particular value of the threshold is denoted as eFC_{th}.

For this process, we considered only the S200 parcellation scheme to simplify the analysis. Once all the eFC matrices were thresholded, the Shannon entropy was recalculated for the eFC matrices of the individual subjects at each threshold and, therefore, denoted as $H(eFC_{th})$. On plotting the values of $H(eFC_{th})$ across varying thresholds, we observed that it monotonically decreases with increasing threshold. This is evident from the box plots in Figure 4.4a, where the plots are observed to shift towards lower values of $H(eFC_{th})$ as the value of threshold is increased. Additionally, we also observe that for a given value of threshold, the box plot of the male group is shifted towards higher values of $H(eFC_{th})$ relative to that of the corresponding female group. This means that although the $H(eFC_{th})$ for individual subject decreases with increasing thresholds, the relative difference in its value between the male group and the corresponding female group remains intact and in the same di-

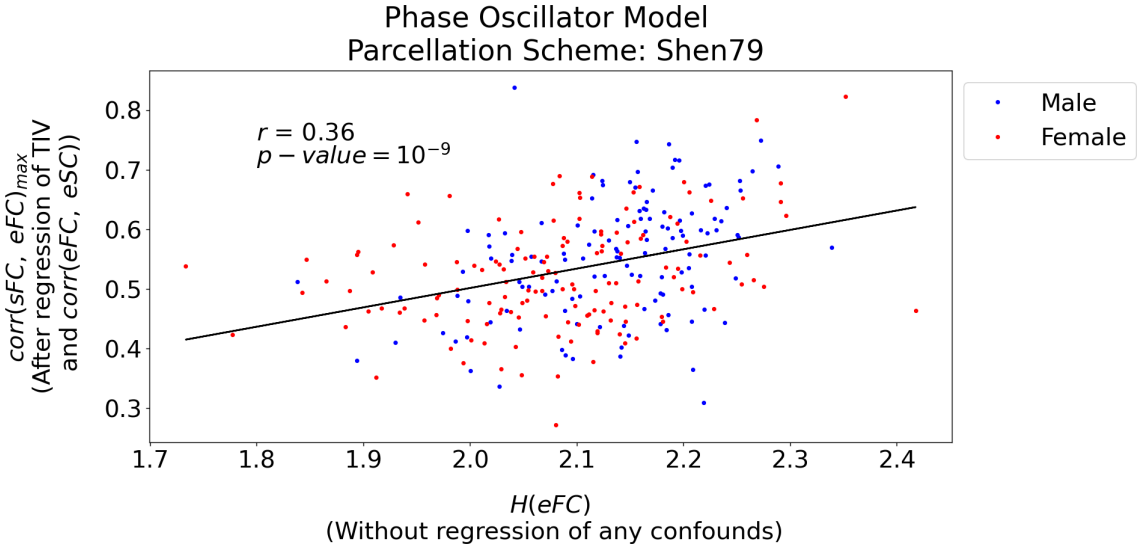

(a)

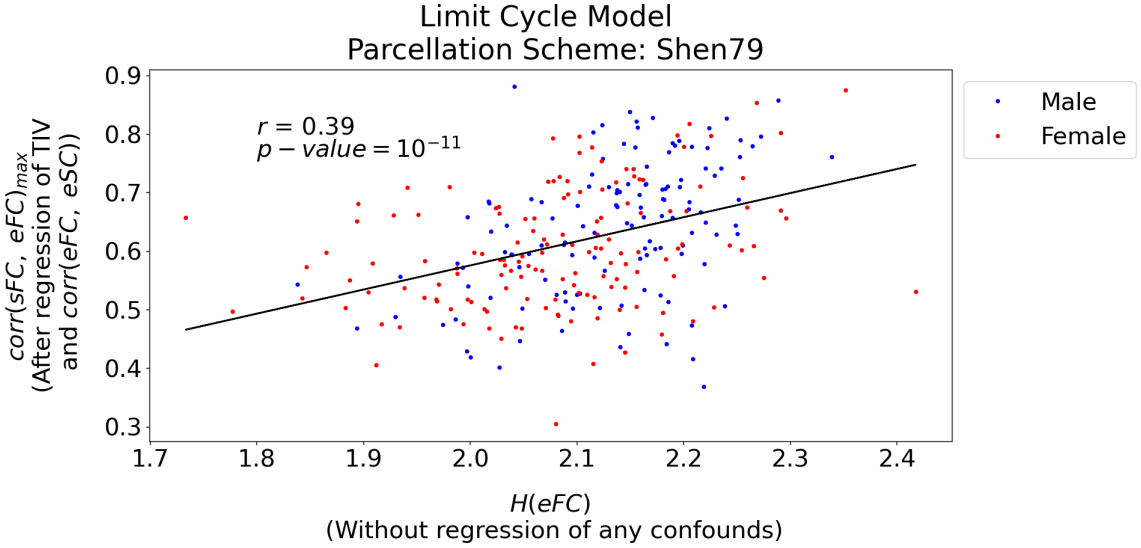

(b)

Figure 4.3: Illustration of the linear relationship between $H(eFC)$ (without regression of any confounds) and $corr(sFC,\ eFC)_{max}$ (after regression of both the TIV and $corr(eFC,\ eSC)$) for the **(a)** phase oscillator model and **(b)** limit cycle model under the Shen79 parcellation scheme; Each dot in the scatter plot corresponds to a subject (blue for males and red for females) and the solid black line represents the line of best fit obtained through linear regression; r is the Pearson's correlation coefficient between the two quantities, and $p - value$ (FDR corrected) represents its statistical significance.

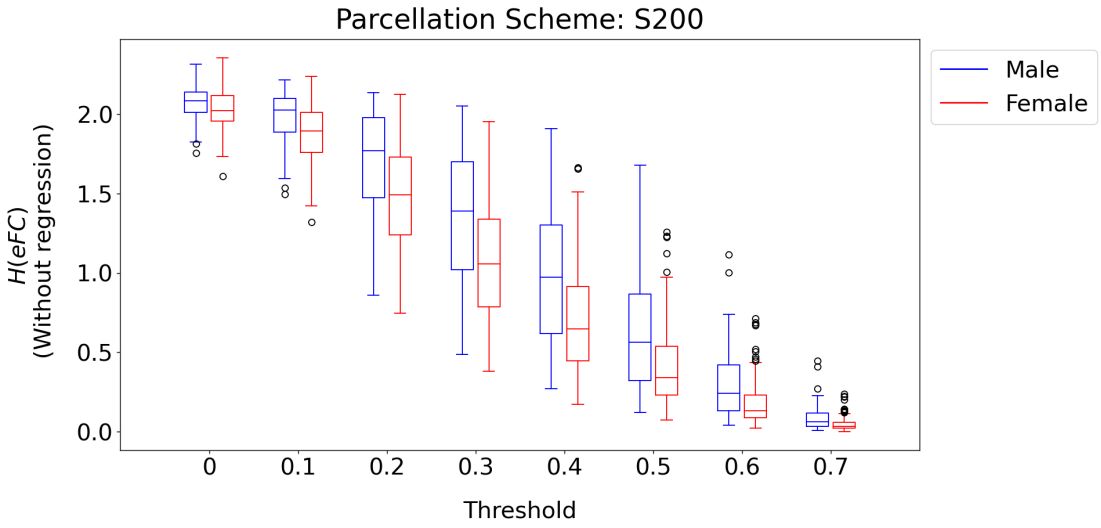

(a)

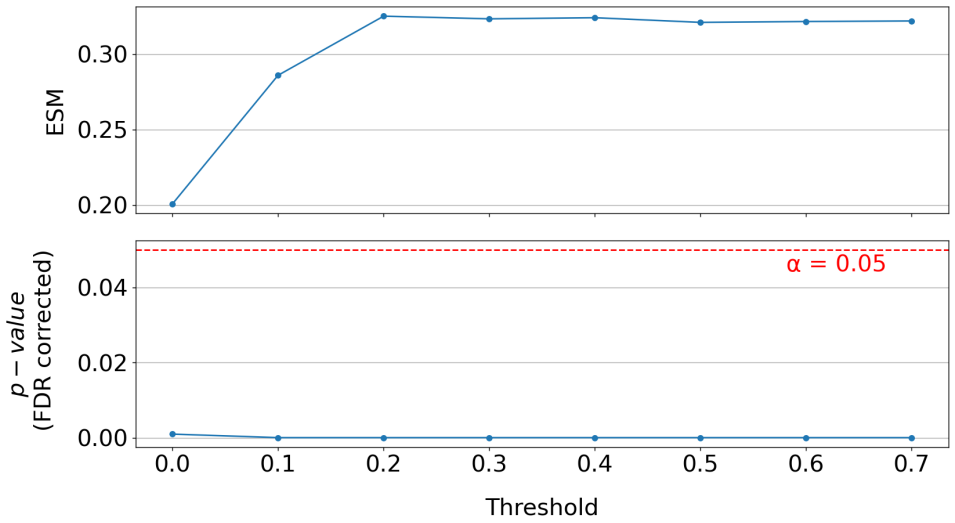

(b)

Figure 4.4: **(a):** Box plots illustrating the monotonic decrease in the value of $H(eFC_{th})$ (without regression of any confounds) with increasing threshold (left to right) and also the qualitative difference in its value between the male group (blue) and that of the female group (red) at each value of the threshold under the S200 parcellation scheme. **(b):** Quantification (ESM) and statistical significance (FDR corrected $p-value$) of the sex differences in $H(eFC)$ (without regression of any confounds) at each threshold under the S200 parcellation scheme; The red line indicates a statistical significance threshold of $\alpha = 0.05$.

rection at all thresholds.

We quantified the observed sex differences within each threshold through the Wilcoxon rank sum test. We found that the ESM at each threshold is positive and statistically significant as the corresponding $p-values$ (FDR corrected) are below the significance threshold of 0.05 as shown in Figure 4.4b. Therefore, it can be concluded that as the threshold increases, the Shannon entropy of the thresholded eFC matrix - $H(eFC_{th})$ monotonically decreases, but at a given threshold, the sex differences in the value of $H(eFC_{th})$ between males and females remain statistically significant, with the group of males having a statistically higher value than the group of females at all the thresholds.

4.1.4 Re-simulation of the goodness-of-fit at Various Thresholds

In order to examine the effect of the thresholding procedure and in turn the effect of altering the $H(eFC)$ on the value of $corr(sFC,\ eFC)_{max}$, we re-simulated the sFC matrices for the phase oscillator model under the S200 parcellation scheme and calculated the new goodness-of-fit between the sFC matrix and each of the thresholded eFC matrix for every individual subject.
However, in addition to examining if the $corr(sFC,\ eFC)_{max}$ is affected by the thresholding of the eFC matrix, another aim of the re-simulation was the elimination of the sex differences induced from the personalisation of models. In the preliminary analysis, the models were personalised for each subject as the individual model parameters were calculated from their respective empirical data (eSC, ePL matrices and fMRI time series signal). Although the two known confounds were regressed out from $corr(sFC,\ eFC)_{max}$, there could possibly be sex differences induced from the individual eSC, ePL matrices and the fMRI time series signal as well. To eliminate this possibility and retain only the eFC matrix as a variant across individual subjects, we re-simulated the non personalised sFC matrices and re-evaluated the $corr(sFC,\ eFC)_{max}$ for every subject.

To fulfill the two aforementioned aims, the $corr(sFC,\ eFC)_{max}$ was calculated for every individual subject at each value of the threshold. The process can be summarised as follows:

1. Firstly, the eSC matrices and the ePL matrices were averaged across all the subjects under the S200 parcellation scheme. This resulted in one averaged eSC matrix and one averaged ePL matrix for the entire population of 272 subjects.

2. The parameters of the Phase Oscillator model such as ω_{jn} and τ_{jn} were then calculated from the averaged eSC and ePL matrix, respectively. Therefore, the parameters ω_{jn} and τ_{jn} are constant across all the subjects.

3. The frequencies f_j corresponding to the jth oscillator were also averaged across all subjects. Hence, every subject has the same f_j for the respective jth oscillator.

4. Subsequently, for every subject, the sFC matrices were generated for all combinations of global propagation delay τ and global coupling strength C.

5. This resulted in one parameter plane per subject at each value of the threshold. Following the procedure of model fitting as described in section 2.6, we extracted the $corr(sFC,\ eFC_{th})_{max}$ from the parameter plane for every subject, and at each value of the threshold. The subscript th represents that the eFC is thresholded at a particular value of the threshold. For example, $corr(sFC,\ eFC_{0.1})_{max}$ represents the goodness-of-fit at the threshold of 0.1.

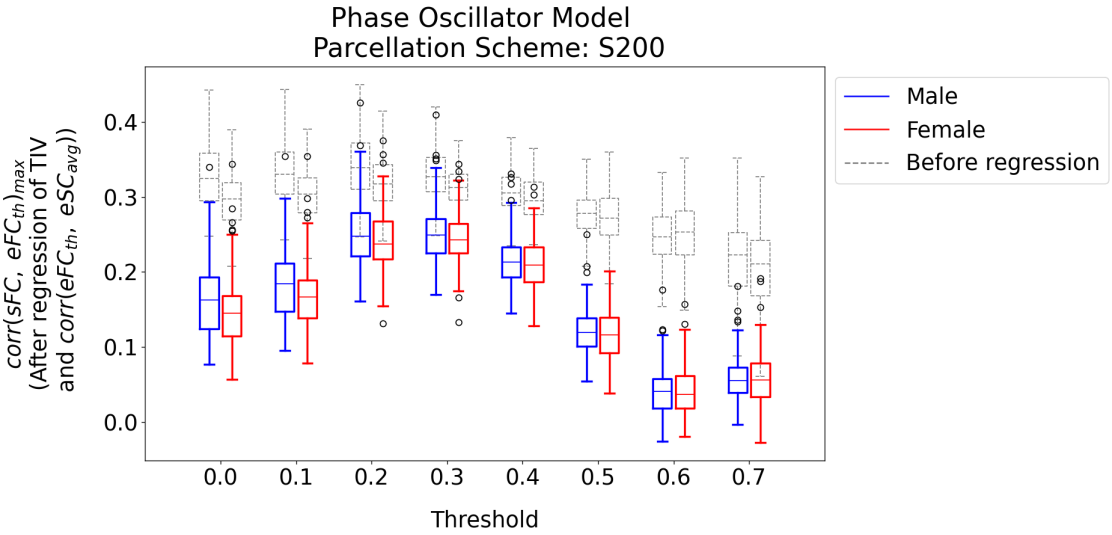

Figure 4.5: Box plots illustrating not only the variation of the value of $corr(sFC,\ eFC_{th})_{max}$ across thresholds, but also the qualitative difference in its value between the male group (blue) and that of the corresponding female group (red) at each threshold. The plots in grey correspond to the case before regression of the confounds and the colored plots represent the case after regression of both the TIV and $corr(eFC_{th},\ eSC_{avg})$

As a result, at each threshold, $corr(sFC,\ eFC_{th})_{max}$ was calculated for every individual subject (272 in total) and the list was subsequently split into two groups of males and females for investigation of the sex differences in the value of $corr(sFC,\ eFC_{th})_{max}$. We then plotted the box plots of both males and females at varying thresholds. The results are as follows:

1. Before regression of the confounds (Figure 7.3 - Appendix), we found that the value of $corr(sFC,\ eFC_{th})_{max}$ remains fairly constant upto the threshold of 0.3, but decreases thereafter. However, at each value of the threshold, the the box plots of the group of males are shifted towards higher values relative to the corresponding group of females.

2. After regressing out just the TIV (Figure 7.4 - Appendix), we found that all the box plots shift downwards relative to their position before regression, but there is a non linear variation of the value of $corr(sFC,\ eFC_{th})_{max}$ across thresholds. Initially there is a slight increase in its value until the threshold of 0.3, then it remains fairly constant until the threshold of 0.5, and decreases thereafter. However, the direction of the relative shift between the box plots of males and females within each threshold remains the same as the case before regression, but with a reduced gap between their respective medians.

3. As shown in Figure 4.5, regressing out the TIV as well as the $corr(eFC_{th},\ eSC_{avg})$ (eSC_{avg} refers to the eSC matrix averaged across all individual subjects) also causes a downward repositioning of all the box plots (in blue and red) relative to the case before regression (in grey). We also observe that the non linear variation of the $corr(sFC,\ eFC_{th})_{max}$ across thresholds becomes more prominent in this case as the value initially increases until the threshold of 0.3 and then decreases thereafter. Even in this case, the direction of the relative shift between the box plots of the male group and the corresponding female group at each value of the threshold remains the same as the case before regression of any confounds, but the gap between their respective medians is negligible.

Hence, under the S200 parcellation scheme, for the phase oscillator model, the results imply that unlike $H(eFC_{th})$, the value of $corr(sFC,\ eFC_{th})_{max}$, after regression of both the confounds, does not decrease monotonically with increasing threshold. Instead, it has a non linear variation across thresholds. This effect is evident from the plot shown in Figure 4.6a where the median of $H(eFC_{th})$ calculated across individual subjects decreasing with increasing thresholds, whereas the median of confound regressed $corr(sFC,\ eFC_{th})_{max}$ calculated across individual subjects at each threshold has a non linear variation across thresholds. To examine the relationship of the $H(eFC_{th})$ (without regressing out the confounds) with $corr(sFC,\ eFC_{th})_{max}$ (with

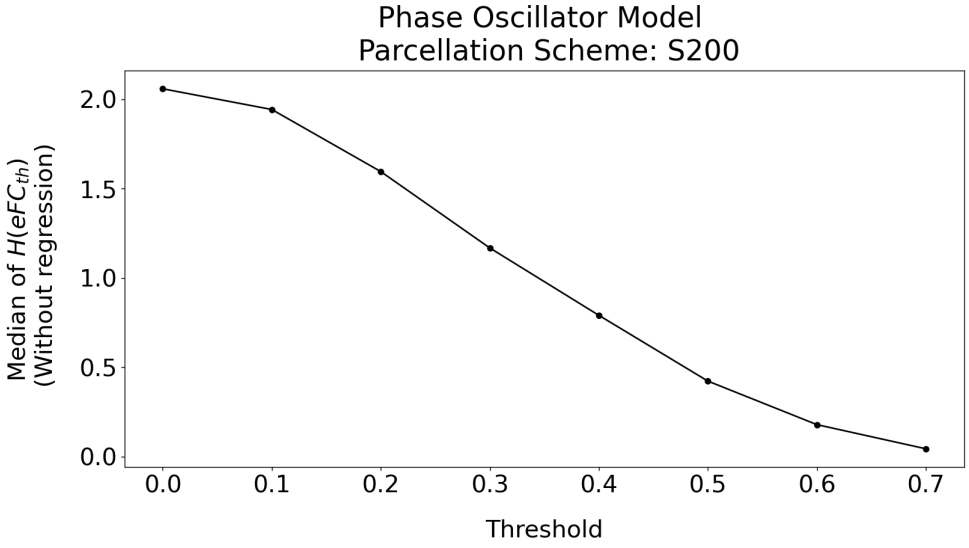

(a)

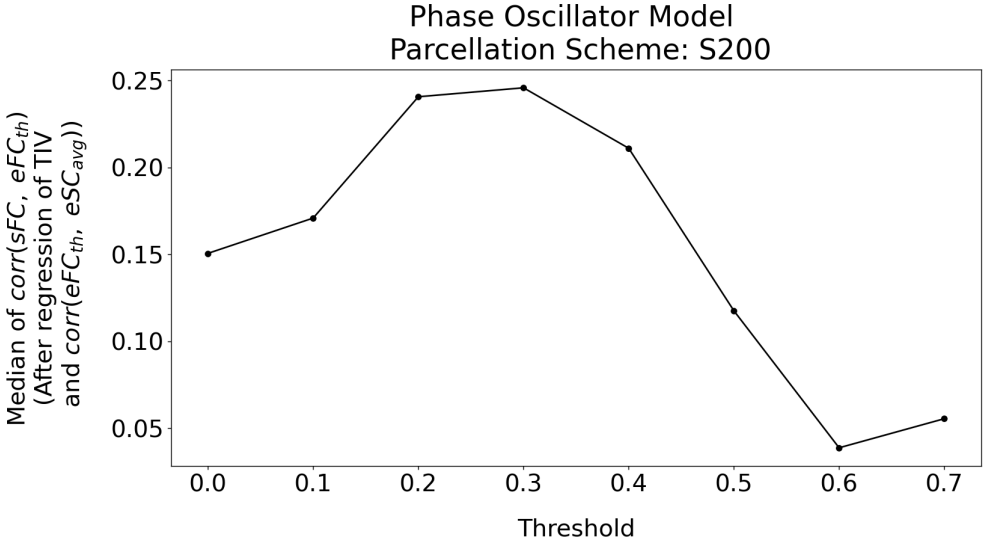

(b)

Figure 4.6: Effect of the thresholding procedure on the value $H(eFC_{th})$ (without regression of any confounds) and also on the value of $corr(sFC,\ eFC_{th})_{max}$ (with regression of both the TIV and $corr(eFC_{th},\ eSC_{avg})$) for the phase oscillator model under S200 parcellation scheme; **(a):** Variation of the median of $H(eFC_{th})$ (calculated across individual subjects at each threshold) with different values at which the eFC matrix is thresholded; **(b):** Variation of the median of confound regressed $corr(sFC,\ eFC_{th})_{max}$ (median is calculated across individual subjects at each threshold) with different values at which the eFC matrix is thresholded.

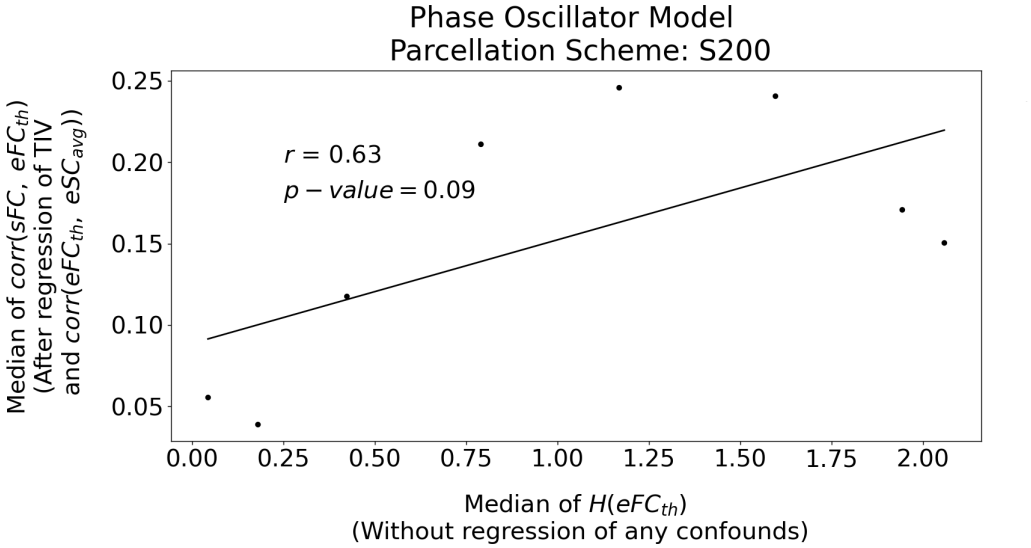

Figure 4.7: Illustration of the relationship between median of $H(eFC_{th})$ (without regression of any confounds) and the median of $corr(sFC,\ eFC_{th})$ (after regression of both the TIV and $corr(eFC_{th},\ eSC_{avg})$ under the phase oscillator model) across different values at which the eFC matrix is thresholded under the S200 parcellation scheme. The solid black line represents the line of best fit obtained through linear regression.

both the confounds regressed out), we calculated the Pearson's correlation coefficient r between their respective medians across thresholds. This relationship is illustrated in Figure 4.7 and we observe that the value of $r = 0.63$, but since the corresponding $p - value$ (no FDR correction) is above 0.05, the correlation coefficient r is statistically insignificant.

Subsequently, the statistical significance and the magnitude of observed sex differences in all three cases (before regression of the confounds, after regression of just the TIV and after regression of both the TIV and $corr(eFC_{th},\ eSC_{avg})$) and at each value of the threshold was quantified through the Wilcoxon rank sum test. The results of the test are shown in Figure 4.8, where we observe that for the case before regression of any confounds (in blue) the ESM at each threshold is positive, but decreases in magnitude as the threshold increases. Additionally, at a given threshold, the ESM also decreases in magnitude as the confounds are regressed out (in orange and green) compared to its value before regression (in blue). We also found that the $p - value$ (FDR corrected) at each threshold before regression (in blue) is below 0.05 (threshold of statistical significance) only till a threshold of 0.4, implying that

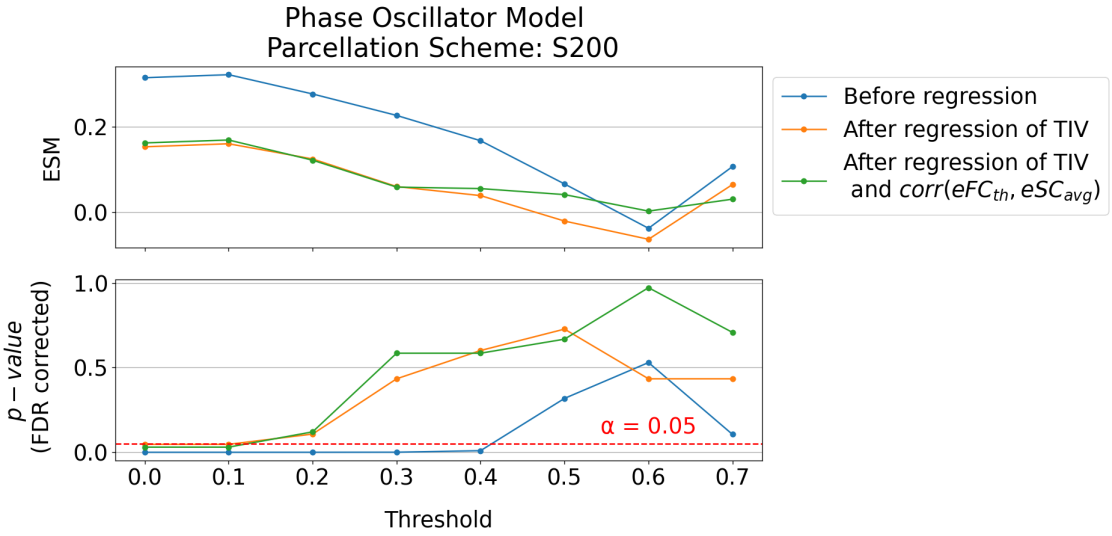

Figure 4.8: Quantification (ESM) and statistical significance (FDR corrected $p - value$) of the sex differences in $corr(sFC,\ eFC_{th})_{max}$ at each threshold, before regression of confounds (in blue), after regression of only the TIV (in orange) and after regression of both the TIV and $corr(eFC_{th},\ eSC_{avg})$ (in green); The red line indicates a statistical significance threshold of $\alpha = 0.05$.

the ESM is statistically significant only for the threshold values from 0.0 to 0.4. In both the cases of regressing out the confounds (in orange and green), the $p - value$ remains below 0.05 only for the threshold of 0 and 0.1. Hence, after the regression of the confounds, the ESM is statistically significant only for the threshold values of 0 and 0.1, implying that at these two values of the threshold, the difference in the value of $corr(sFC,\ eFC_{th})_{max}$ (with both the confounds regressed out) between the group of males and the group of females is statistically significant, with a higher value corresponding to the group of males.

Another important observation is that at the threshold of 0 and 0.1, the sex differences in the value of $corr(sFC,\ eFC)_{max}$ are statistically significant inspite of using non personalised model parameters and regressing out the two known confounds. Moreover, beyond the threshold of 0.1, the sex differences in the $H(eFC)$ are statistically significant (Figure 4.4b), whereas the differences in $corr(sFC,\ eFC)_{max}$ (with both the confounds regressed out) are not (Figure 4.8).

4.2 Standard Deviation of the eFC Matrix - $\sigma(|eFC|)$

4.2.1 Sex Differences in $\sigma(|eFC|)$

For a selected parcellation scheme, $\sigma(|eFC|)$ was calculated for all the subjects (272 in total) and the list was subsequently split into two groups of males (128) and females (144). These two groups were then investigated for sex differences - qualitatively though box plots, and quantitatively through the Wilcoxon rank sum test, which yielded a $p - value$ as well as a test-statistic that was used to calculate the ESM for every parcellation scheme.

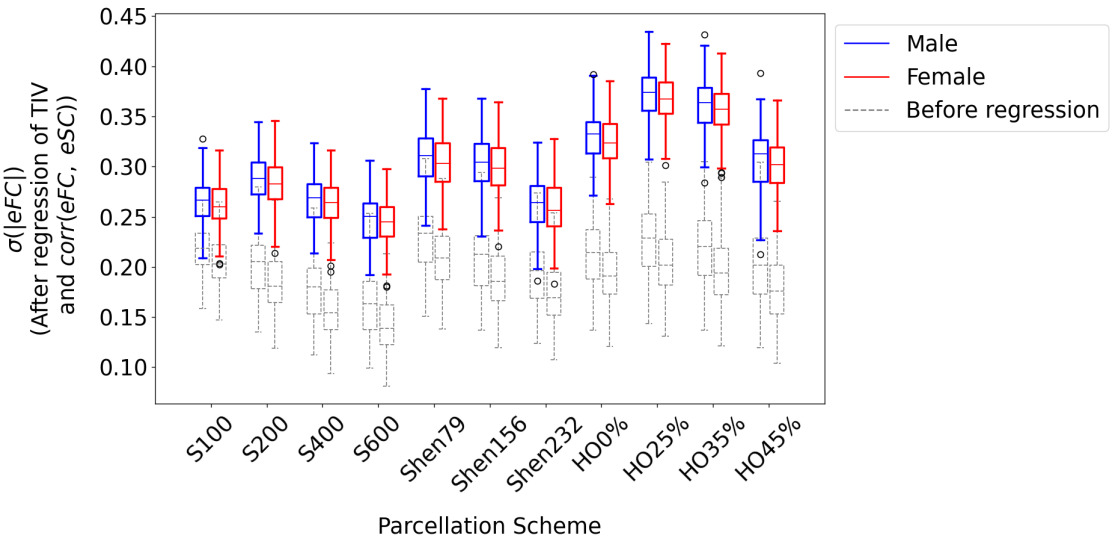

Figure 4.9: Box plots illustrating the qualitative difference in the value of $\sigma(|eFC|)$ between the male group (blue) and that of the female group (red) within each of the 11 parcellation schemes. The plots in grey correspond to $\sigma(|eFC|)$ before regression of the confounds and the colored plots represent its value after regression of both the TIV and $corr(eFC,\ eSC)$

Qualitatively, in all three cases - before regression of any confounds (Figure 7.5 - Appendix), after regression of just the TIV (Figure 7.6 - Appendix) and after regression of both the TIV and $corr(eFC,\ eSC)$, we found that within each parcellation scheme, the box plot of the group of males is shifted relatively above that of the corresponding group of females. We also found that regression of just the TIV causes a downward repositioning of all the box plots, indicating a consistent decrease in the value of $\sigma(|eFC|)$ across all parcellation schemes. Figure 4.9 shows the case where

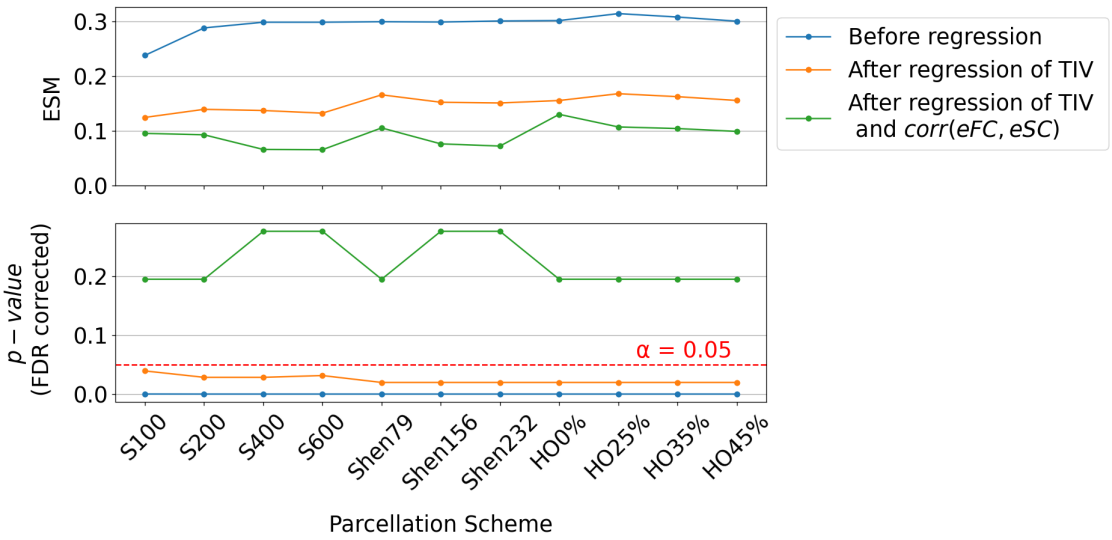

Figure 4.10: Quantification (ESM) and statistical significance (FDR corrected $p-value$) of the sex differences in $\sigma(|eFC|)$ within each of the 11 parcellation schemes before regression of confounds (in blue), after regression of the TIV (in orange) and after regression of both the TIV and $corr(eFC,\ eSC)$ (in green); The red line indicates a statistical significance threshold of $\alpha = 0.05$.

both the confounds have been regressed out (colored plots) and we observe that all the box plots reposition upwards relative to those before regression (in grey). However, as mentioned earlier, even as each confound is regressed out, the direction of relative shift between the plots of the group of males and the group of females within a given parcellation scheme stays the same as the case before regression, but with a reduced gap between their respective medians.

The magnitude (ESM) and statistical significance ($p - value$) of the observed sex differences in $\sigma(|eFC|)$ as evaluated through the Wilcoxon rank sum test both before (in blue) and after regression of the confounds (in orange and green) are shown in Figure 4.10, where it can be seen that the ESM evaluated in order to quantify the difference in the value of $\sigma(|eFC|)$ between males and females with each parcellation scheme, is positive, but decreases in magnitude as each confound is regressed out. Besides, the $p - value$ is below the significance threshold of 0.05 before regression of any confound (in blue) and also after regression of just the TIV (in orange), implying that the ESM is statistically significant only in the these two cases. As the $p - value$ exceeds the threshold of 0.05 after regression of both the confounds (in green) for all the parcellations schemes, the ESMs corresponding to this case are statistically insignificant.

We, therefore, concluded that within each of the 11 parcellation schemes, the group of males has a statistically and significantly higher $\sigma(|eFC|)$ than that of the corresponding group of females both before regression of any confounds and after regressing out only the brain size (TIV). In order to eliminate the confounding effects, but retain the statistically significant sex differences in $\sigma(|eFC|)$, we considered its value after regression of the TIV alone for our further analysis.

Parcellation Scheme	**Phase Oscillator Model**		**Limit Cycle Model**	
	r	$p-value$ (FDR corrected)	r	$p-value$ (FDR corrected)
S200	0.31	10^{-7}	0.46	10^{-16}
S400	0.27	10^{-6}	0.39	10^{-11}
S600	0.35	10^{-9}	-	-
Shen79	0.55	10^{-23}	0.64	10^{-32}
Shen156	0.46	10^{-16}	0.57	10^{-24}
Shen232	0.42	10^{-13}	-	-
HO0%	0.38	10^{-11}	0.46	10^{-15}
HO25%	0.29	10^{-7}	0.38	10^{-11}
HO35%	0.34	10^{-9}	0.41	10^{-12}
HO45%	0.39	10^{-11}	0.43	10^{-14}

Table 4.2: Pearson's correlation coefficient r between $\sigma(|eFC|)$ (after regression of the TIV) and $corr(sFC,\ eFC)_{max}$ (after regression of both the confounds) and its statistical significance (FDR corrected $p-value$) for the phase oscillator model and the limit cycle model under each of the 11 parcellation schemes.

4.2.2 Relationship of $\sigma(|eFC|)$ with $corr(sFC,\ eFC)_{max}$

Within each of the 10 and 8 parcellation schemes of interest under the phase oscillator and limit cycle model, respectively, the relationship between $\sigma(|eFC|)$ (after regression of the TIV) and $corr(sFC,\ eFC)_{max}$ (after regression of both the confounds) was examined through the evaluation of the Pearson's correlation coefficient r between the two quantities. The various values of r and the corresponding statistical significance (FDR corrected $p-values$) for both phase oscillator model and the limit cycle model under their respective parcellation schemes of interest are shown

in Table 4.2. We found that for both the models, within each of the parcellation schemes, the correlation coefficients r are positive and vary from values close to 0.2 to 0.6. Since the corresponding $p-values$ (FDR corrected) are all much lesser than the significance threshold of 0.05, the correlation coefficients r are statistically significant.

For both the models, the highest value of r is obtained for the Shen79 parcellation scheme. However, the lowest r corresponds to the S400 and HO25% parcellation scheme under the phase oscillator model and the limit cycle model, respectively. The relationship for the Shen79 parcellation scheme is illustrated in Figure 4.11a for the phase oscillator model where we observe that the value of the correlation coefficient is $r = 0.55$ and it is statistically significant ($p-value << 0.05$). Similarly, Figure 4.11b shows the relationship for the limit cycle model which also displays a statistically significant correlation coefficient of $r = 0.64$ for the Shen79 parcellation scheme. The plots for the remaining parcellation schemes of interest are included in the subsection 7.2.1 of the Appendix.

4.3 Area under the Eigen Value Curve of the eFC Matrix - $A(\lambda_{eFC})$

4.3.1 Sex Differences in $A(\lambda_{eFC})$

The $A(\lambda_{eFC})$ was calculated for all the 272 subjects within a selected parcellation scheme and the list was subsequently split into two groups: males and females. The two groups were then investigated for sex differences in the value of $A(\lambda_{eFC})$ (both before and after regression of the confounds) through the wilcoxon's sum ranks test.

Before regression of any confounds (Figure 7.7 - Appendix), we found that within a given parcellation scheme, the box plot of the female group is relatively shifted towards higher values of $A(\lambda_{eFC})$ as compared to that of the corresponding male group. After regression of just the TIV (Figure 7.7 - Appendix), we observed an upward repositioning of the box plots of both males and females, indicating an increase in the value of $A(\lambda_{eFC})$ across all the parcellation schemes. In Figure 4.12, the colored box plots show the case where both the TIV and the $corr(eFC,\ eSC)$ have been regressed out of $A(\lambda_{eFC})$ and the grey plots correspond to the case before the regression of any confounds (for comparison). In this case, it can be seen that except for the S100 parcellation, there is a consistent decrease in the value of $A(\lambda_{eFC})$ across all the parcellation schemes as the box plots reposition themselves towards lower values. However, in both the cases of regression - after regression of just the TIV and after

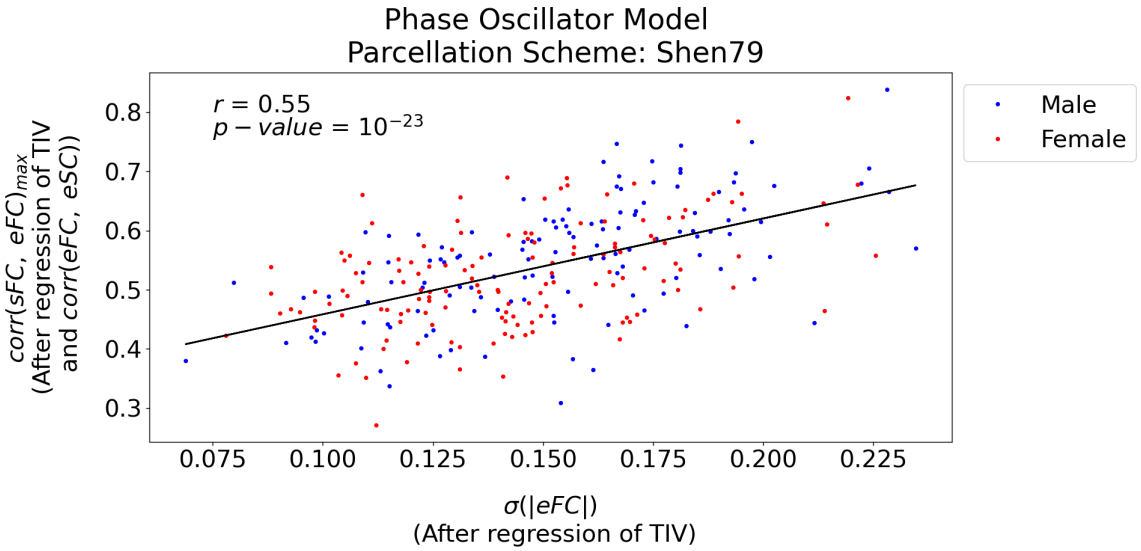

(a)

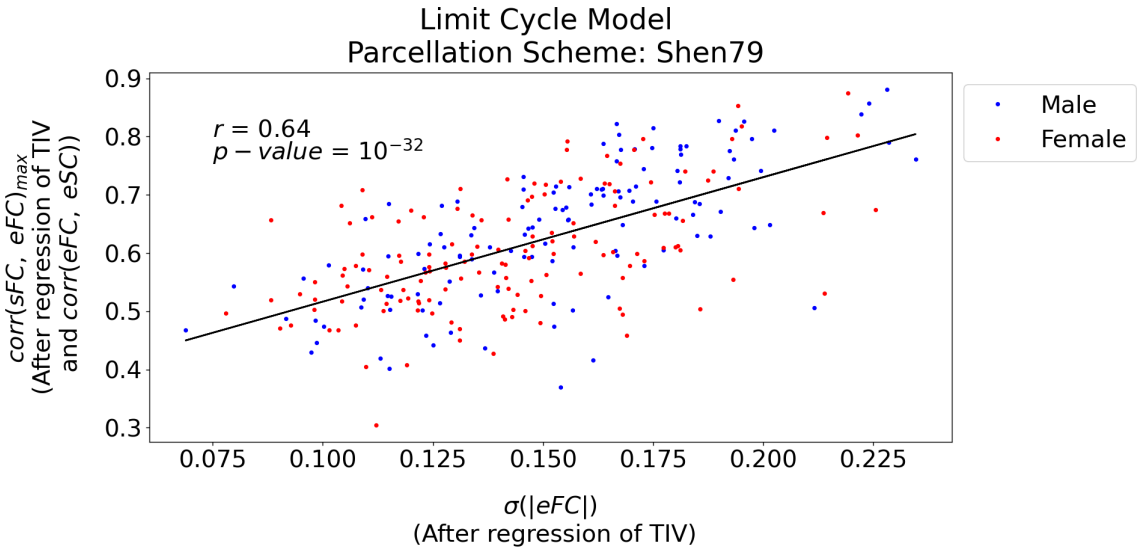

(b)

Figure 4.11: Illustration of the relationship between $\sigma(|eFC|)$ (after regression of the TIV) and $corr(sFC,\ eFC)_{max}$ (after regression of both the confounds) for **(a)** the phase oscillator model and **(b)** the limit cycle model under the Shen79 parcellation scheme; Each dot in the scatter plot corresponds to a subject (blue for males and red for females) and the solid black line represents the line of best fit obtained through linear regression; r is the Pearson's correlation coefficient between the two quantities, and $p - value$ represents its statistical significance.

regression of both the TIV as well as $corr(eFC,\ eSC)$, within each of the 11 parcellation schemes, the box plot of the group of females remains shifted towards higher values of $A(\lambda_{eFC})$ than that of the corresponding group of males, but with a reduced gap between their respective medians.

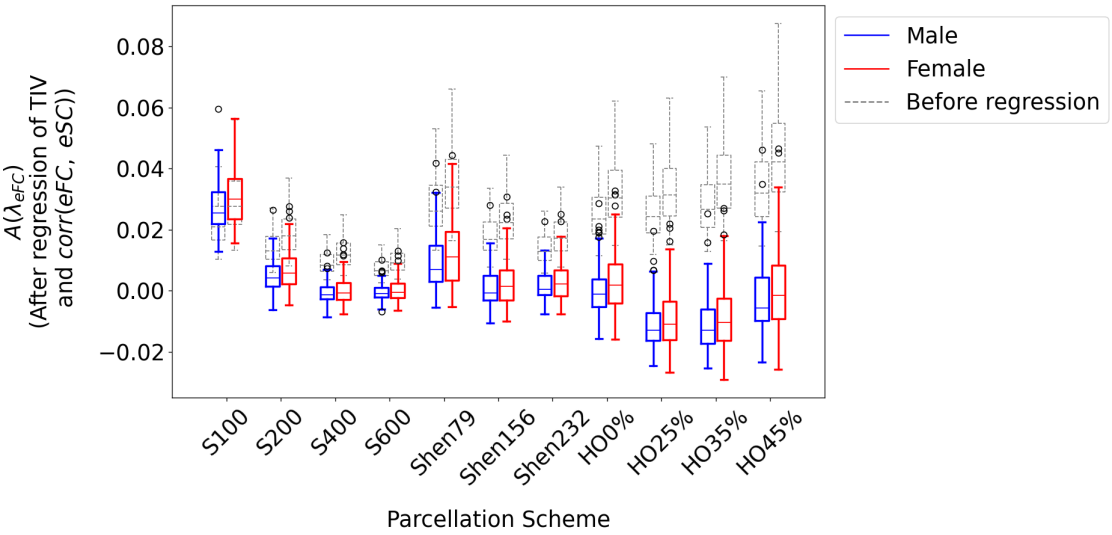

Figure 4.12: Box plots illustrating the qualitative difference in the value of $A(\lambda_{eFC})$ between the male group (blue) and that of the female group (red) within each of the 11 parcellation schemes. The plots in grey correspond to $A(\lambda_{eFC})$ before regression of the confounds and the colored plots represent its value after regression of both the TIV and $corr(eFC,\ eSC)$.

The observed sex differences were tested and quantified through the Wilcoxon rank sum test whose results are shown in Figure 4.13. We found that the ESM is negative for all parcellation schemes, however, its magnitude decreases each time a confound is regressed out. The $p-value$ is below the significance threshold both before regression of the confounds as well as after regression of just the TIV, but surpasses the threshold once both the known confounds are regressed out of $A(\lambda_{eFC})$. This implies that the ESM that quantifies the difference in the value of $A(\lambda_{eFC})$ between the group of males and females within a given parcellation scheme, is statistically significant in two cases - before regression of any confounds and after regression of just the TIV.

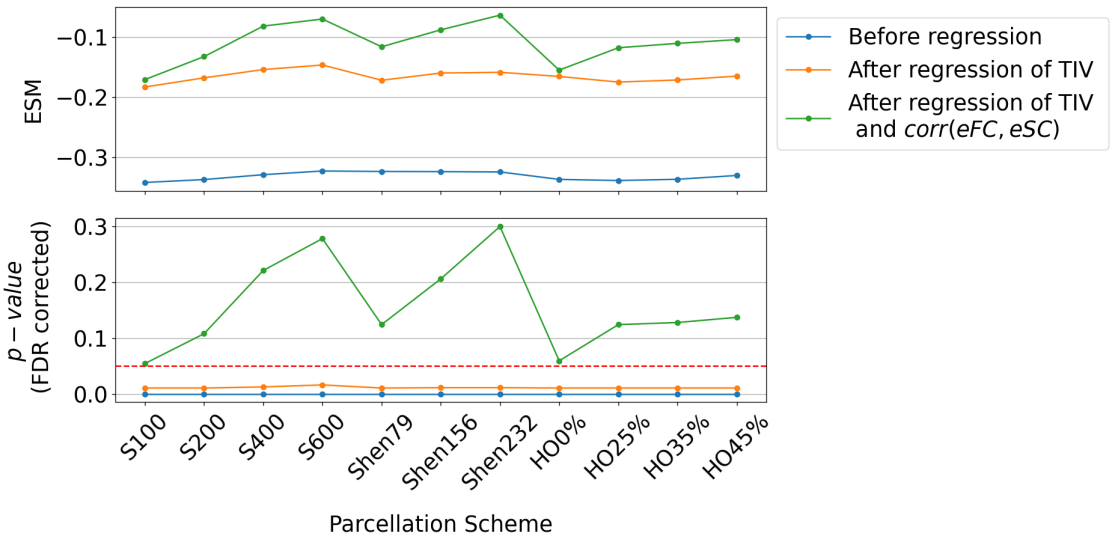

Figure 4.13: Quantification (ESM) and statistical significance (FDR corrected $p - value$) of the sex differences in $A(\lambda_{eFC})$ within each of the 11 parcellation schemes before regression of confounds (in blue), after regression of the TIV (in orange) and after regression of both the TIV and $corr(eFC,\ eSC)$; The red line indicates a statistical significance threshold of $\alpha = 0.05$.

It can, therefore, be concluded that, within any selected parcellation scheme, the value of $A(\lambda_{eFC})$ for the group of females is statistically and significantly higher in comparison with the respective group of males, not only before regression of the confounds, but also after regression of the TIV. Therefore, in all further analysis involving $A(\lambda_{eFC})$, we used its value after regression of the TIV.

4.3.2 Relationship of $A(\lambda_{eFC})$ with $corr(sFC,\ eFC)_{max}$

In order to study the relationship between $A(\lambda_{eFC})$ and $corr(sFC,\ eFC)_{max}$, for a selected parcellation scheme of interest, we determined the Pearson's correlation coefficient r between $A(\lambda_{eFC})$ (after regression of only the TIV) and the respective $corr(sFC,\ eFC)_{max}$ (after regression of both the confounds - TIV and $corr(eFC,\ eSC)$) for the phase oscillator model as well as the limit cycle model.

For both the models, within their respective parcellation schemes of interest, we found that the correlation coefficients r are negative (see Table 4.3) and range from values close to -0.3 to -0.6, with the corresponding $p - values$ (FDR corrected) well below the significance threshold of 0.05. Consequently, the values of r evaluated are

statistically significant for both the models and for each of the parcellation schemes. However, the highest (in magnitude) r is observed for the Shen79 parcellation scheme for both the models, whereas, the lowest r corresponds to the S400 for the phase oscillator model and S400 and HO25% (equal values) parcellation schemes for the limit cycle model.

Under the Shen79 parcellation scheme, Figure 4.14a shows the relationship for the phase oscillator model, where we observe a statistically significant ($p-value << 0.05$) negative correlation coefficient of $r = -0.63$ and Figure 4.14b shows the relationship for the limit cycle model with a statistically significant $r = -0.70$. Similar plots for the remaining parcellation schemes of interest are included in the subsection 7.3.1 of the Appendix.

Parcellation Scheme	**Phase Oscillator Model**		**Limit Cycle Model**	
	r	$p - value$ (FDR corrected)	r	$p - value$ (FDR corrected)
S200	-0.41	10^{-12}	-0.55	10^{-22}
S400	-0.32	10^{-8}	-0.43	10^{-13}
S600	-0.41	10^{-12}	-	-
Shen79	-0.63	10^{-31}	-0.70	10^{-41}
Shen156	-0.54	10^{-21}	-0.61	10^{-27}
Shen232	-0.46	10^{-15}	-	-
HO0%	-0.46	10^{-15}	-0.53	10^{-20}
HO25%	-0.36	10^{-10}	-0.43	10^{-13}
HO35%	-0.41	10^{-12}	-0.46	10^{-15}
HO45%	-0.46	10^{-15}	-0.49	10^{-18}

Table 4.3: Pearson's correlation coefficient r between $A(\lambda_{eFC})$ (after regression of the TIV) and $corr(sFC,\ eFC)_{max}$ (after regression of both the confounds) and its statistical significance (FDR corrected $p - value$) for the phase oscillator model and the limit cycle model under each of the 11 parcellation schemes.

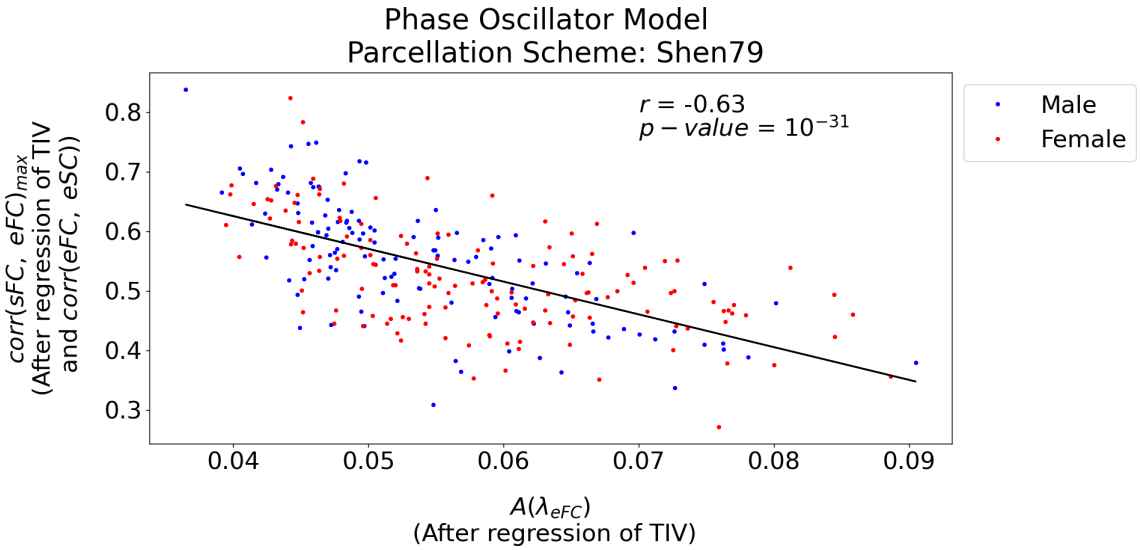

(a)

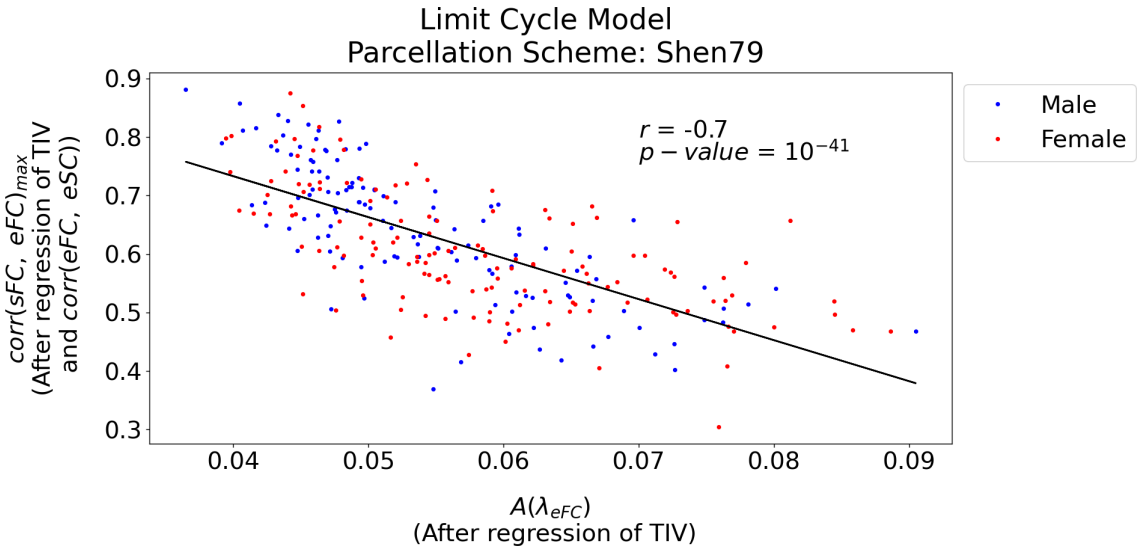

(b)

Figure 4.14: Illustration of the relationship between $A(\lambda_{eFC})$ (after regression of the TIV) and $corr(sFC,\ eFC)_{max}$ (after regression of both the confounds) for **(a)** the phase oscillator model and **(b)** limit cycle model under the Shen79 parcellation scheme; Each dot in the scatter plot corresponds to a subject (blue for males and red for females) and the solid black line represents the line of best fit obtained through linear regression; r is the Pearson's correlation coefficient between the two quantities, and $p - value$ (FDR corrected) represents its statistical significance.

Chapter 5

Discussion

Through this project, we aimed to investigate the possible sex differences that may exist in the goodness-of-fit, that is, the $corr(sFC,\ eFC)_{max}$ extracted separately for all the subjects for the phase oscillator model as well as the limit cycle model under 11 different parcellation schemes. The aim of the project, however, was not to reason the variation of the goodness-of-fit across parcellation schemes as studied in [8] and [31]. Instead, we intended to examine the presence of sex differences in the goodness-of-fit within a selected parcellation scheme and also to investigate if the variation of the goodness-of-fit between males and females despite the removal of confounding variables, could be attributed to the variation in the properties of the eFC matrix since it was employed for model validation. Such an investigation was performed independently under each of the 11 parcellation schemes and each of the two models.

In the preliminary analysis, we observed that for both the models studied, the value of $corr(sFC,\ eFC)_{max}$ within a given parcellation scheme is statistically higher for the group of males as compared to the corresponding group of females, with the difference being statistically significant and this observation is persistent in all the parcellation schemes before regressing out the known confounds. However, when the two known confounds - the brain size (TIV) and the empirical structure function correspondence ($corr(eFC,\ eSC)$) were regressed out from $corr(sFC,\ eFC)_{max}$, the sex differences remained statistically significant and in the same direction (as before regressing out the confounds) within all the parcellation schemes except for S100 for the phase oscillator model and S100, S600 and Shen232 for the limit cycle model. We, therefore, concluded that despite the elimination of the possible influences from the confounds, the statistically significant sex differences in the goodness-of-fit persist for 10 and 8 parcellation schemes of interest for the phase oscillator model and the limit cycle model, respectively. This implies that for those parcellation schemes, the sex differences in the goodness-of-fit do not emerge from the sex differences in the

brain size and the empirical structure-function correspondence. Additionally, particularly for the S200 parcellation scheme, we re-simulated the phase oscillator model where the eSC, ePL matrices and the frequencies corresponding to every brain region were averaged across individual subjects in order to eliminate the sex differences induced due to personalization of models. In this case, we found that the differences in the value of $corr(sFC,\ eFC)_{max}$ between the group of males and the corresponding group of females, are statistically significant, with a relatively higher values for the group of males, inspite of removal of both the confounds as well as implementation of non personalized model parameters. This is an indication that, at least for the S200 parcellation scheme, the presence of statistically significant sex differences in the goodness-of-fit (generated through the phase oscillator model) is not only independent of the two confounds (brain size and empirical structure-function correspondence), but also independent of the inter-individual differences that stem from the personalised model parameters. However, whether implementation of non personalised models preserves the aforementioned sex differences for the other parcellation schemes and also the limit cycle model, needs further investigation.

In order to explain the statistically significant higher value of the goodness-of-fit for the group of males relative to that of the group of females within a selected parcellation scheme, despite the removal of both the confounds, we speculated that a potential reason for such an observation could be the sex differences in the 'complexity' of the eFC matrix used to validate the model, that may in turn affect the quality of model fitting. We hypothesised that the presence of high 'complexity' in the eFC matrix implies a lower goodness-of-fit and therefore, the eFC matrices corresponding to the group of females are more 'complex' than that of the group of males. To test our hypothesis, we considered three quantities calculated from the eFC matrices of individual subjects as potential 'complexity' measures and examined if they also exhibited sex differences in them and if the measures were negatively correlated with the confound regressed goodness-of-fit within a given parcellation scheme, as per our hypothesis.

On considering the Shannon entropy of the eFC matrix - $H(eFC)$ as a potential measure of 'complexity', we found that, without regressing out any confounds, the group of males has a statistically significant higher value relative to that of the group of females within every parcellation scheme except S100, where the difference is not statistically significant. This implies that within a parcellation scheme (except S100), the group of males have a higher uncertainty associated with the synchronization of activities between different pairs of brain regions, as compared to that of the corresponding group of females. Besides, irrespective of whether only the TIV is regressed out, or both the TIV and $corr(eFC,\ eSC)$ are regressed out, the sex differ-

ences in $H(eFC)$ within all the parcellation schemes, turn statistically insignificant. This implies that the variation of the Shannon entropy of the eFC matrix between males and females, is not independent of the influence from the other covariates with sex, namely the brain size and the empirical structure-function correspondence. It is, therefore, imperative that the confounds are not regressed out from $H(eFC)$, in order to not only detect statistically significant sex differences in it, but to also use this measure to account for the sex differences in $corr(sFC,\ eFC)_{max}$ (from which both the confounds have been regressed out).
Moreover, for both the models, the $H(eFC)$ (without regression of confounds) positively, but weakly correlates with the $corr(sFC,\ eFC)_{max}$ (after regression of both the confounds) across individual subjects within a selected parcellation scheme of interest, that is, the Shannon entropy of the eFC matrix, along with the confounds, can account for a very small percentage of the variation in the confound regressed goodness-of-fit from one subject to another within a selected parcellation scheme. The exact percentage of variance explained depends on the model and the parcellation scheme. However, further analysis under the S200 parcellation scheme for the phase oscillator model revealed that a monotonic decrease in the $H(eFC)$ (without regression) due to the thresholding process, does not imply a monotonic decrease in the $corr(sFC,\ eFC)_{max}$ (with both the confounds regressed out) across varying thresholds for an individual subject. This is evident from the fact that the correlation coefficient between the respective medians of the two quantities across varying thresholds is statistically insignificant. A potential reason for the non linear variation in the goodness-of-fit across varying thresholds could be that besides affecting the Shannon entropy of the eFC matrix, the thresholding procedure may also influence other properties of the eFC matrix, which could collectively cause a non linear variation in the goodness-of-fit of an individual subject across varying thresholds. Therefore, if we intend to examine the the effect of altering only the Shannon entropy of the eFC matrix, on the value of the goodness-of-fit for an individual subject, that is, at an intra-individual level, the thresholding process may not be the optimal way and further investigation is required in this aspect.

Furthermore, under the S200 parcellation scheme, we also found that although the sex differences in the value of $H(eFC_{th})$ (without regression of confounds) are statistically significant at all values of the threshold, the sex differences in the value of $corr(sFC,\ eFC_{th})_{max}$ (with both the confounds regressed out) are statistically significant only at the threshold of 0 and 0.1. Hence, beyond the threshold of 0.1, the presence of sex differences in the Shannon entropy of the eFC matrix, does not necessarily mean that the goodness-of-fit (after regression of both the confounds) will also have sex differences in it. The reason for such an observation is still unclear, but a reasonable speculation could be that it may be due to the fact that the two

quantities are weakly correlated ($r = 0.13$) across individual subjects for the phase oscillator model, under the S200 parcellation scheme.

The second potential 'complexity' measure that we considered was the standard deviation of the eFC matrix - $\sigma(|eFC|)$ where we observed that the sex differences in its value are statistically significant, with the group of males having a statistically higher value than that of the corresponding group of females, within all the 11 parcellation schemes before regressing out any confounds and also after the regressing out the TIV, but not when both the TIV and $corr(eFC,\ eSC)$ are regressed out. This implies that even after regressing out the brain size, the males have a statistically higher spread in their respective eFC matrices as compared to that of the corresponding females within a selected parcellation scheme. That is, from a statistical perspective, there exist some pairs of brain regions whose activities are synchronised very differently from that of the other pairs for males, whereas, females have a relatively more similar extent of synchronised co-activation between different pairs of brain regions and that these sex differences observed in the standard deviation of the eFC matrix are independent of influence from the sex differences in the brain size (TIV), but are dependent on the influence of the sex differences in the empirical structure-function correspondence ($corr(eFC,\ eSC)$). Therefore, in order to observe statistically significant differences in the value of $\sigma(|eFC|)$ between the group of males and females, or to use it to account for the sex differences in another quantity such as $corr(sFC,\ eFC)_{max}$, the value of $\sigma(|eFC|)$ cannot be considered independent of $corr(eFC,\ eSC)$; the TIV, however, can be regressed out from it. Moreover, for both the models considered, since the correlation coefficient between $\sigma(|eFC|)$ (after regression of the TIV) and $corr(sFC,\ eFC)_{max}$ (after regression of both the confounds) across individual subjects within a selected parcellation scheme of interest is positive, moderate in magnitude as well as statistically significant, it signifies that a more broadly distributed eFC matrix implies a better quality of the model fit and that $\sigma(|eFC|)$ (after regression of the TIV) accounts for a reasonable proportion of the variation in $corr(sFC,\ eFC)_{max}$ (after regression of both the confounds) between males and females within a selected parcellation scheme. The exact percentage of the variance explained, however, depends on the model and the parcellation scheme.

The third measure of 'complexity' considered in this study was the area under the eigen value curve of the eFC matrix - $A(\lambda_{eFC})$. We found that from a statistical standpoint, this measure is significantly higher for the group of females relative to the corresponding group of males within all of the parcellation schemes, not only before regressing out the confounds, but also after regressing out the brain size (TIV). However, the sex differences become statistically insignificant after regressing out both the TIV as well as the $corr(eFC,\ eSC)$. The statistically higher value of $A(\lambda_{eFC})$

for the group of females suggests that the eigen value curve of the eFC matrices of the females decays at a slower rate (gradual fall), while the curve corresponding to the males within the same parcellation scheme decays at a much faster rate (steep fall). In other words, within a selected parcellation scheme, the reconstruction of the eFC matrix back to its original vector space involves a significant contribution of a relatively larger number of eigen values in the case of females, as compared to the case of males. This is true even after the major differentiating factor, that is, the brain size has been regressed out from $A(\lambda_{eFC})$. The fact that the sex differences are statistically significant even after regressing out the TIV, but not after regressing out both the TIV as well as $corr(eFC,\ eSC)$ implies that similar to the observation in the case of $\sigma(|eFC|)$, the difference in the value of $A(\lambda_{eFC})$ between males and females within a given parcellation scheme is independent of the influence from the sex differences in the brain size (TIV), but is influenced by the sex differences in the empirical structure-function correspondence ($corr(eFC,\ eSC)$). Hence, the observed sex differences in both $\sigma(|eFC|)$ as well as $A(\lambda_{eFC})$ emerge from the sex differences in $corr(eFC,\ eSC)$ and, therefore, regressing it out also takes away the statistical significance of the sex differences from both the measures. Accordingly, to observe statistically significant difference in the value of $A(\lambda_{eFC})$ between the group of males and females, or to use this measure to explain the sex differences in $corr(sFC,\ eFC)_{max}$, it must be considered without regressing out $corr(eFC,\ eSC)$ from it. Furthermore, unlike the first two measures of 'complexity', the $A(\lambda_{eFC})$ (with the TIV regressed out) is found to be negatively correlated with the $corr(sFC,\ eFC)_{max}$ (with both the confounds regressed out) within a selected parcellation scheme. In addition to being negative, the correlation coefficient is also statistically significant and has a moderate to strong magnitude. This implies that a higher value of $A(\lambda_{eFC})$ (with the TIV regressed out) corresponds to a lower value of $corr(sFC,\ eFC)_{max}$ (with both the confounds regressed out) and the former accounts for a reasonable percentage of variation in the latter between the group of males and females for both the models within their respective parcellation schemes of interest. The exact percentage, however, depends on the model and the parcellation scheme considered.

Comparing all the three measures, the maximum proportion of the variance in the $corr(sFC,\ eFC)_{max}$ (with both the confounds regressed out) across individual subjects, within a parcellation scheme is explained by the $A(\lambda_{eFC})$ (with the TIV regressed out), followed by $\sigma(|eFC|)$ (with TIV regressed out) and least proportion is accounted for, by $H(eFC)$ (without regression of any confounds). However, correlation does not imply causation. Therefore, it cannot be claimed that the sex differences in these three measures cause the variation in the goodness-of-fit between males and females. Although an attempt was made to test the causality of $H(eFC)$ on the goodness-of-fit, the thresholding procedure does not assure an alteration of just the

$H(eFC)$. Therefore, further investigation is required in order to test the causality of any of the 'complexity' measures on the confound regressed goodness-of-fit.

For each of the three potential measures of 'complexity' considered in the project, we speculated that a high value of the measure corresponds to a higher 'complexity' of the eFC matrix, and according to our hypothesis proposed in section 3.3, we expected the group of females to have a statistically significant higher value of the 'complexity' measure relative to the group of males within a given parcellation scheme. Therefore, the 'complexity' measures and the confound regressed goodness-of-fit for both the models under their respective parcellation schemes of interest were expected to be negatively correlated with each other. However, it is not straightforwardly clear as to whether to accept or reject the hypothesis, because in the case of two measures, namely, $H(eFC)$ and $\sigma(|eFC|)$, we observed surprising results that are contradictory to our expectations and $A(\lambda_{eFC})$ is the only measure (amongst the ones considered) for which the hypothesis stands validated. The hypothesis proposed by us is, therefore, inconsistent across different measures of 'complexity' considered in the study. Furthermore, since the exact definition of 'complexity' of a connectome has not been clearly established yet, it is also unclear as to whether any of the properties of the eFC matrix that we speculated as "potential measures of complexity" actually reflect the underlying complexity of the functional connectivity between different brain regions in a neuro-physiological context. As different measures have different interpretations, it is difficult to specify which sex has a statistically more 'complex' eFC matrix and whether a lower 'complexity' always implies a better model fit.

Essentially, in this project, we were successful in establishing the statistical differences in the goodness-of-fit between the group of males and the corresponding group of females within most parcellation schemes even after regressing out the confounds for both of the whole brain dynamical models studied. We identified 10 and 8 such parcellation schemes for the phase oscillator model and the limit cycle model, respectively. Besides, we also discovered a few properties of the eFC matrix that display sex differences in them and also account for different proportion of variance in the confound regressed goodness-of-fit across individual subjects within a selected parcellation scheme of interest. However, a precise and valid quantification and interpretation of the term 'complexity' of a connectome and its correlation (and/or causation) with the goodness-of-fit remains obscure. The project, therefore, requires an additional investigation in this aspect.

Chapter 6

Limitations and Future Prospects

In addition to the aspects of the projects which need further investigation (as discussed in the previous chapter), the materials and statistical methods implemented in the project also have their own limitations. In this chapter, we will enumerate some of those shortcomings and also propose potential future directions of the project.

The parcellation schemes employed in the project are non personalised, that is to say, they are based on a universal map of the brain defined in the standard space, rather than the native space of the individual subject. The standard space fixes the same number of brain regions for all the subjects under a specific parcellation scheme. Since the level of organization in the brain differs across individuals, fixing the same number of brain regions for all the subjects may not be the most optimal method. Besides, standardising the granularity (number of parcels) across individual subjects may also mitigate the potential inter-individual differences with regards to their respective functional or structural connectomes. It could, therefore, be interesting to consider personalised delineation of the brain for each subject and then investigate the sex differences in the properties of their respective connectomes.

In the context of statistical hypothesis tests, although the Wilcoxon rank sum test does not require the distribution of the data to be of a specific kind (therefore applicable even in cases of normally distributed data), the Student's t test is statistically more powerful in cases where the distribution of the data is close to a normal distribution. In our study, we did not perform a thorough investigation of the nature of the distribution followed by the data in every segment of the analysis and we, therefore, employed the non parametric Wilcoxon rank sum test so as to remain consistent throughout the project. However, in order to achieve statistically more accurate results, the choice of the hypothesis tests should be situation specific.

Moreover, previous studies have also shown that the $p - value$ depends on the standard error, which is in turn dependant on the sample size of the data. Increasing the sample size decreases the standard error and, therefore, also decreases the $p - value$. The $p - value$ is, therefore, said to be confounded by the sample size [35]. In our study, it is possible that we obtain a smaller $p - value$ in cases where the sample size of the data is large, for example, in Figure 3.6a, we see that the $p - value$ corresponding to the S200 parcellation scheme is lower than that of S100 parcellation scheme. Such a result is observed not only because the parcellation criteria is different between S100 and S200, but also because of a mere increase in the sample size of the data (increase in dimension of the connectomes from 100x100 to 200x200). Although, we performed the FDR correction on the $p - value$ to correct for multiple comparison across different parcellation schemes, it is important to note that the sample size dependence of the $p - value$ cannot be overlooked.

Besides, as already mentioned earlier, we did not apply the Fisher's Z transformation on the elements of the eFC matrices (which are themselves correlation coefficients) prior to the calculation of the quality of model fit, that is, the $corr(sFC,\ eFC)$. However, from a strict statistical perspective, all correlation coefficients must technically be Fisher's Z transformed prior to any arithmetic or statistical operations. It could, therefore, be useful to inspect if the implementation of the Fisher's Z transformation on the eFC matrix elements prior to the calculation of $corr(sFC,\ eFC)$ (as done in a very recent study [2]), affects the magnitude and statistical significance of the sex differences in it in any way.

In this project, we considered two similar whole brain dynamical models based on an ensemble of phase oscillators. Although the models are useful in simulating the resting state activity of the brain regions, other biologically inspired models like the neuronal mass model [8] can also be additionally considered so as to examine if the sex differences in the goodness-of-fit persist under the implementation of a conceptually different model.
Moreover, in both the phase oscillator model as well as the limit cycle model, we optimised the goodness-of-fit with respect to just two global model parameters - global propagation delay τ and global coupling strength C. However, the dimension of the parameter space can be increased (from 2D) by introducing more global parameters in the model and the goodness-of-fit can subsequently be optimised with respect to a higher number of global parameters. This may potentially influence the value of the goodness-of-fit and consequently influence the magnitude and statistical significance of the sex differences observed in it.

Thus far, the connectivity matrices we worked with are whole brain connectomes, that is, we considered the anatomical or functional connections (empirical and simulated) between regions defined over the entire brain. However, there have been previous studies showing that the whole brain can be divided into 6 subnetworks called Resting State Networks (RSNs) [19] each consisting of a certain number of brain regions (obtained through a selected parcellation scheme). Therefore, in addition to the whole brain connectomes, RSN specific connectivity matrices can also be considered in order to explore if sex differences persist in the goodness-of-fit extracted between region specific connectomes.

In the segment on 'complexity' analysis, although we considered three quantities derived from the eFC matrices as potential measures of 'complexity', other properties of the eFC matrix can also be considered in order to investigate the existence of sex differences in them and their ability to account for the sex differences in the goodness-of-fit. For instance, viewing the eFC matrix from a graph theoretical perspective, measures such as the shape and scale parameters of the degree distribution of the eFC matrix, modularity and clustering coefficient of the eFC matrix, etc can also be considered as discussed in the study [8].
In addition to examining the various properties of the static eFC matrix, the analysis can be extended to evaluation of the 'complexity' of the dynamic eFC matrix and also of the BOLD fMRI time series signal that is employed to construct the eFC matrices. As mentioned earlier, recent studies such as [26], [37], [27], [19] etc. have quantified the 'complexity' of the fMRI time varying signal, or of dynamical functional connectivity matrix in terms of entropy measures like the sample entropy, approximate entropy, multi-scale entropy etc. Hence, evaluation of such measures in the context of this study, could potentially provide a deeper understanding of the interpretation of the complexity of the time series signal, whether and how it is different between males and females and also its impact (correlation, causation) on the sex differences in the goodness-of-fit.

The project, therefore, has many prospects to be explored in the future and further research in this domain has the potential to furnish great insights into how males and females differ in their brain dynamics and consequently, in their behaviour.

Chapter 7

Appendix

In this chapter, we include all the extra plots that support the analysis and results of the project.

7.1 Shannon Entropy of the eFC Matrix - $H(eFC)$

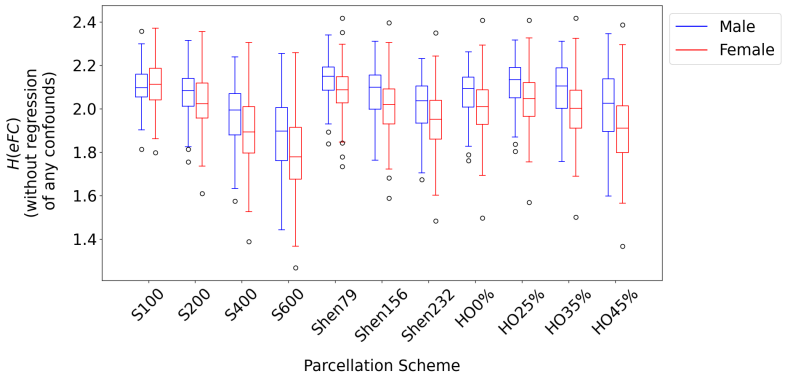

Figure 7.1: Box plots illustrating the qualitative difference in the value of $H(eFC)$ between the male group (blue) and that of the female group (red) within each of the 11 parcellation schemes, for the case before regression of any confounds.

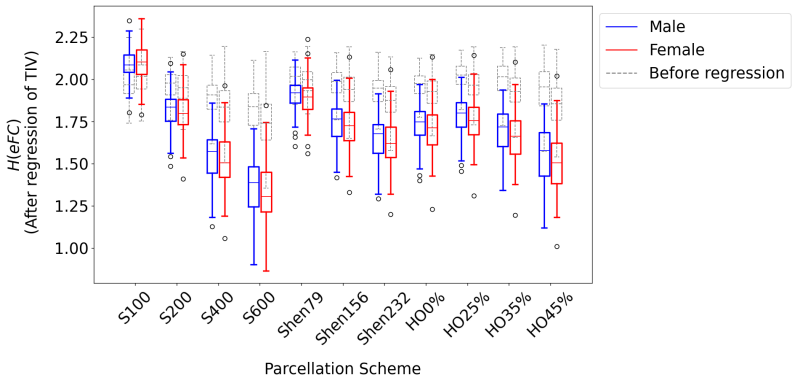

Figure 7.2: Box plots illustrating the qualitative difference in the value of $H(eFC)$ between the male group (blue) and that of the female group (red) within each of the 11 parcellation schemes, for the case after regression of only the brain size (TIV).

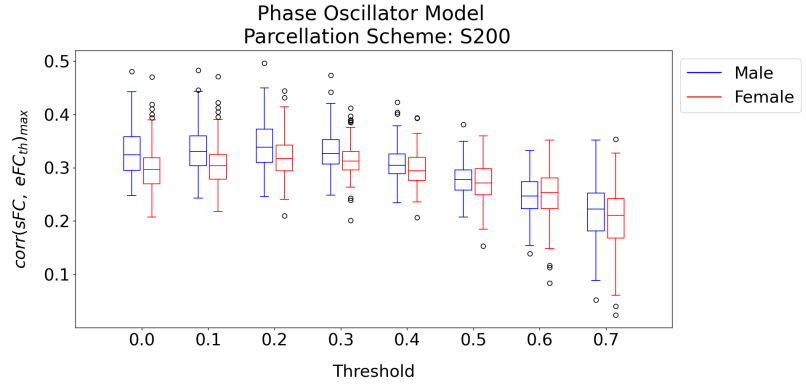

Figure 7.3: Box plots illustrating not only the variation of $corr(sFC,\ eFC_{th})_{max}$ across thresholds but also the qualitative difference in its value between the male group (in blue) and that of the female group (in red) at each threshold, for the case before regressing out any confounds.

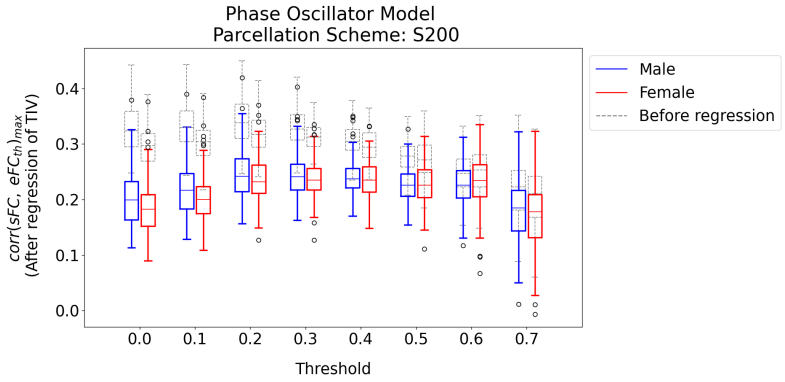

Figure 7.4: Box plots illustrating not only the variation of $corr(sFC,\ eFC_{th})_{max}$ across thresholds but also the qualitative difference in its value between the male group (in blue) and that of the female group (in red) at each threshold, for the case where only the TIV was regressed out.

7.1.1 Relationship between $H(eFC)$ and $corr(sFC,\ eFC)_{max}$

The following plots illustrate the relationship between the $H(eFC)$ (without regression of any confounds) and the $corr(sFC,\ eFC)_{max}$ (after regression of both the TIV and $corr(eFC,\ eSC)$) within a parcellation scheme. Each dot in the scatter plot corresponds to a subject (blue for males and red for females) and the solid black line represents the line of best fit obtained through linear regression; r is the Pearson's correlation coefficient between the two quantities and the $p-value$ (FDR corrected) represents its statistical significance. Below, we illustrate the plots for all the parcellation schemes of interest for the phase oscillator model followed by the plots for those of the limit cycle model.

Phase Oscillator Model

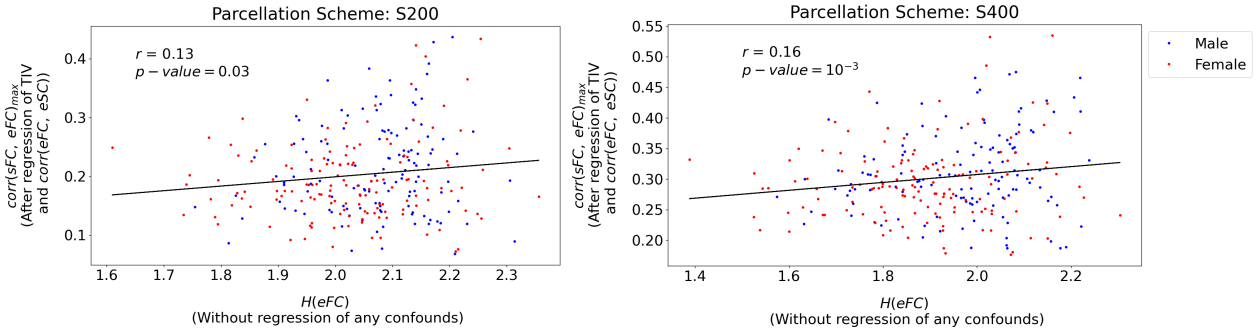

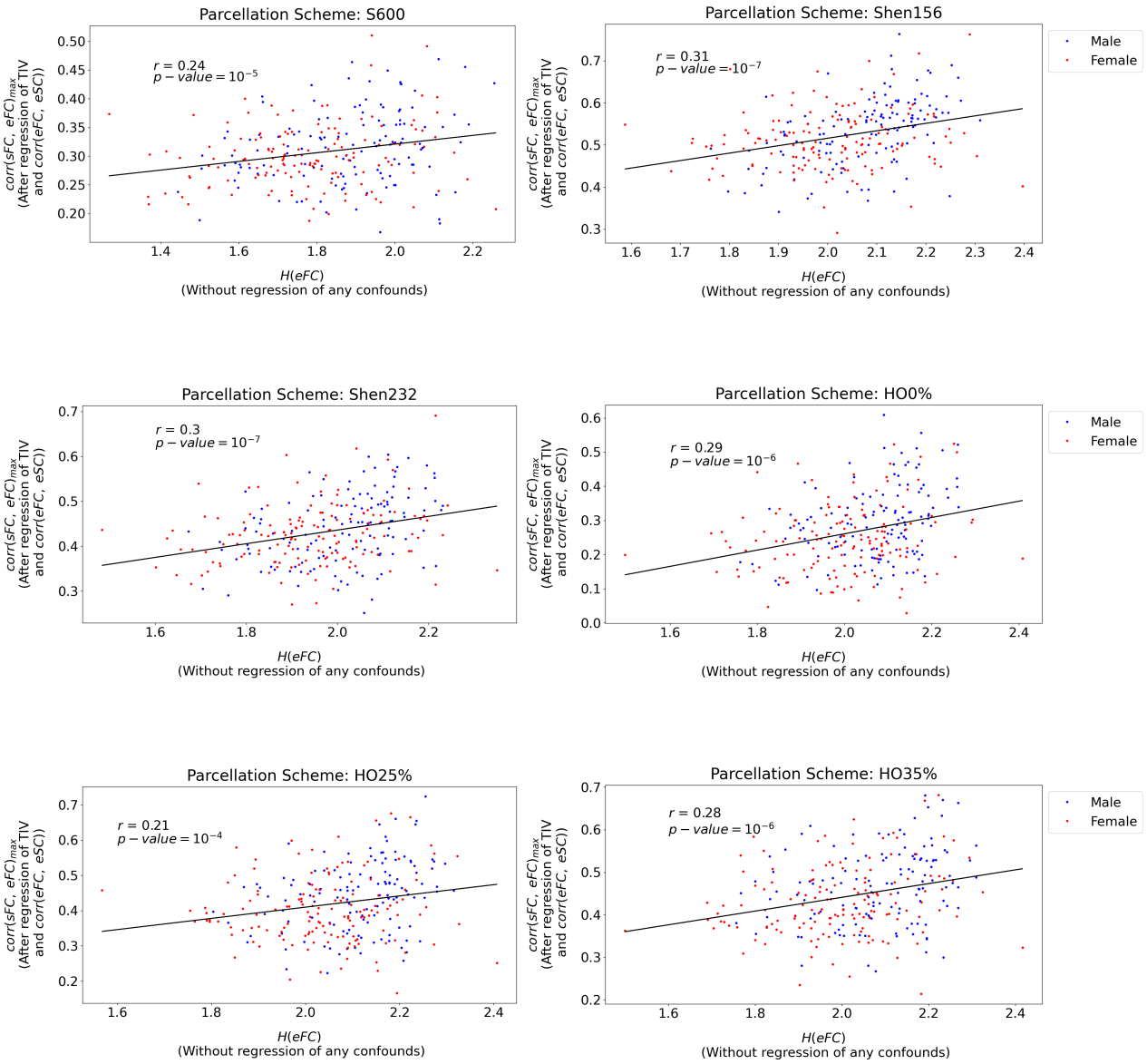
Parcellation Scheme: S600
r = 0.24
p − value = 10^−5
corr(sFC, eFC)max
(After regression of TIV
and corr(eFC, eSC))
H(eFC)
(Without regression of any confounds)
Parcellation Scheme: Shen156
r = 0.31
p − value = 10^−7
Male
Female
Parcellation Scheme: Shen232
r = 0.3
p − value = 10^−7
Parcellation Scheme: HO0%
r = 0.29
p − value = 10^−6
Parcellation Scheme: HO25%
r = 0.21
p − value = 10^−4
Parcellation Scheme: HO35%
r = 0.28
p − value = 10^−6

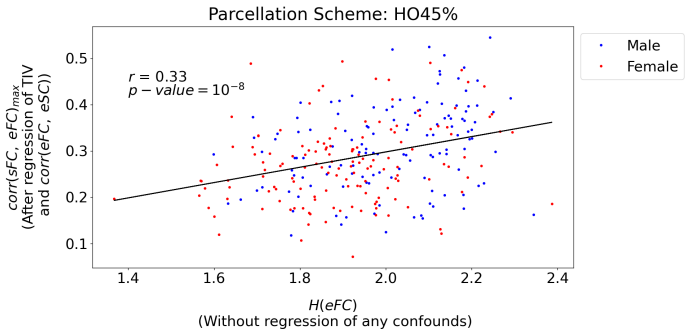

Limit Cycle Model

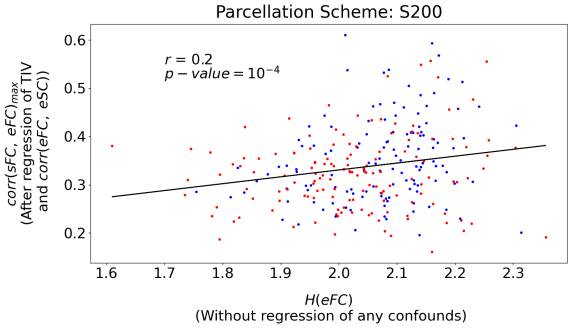

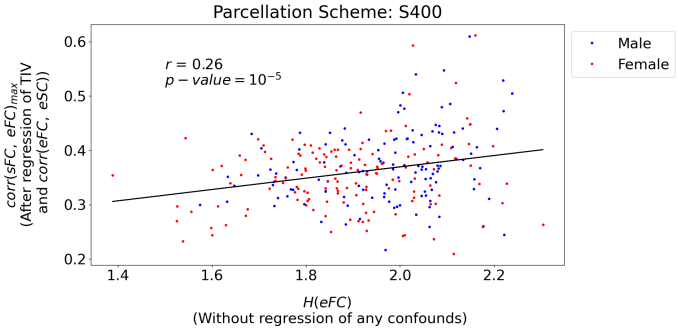

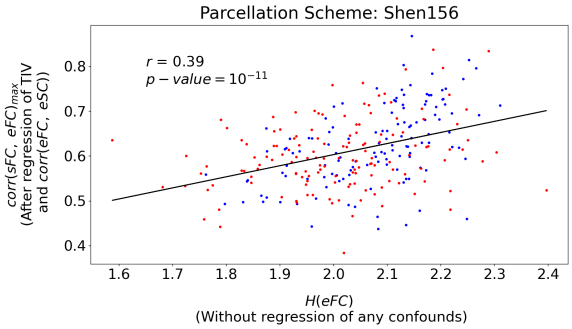

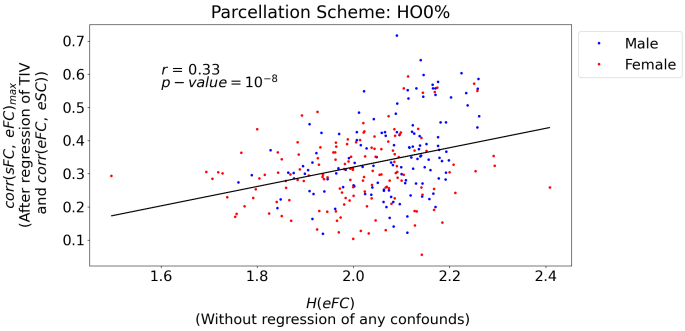

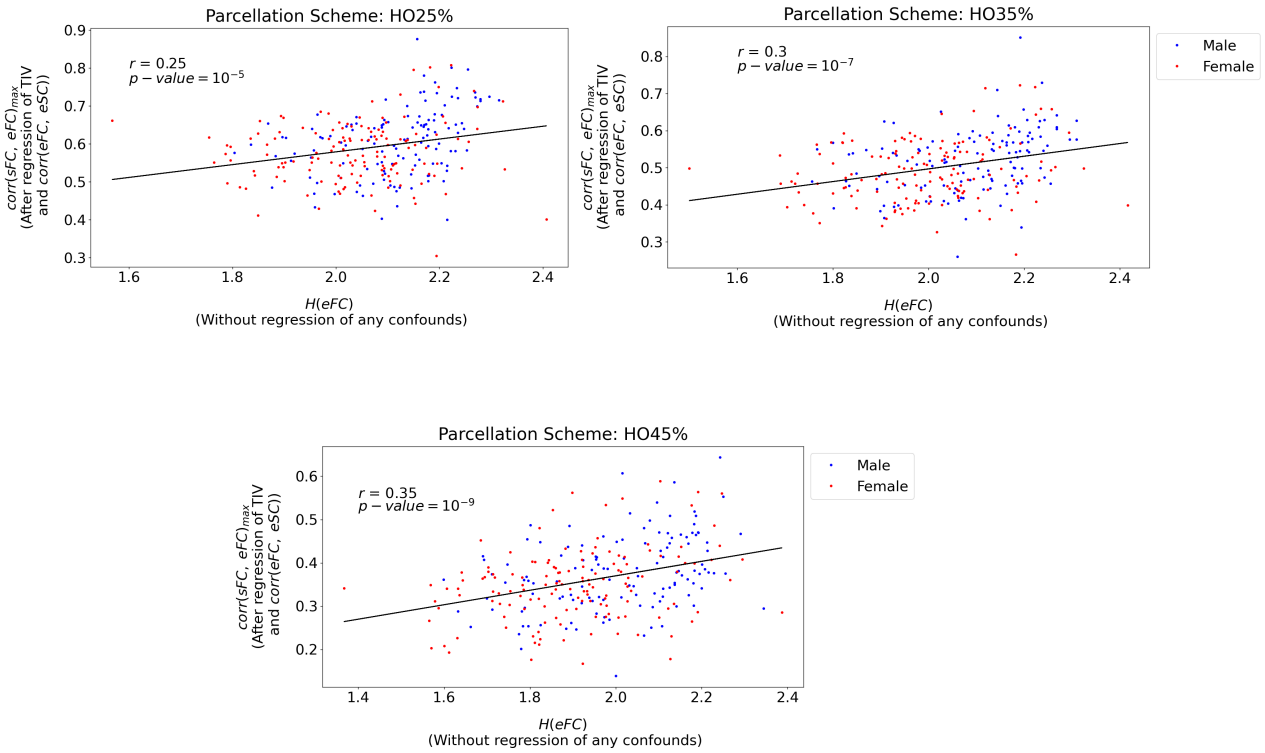

7.2 Standard Deviation of the eFC Matrix - $\sigma(|eFC|)$

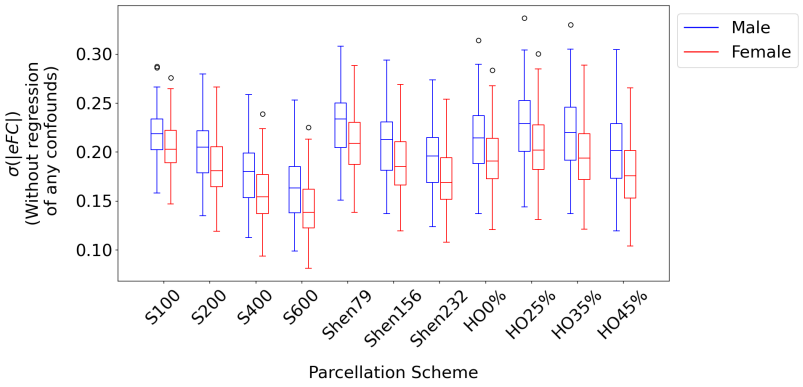

Figure 7.5: Box plots illustrating the qualitative difference in the value of $\sigma(|eFC|)$ between the male group (blue) and that of the female group (red) within each of the 11 parcellation schemes, for the case before regression of any confounds.

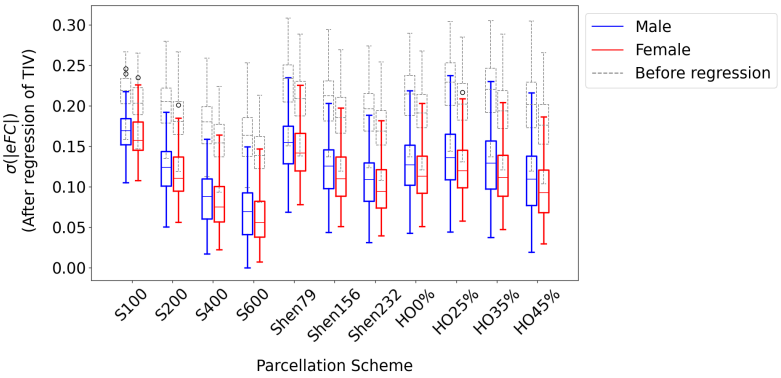

Figure 7.6: Box plots illustrating the qualitative difference in the value of $\sigma(|eFC|)$ between the male group (blue) and that of the female group (red) within each of the 11 parcellation schemes, for the case after regression of only the brain size (TIV).

7.2.1 Relationship between $\sigma(|eFC|)$ and $corr(sFC,\ eFC)_{max}$

The following plots illustrate the relationship between the $\sigma(|eFC|)$ (after regression of just the TIV) and the $corr(sFC,\ eFC)_{max}$ (after regression of both the TIV and $corr(eFC,\ eSC)$) within a parcellation scheme. Each dot in the scatter plot corresponds to a subject (blue for males and red for females) and the solid black line represents the line of best fit obtained through linear regression; r is the Pearson's correlation coefficient between the two quantities and the $p-value$ (FDR corrected) represents its statistical significance. The plots for both the models are shown below.

Phase Oscillator Model

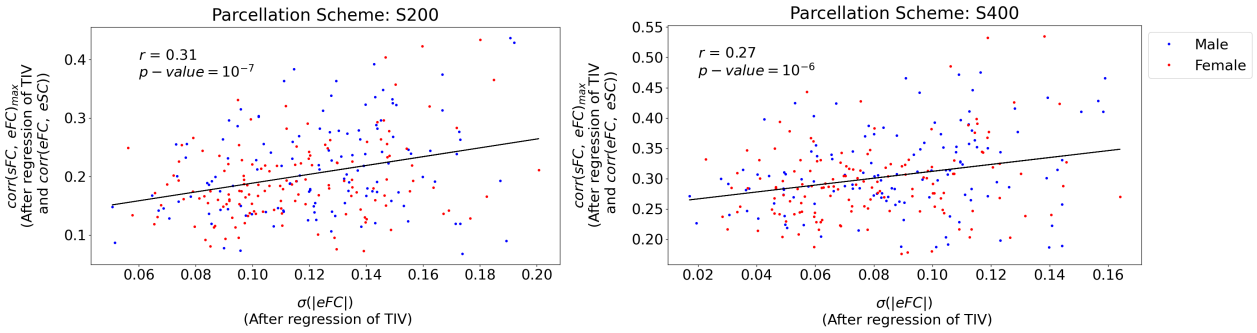

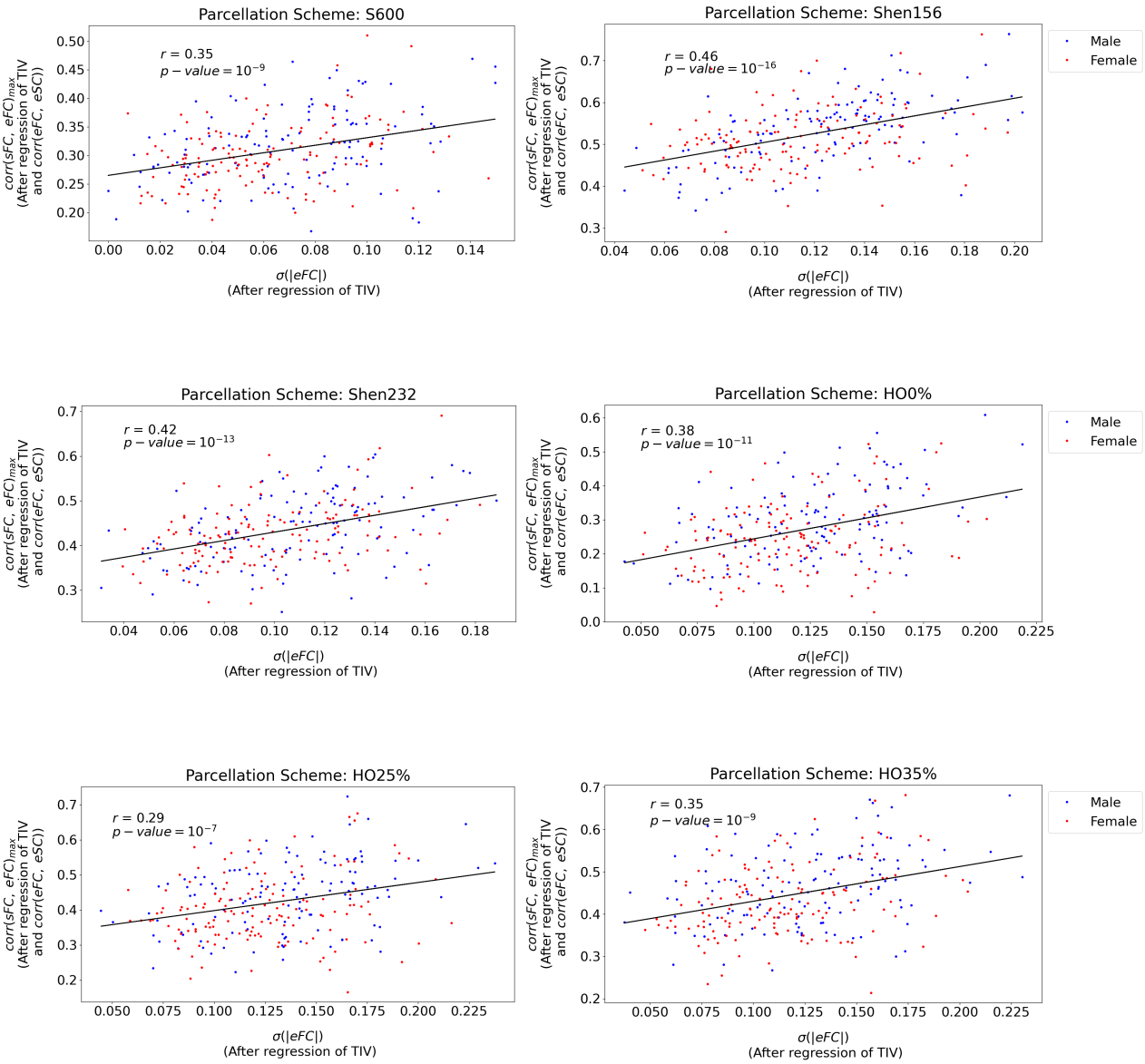
Parcellation Scheme: S600
r = 0.35
p − value = 10^−9
Parcellation Scheme: Shen156
r = 0.46
p − value = 10^−16
Parcellation Scheme: Shen232
r = 0.42
p − value = 10^−13
Parcellation Scheme: HO0%
r = 0.38
p − value = 10^−11
Parcellation Scheme: HO25%
r = 0.29
p − value = 10^−7
Parcellation Scheme: HO35%
r = 0.35
p − value = 10^−9
corr(sFC, eFC)max (After regression of TIV and corr(eFC, eSC))
σ(|eFC|) (After regression of TIV)
Male
Female

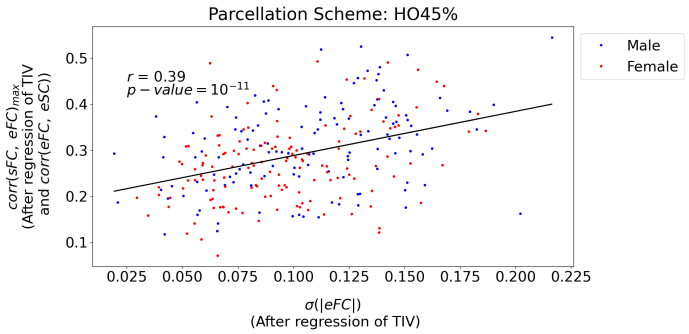

Limit Cycle Model

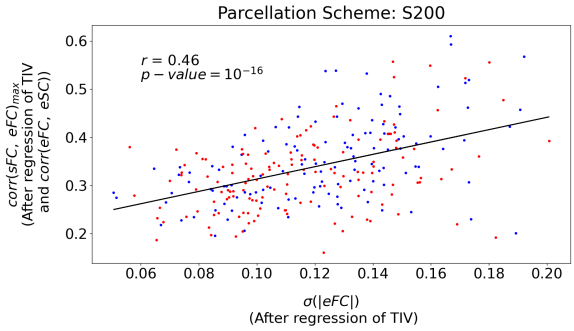

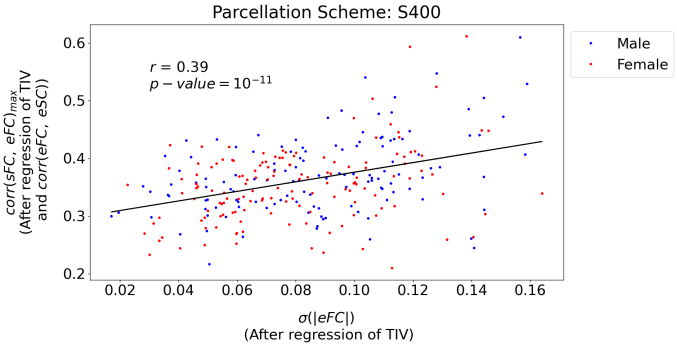

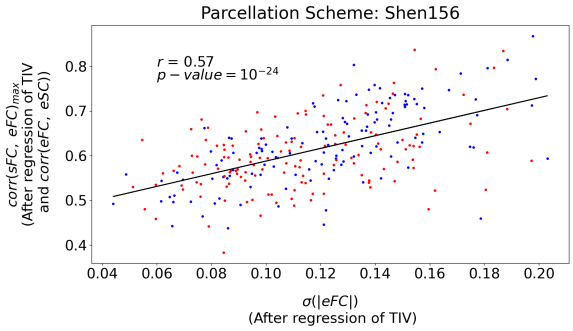

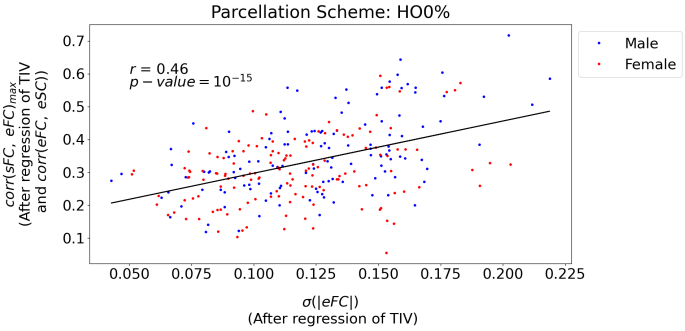

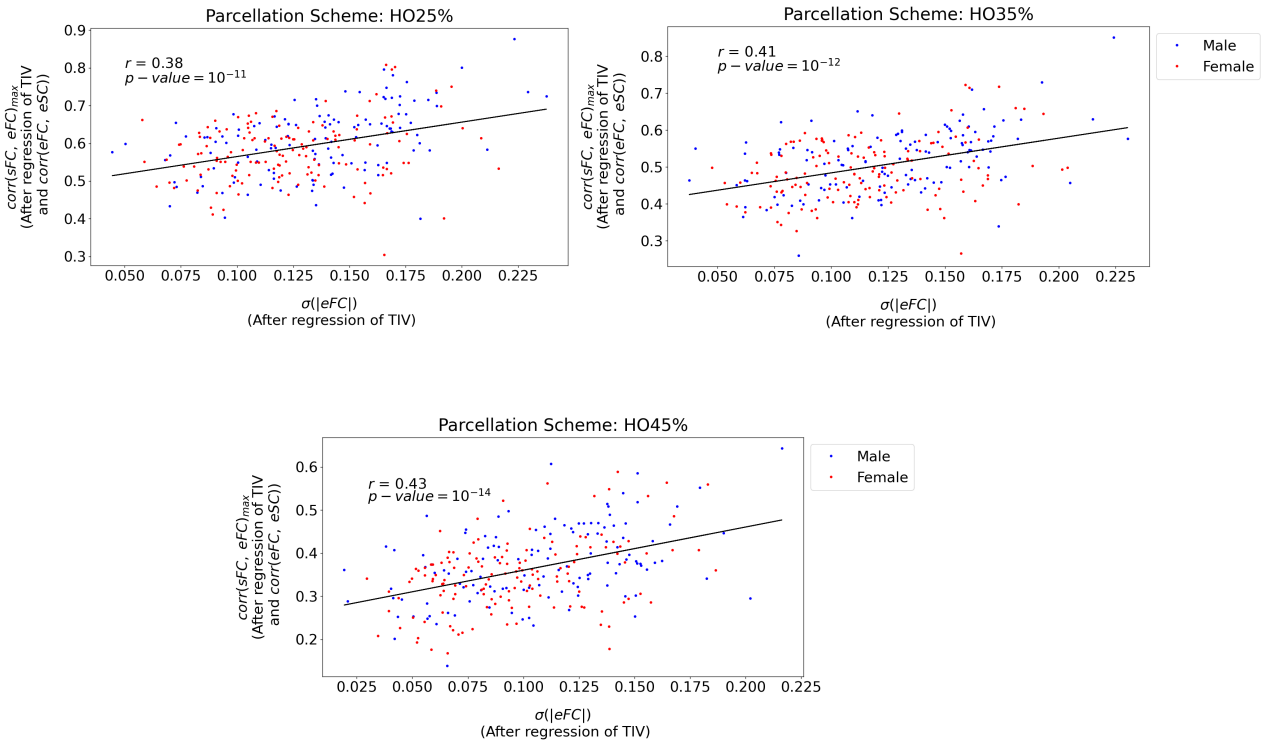

7.3 Area under the Eigen Value Curve of the eFC Matrix - $A(\lambda_{eFC})$

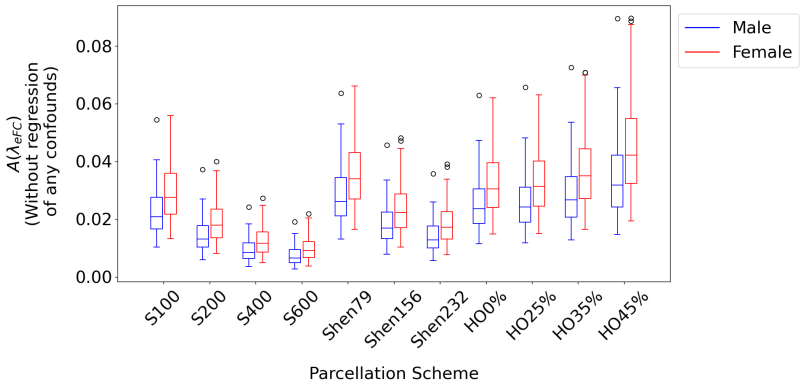

Figure 7.7: Box plots illustrating the qualitative difference in the value of $A(\lambda_{eFC})$ between the male group (blue) and that of the female group (red) within each of the 11 parcellation schemes, for the case before regression of any confounds.

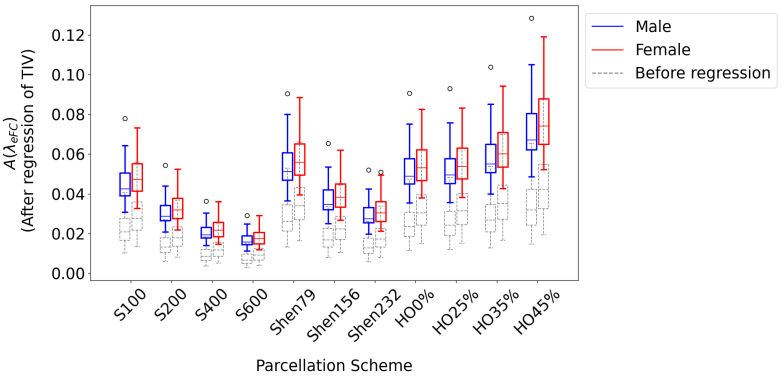

Figure 7.8: Box plots illustrating the qualitative difference in the value of $A(\lambda_{eFC})$ between the male group (blue) and that of the female group (red) within each of the 11 parcellation schemes, for the case after regression of only the brain size (TIV).

7.3.1 Relationship between $A(\lambda_{eFC})$ and $corr(sFC,\ eFC)_{max}$

The following plots illustrate the relationship between the $A(\lambda_{eFC})$ (without regression of any confounds) and the $corr(sFC,\ eFC)_{max}$ (after regression of both the TIV and $corr(eFC,\ eSC)$) within a parcellation scheme. Each dot in the scatter plot corresponds to a subject (blue for males and red for females) and the solid black line represents the line of best fit obtained through linear regression; r is the Pearson's correlation coefficient between the two quantities and the $p-value$ (FDR corrected) represents its statistical significance. The plots for both the models are shown below.

Phase Oscillator Model

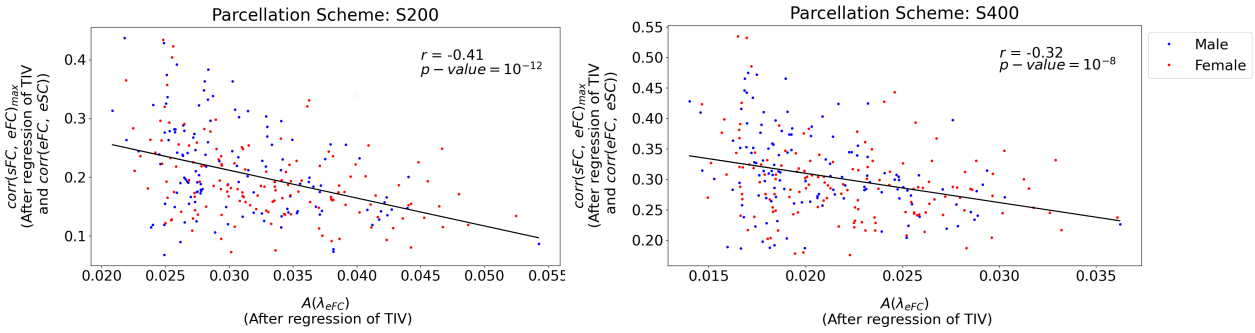

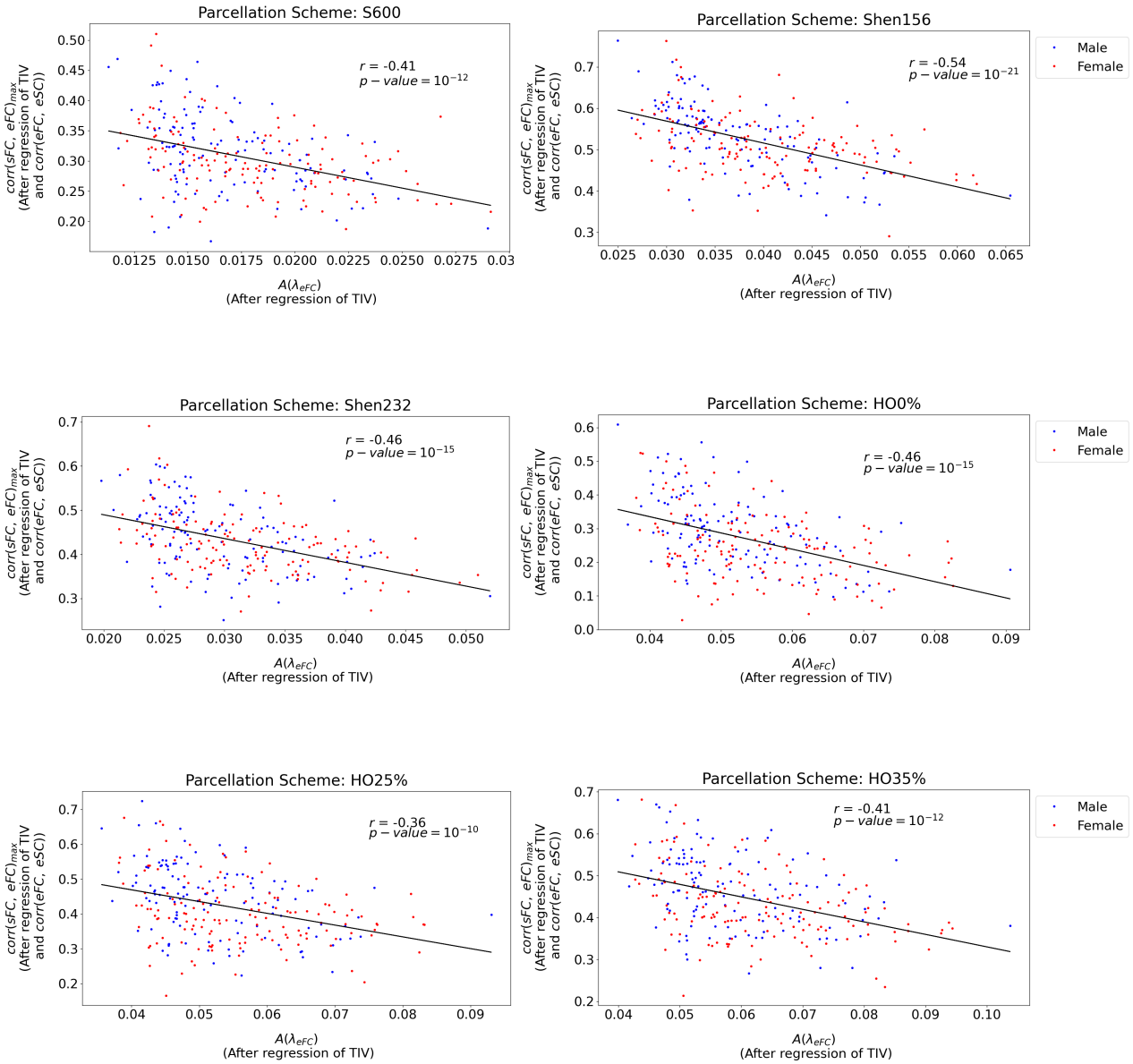
Parcellation Scheme: S600
r = -0.41
p − value = 10^−12
corr(sFC, eFC)max
(After regression of TIV
and corr(eFC, eSC))
A(λeFC)
(After regression of TIV)
Parcellation Scheme: Shen156
r = -0.54
p − value = 10^−21
Male
Female
Parcellation Scheme: Shen232
r = -0.46
p − value = 10^−15
Parcellation Scheme: HO0%
r = -0.46
p − value = 10^−15
Parcellation Scheme: HO25%
r = -0.36
p − value = 10^−10
Parcellation Scheme: HO35%
r = -0.41
p − value = 10^−12

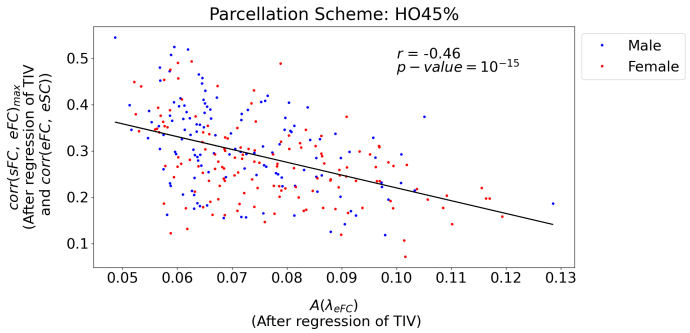

Limit Cycle Model

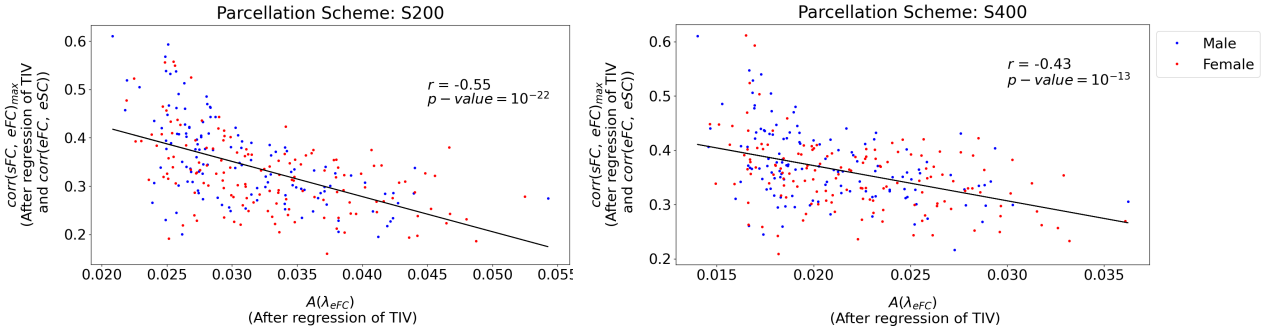

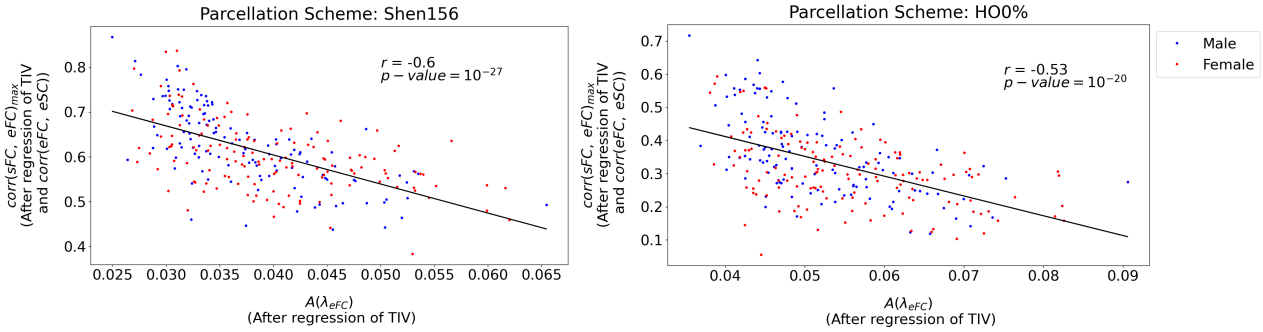

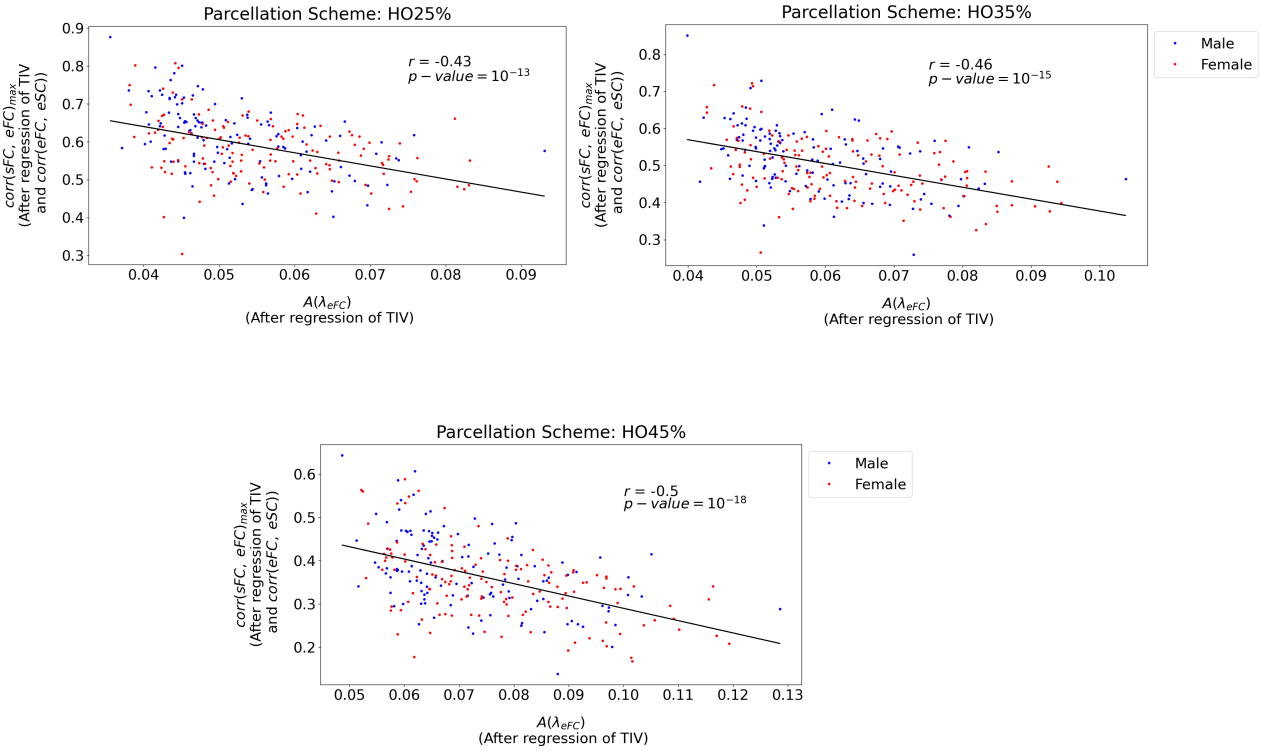
Parcellation Scheme: HO25%
r = -0.43
p − value = 10^−13
corr(sFC, eFC)max
(After regression of TIV
and corr(eFC, eSC))
A(λeFC)
(After regression of TIV)
Parcellation Scheme: HO35%
r = -0.46
p − value = 10^−15
Male
Female
Parcellation Scheme: HO45%
r = -0.5
p − value = 10^−18

Bibliography

[1] Analysing a binary vs. ordinal variable. https://peterstatistics.com/CrashCourse/3-TwoVarUnpair/BinOrd/BinOrd-2b-EffectSize.html#:~:text=The%20Rosenthal%20correlation%20is%20a,it%20with%20other%20correlation%20coefficients).

[2] Kevin M Aquino, Ben Fulcher, Stuart Oldham, Linden Parkes, Leonardo Gollo, Gustavo Deco, and Alex Fornito. On the intersection between data quality and dynamical modelling of large-scale fmri signals. *NeuroImage*, 256:119051, 2022.

[3] Brain Transcriptomics. http://www.altmann.eu/research/?page_id=515.

[4] Michael Breakspear, Stewart Heitmann, and Andreas Daffertshofer. Generative models of cortical oscillations: neurobiological implications of the kuramoto model. *Frontiers in human neuroscience*, 4:190, 2010.

[5] The SciPy community. scipy.stats.ranksums. https://docs.scipy.org/doc/scipy/reference/generated/scipy.stats.ranksums.html.

[6] Connectome. https://en.wikipedia.org/wiki/Connectome#:~:text=A%20connectome%20(%2Fk%C9%99%CB%88,neurons%20which%20communicate%20through%20synapses.

[7] Case Event Data and AE Using Descriptive Statistics Bartz. *Basic statistical concepts*. New York: Macmillan. Devore, J., and Peck, 1988.

[8] Justin WM Domhof, Kyesam Jung, Simon B Eickhoff, and Oleksandr V Popovych. Parcellation-induced variation of empirical and simulated brain connectomes at group and subject levels. *Network Neuroscience*, 5(3):798–830, 2021.

[9] Simon B Eickhoff, BT Yeo, and Sarah Genon. Imaging-based parcellations of the human brain. *Nature Reviews Neuroscience*, 19(11):672–686, 2018.

[10] Eigenvalues and eigen vectors. https://en.wikipedia.org/wiki/Eigenvalues_and_eigenvectors.

[11] Entropy (information theory). https://en.wikipedia.org/wiki/Entropy_(information_theory).

[12] False discovery rate. https://en.wikipedia.org/wiki/False_discovery_rate.

[13] False Discovery Rate. https://www.publichealth.columbia.edu/research/population-health-methods/false-discovery-rate.

[14] Fisher Transformation. https://en.wikipedia.org/wiki/Fisher_transformation.

[15] Jay N Giedd, Armin Raznahan, Kathryn L Mills, and Rhoshel K Lenroot. magnetic resonance imaging of male/female differences in human adolescent brain anatomy. *Biology of sex differences*, 3(1):1–9, 2012.

[16] Zijin Gu, Keith Wakefield Jamison, Mert Rory Sabuncu, and Amy Kuceyeski. Heritability and interindividual variability of regional structure-function coupling. *Nature Communications*, 12(1):1–12, 2021.

[17] Adam Hayes. Multiple Linear Regression (MLR). https://www.investopedia.com/terms/m/mlr.asp#:~:text=Key%20Takeaways-,Multiple%20linear%20regression%20(MLR)%2C%20also%20known%20simply%20as%20multiple,uses%20just%20one%20explanatory%20variable.

[18] Shubhangi Hora. Parametric Tests - the t test. https://towardsdatascience.com/parametric-tests-the-t-test-c9b17faabfb0, 2021.

[19] Yanbing Jia, Huaguang Gu, and Qiang Luo. Sample entropy reveals an age-related reduction in the complexity of dynamic brain. *Scientific reports*, 7(1):1–10, 2017.

[20] Jonathan Taylor statsmodels-developers Josef Perktold, Skipper Seabold. statsmodels.stats.multitest.fdrcorrection. https://www.statsmodels.org/dev/generated/statsmodels.stats.multitest.fdrcorrection.html.

[21] Linear Regression. https://en.wikipedia.org/wiki/Linear_regression.

[22] Richard Lynn. Sex differences in intelligence and brain size: A developmental theory. *Intelligence*, 27(1):1–1, 1999.

[23] Guillermo Macbeth, Eugenia Razumiejczyk, and Rubén Daniel Ledesma. Cliff's delta calculator: A non-parametric effect size program for two groups of observations. *Universitas Psychologica*, 10(2):545–555, 2011.

[24] Mann–Whitney U test. https://en.wikipedia.org/wiki/Mann%E2%80%93Whitney_U_test#Assumptions_and_formal_statement_of_hypotheses.

[25] S. A. McLeod. What a p-value tells you about statistical significance. Simply Psychology. www.simplypsychology.org/p-value.html, 2019.

[26] Maysam Nezafati, Hisham Temmar, and Shella D Keilholz. Functional mri signal complexity analysis using sample entropy. *Frontiers in Neuroscience*, 14:700, 2020.

[27] Amir Omidvarnia, Andrew Zalesky, Dimitri Van De Ville, Graeme D Jackson, Mangor Pedersen, et al. Temporal complexity of fmri is reproducible and correlates with higher order cognition. *NeuroImage*, 230:117760, 2021.

[28] p-Value. https://en.wikipedia.org/wiki/P-value.

[29] Hae-Jeong Park and Karl Friston. Structural and functional brain networks: from connections to cognition. *Science*, 342(6158):1238411, 2013.

[30] Steven M Pincus. Approximate entropy as a measure of system complexity. *Proceedings of the National Academy of Sciences*, 88(6):2297–2301, 1991.

[31] Oleksandr V Popovych, Kyesam Jung, Thanos Manos, Sandra Diaz-Pier, Felix Hoffstaedter, Jan Schreiber, BT Thomas Yeo, and Simon B Eickhoff. Inter-subject and inter-parcellation variability of resting-state whole-brain dynamical modeling. *Neuroimage*, 236:118201, 2021.

[32] Stuart J Ritchie, Simon R Cox, Xueyi Shen, Michael V Lombardo, Lianne M Reus, Clara Alloza, Mathew A Harris, Helen L Alderson, Stuart Hunter, Emma Neilson, et al. Sex differences in the adult human brain: evidence from 5216 uk biobank participants. *Cerebral cortex*, 28(8):2959–2975, 2018.

[33] Renato ME Sabbatini. Are there differences between the brains of males and females. *Brain & Mind Online Magazine*, 12(11), 1997.

[34] Standard Deviation. https://en.wikipedia.org/wiki/Standard_deviation.

[35] Maciej Tomczak and Ewa Tomczak. The need to report effect size estimates revisited. an overview of some recommended measures of effect size. *Trends in sport sciences*, 1(21):19–25, 2014.

[36] Raphael Vallat. pingouin.compute_effsize_from_t. https://pingouin-stats.org/generated/pingouin.compute_effsize_from_t.html#pingouin.compute_effsize_from_t.

[37] Danny JJ Wang, Kay Jann, Chang Fan, Yang Qiao, Yu-Feng Zang, Hanbing Lu, and Yihong Yang. Neurophysiological basis of multi-scale entropy of brain complexity and its relationship with functional connectivity. *Frontiers in neuroscience*, 12:352, 2018.

[38] PhD MPH Wayne W. LaMorte, MD. Mann Whitney U Test (Wilcoxon Rank Sum Test). https://sphweb.bumc.bu.edu/otlt/mph-modules/bs/bs704_nonparametric/bs704_nonparametric4.html#:~:text=The%20Mann%20Whitney%20U%20test%2C%20sometimes%20called%20the%20Mann%20Whitney,populations%20have%20the%20same%20shape)., 2017.

[39] Susanne Weis, Kaustubh R Patil, Felix Hoffstaedter, Alessandra Nostro, BT Thomas Yeo, and Simon B Eickhoff. Sex classification by resting state brain connectivity. *Cerebral cortex*, 30(2):824–835, 2020.

[40] Xi Zhang, Meng Liang, Wen Qin, Baikun Wan, Chunshui Yu, and Dong Ming. Gender differences are encoded differently in the structure and function of the human brain revealed by multimodal mri. *Frontiers in Human Neuroscience*, 14:244, 2020.

Erklärung

Hiermit versichere ich an Eides statt, dass ich die vorliegende Arbeit selbstständig und ohne die Benutzung anderer als der angegebenen Hilfsmittel angefertigt habe. Alle Stellen, die wörtlich oder sinngemäß aus veröffentlichten und nicht veröffentlichten Schriften entnommen wurden, sind als solche kenntlich gemacht. Die Arbeit ist in gleicher oder ähnlicher Form oder auszugsweise im Rahmen einer anderen Prüfung noch nicht vorgelegt worden. Ich versichere, dass die eingereichte elektronische Fassung der eingereichten Druckfassung vollständig entspricht.

Köln, 10.Juni 2022
Shraddha P. Jain